Forschungszentrum Jülich
in der Helmholtz-Gemeinschaft

Effect of water vapour on growth and adherence of chromia scales on pure chromium

Marek Michalik, Michael Hänsel, Willem J. Quadakkers

Energietechnik
Energy Technology

Schriften des Forschungszentrums Jülich
Reihe Energietechnik / Energy Technology Band / Volume 67

Forschungszentrum Jülich GmbH
Institut für Energieforschung (IEF)
Werkstoffstruktur und Eigenschaften (IEF-2)

Effect of water vapour on growth and adherence of chromia scales on pure chromium

Marek Michalik*, Michael Hänsel, Willem J. Quadakkers

* Dissertation

Schriften des Forschungszentrums Jülich
Reihe Energietechnik / Energy Technology Band / Volume 67

ISSN 1433-5522 ISBN 978-3-89336-486-2

Bibliographic information published by the Deutsche Nationalbibliothek.
The Deutsche Nationalbibliothek lists this publication in the Deutsche Nationalbibliografie; detailed bibliographic data are available in the Internet at http://dnb.d-nb.de.

Publisher and Distributor:	Forschungszentrum Jülich GmbH Zentralbibliothek, Verlag D-52425 Jülich phone: +49 02461 61-5368 · fax: +49 2461 61-6103 e-mail: zb-publikation@fz-juelich.de Internet: http://www.fz-juelich.de/zb
Cover Design:	Grafische Medien, Forschungszentrum Jülich GmbH
Printer:	Grafische Medien, Forschungszentrum Jülich GmbH
Copyright:	Forschungszentrum Jülich 2007

Schriften des Forschungszentrums Jülich
Reihe Energietechnik / Energy Technology Band / Volume 67

D 82 (Diss., Aachen, RWTH, 2007)

ISSN 1433-5522
ISBN 978-3-89336-486-2

The complete volume is freely available on the Internet on the Jülicher Open Access Server (JUWEL) at http://www.fz-juelich.de/zb/juwel

Zusammenfassung

Das Oxidationsverhalten von Chromoxid verschiedener Reinheitsgrade wurde im Temperaturbereich von 950 bis 1050°C in verschiedenen Atmosphären wie Ar-O_2, Ar-H_2-H_2O sowie komplexere wie N_2-O_2-H_2O und N_2-H_2-H_2O untersucht. Dadurch konnte das Oxidationsverhalten von Chromoxid bei verschiedenen Sauerstoff- und Wasserdampfpartialdrücken studiert werden.

Es konnte gezeigt werden, dass die Bildung von Oxidschichten in Ar-O_2 vom Sauerstoffpartialdruck abhängt. Abnehmender pO_2 führte in derartigen Gasmischungen zu niedrigeren Oxidationsraten und verbesserter Haftung der Oxidschichten. In Ar-H_2-H_2O war dies nicht der Fall, die Haftung der Oxidschichten ist in allen Fällen in Gasen mit niedrigem pO_2 hervorragend. Das Absenken des Sauerstoffpartialdrucks (dies wurde durch eine höheres H_2/H_2O Verhältnis erreicht) führte zu einer höheren Oxidationsrate.

Die Haupterkenntnis der Arbeit ist, dass die Morphologie der Oxidschichten, die in Ar-H_2O und Ar-H_2-H_2O gebildet werden, sich erheblich von der in Ar-O_2 geformten unterscheidet. Die Oxidkörner, die in wasserdampfhaltigen Gasen mit niedrigem Sauerstoffpartialdruck gebildet wurden, sind deutlich kleiner, als die in trockenen Gasen mit molekularem Sauerstoff gewachsenen. Es wurde vermutet, dass der Effekt von Wasserdampf auf die Oxidschichtmorphologie mit der schnelleren Adsorption und Dissoziation von Wasserdampf im Vergleich zu O_2 zusammenhängt und der Hauptgrund für einen verstärkten nach innen gerichteten Transport zur Metal/Oxid Grenzfläche ist. Es wurde vorgeschlagen, dass im Wesentlichen die Sauerstoffkorngrenzendiffusion verstärkt wurde aber es wird angenommen, dass molekularer Transport von H_2 und H_2O durch die Oxidschicht ebenfalls möglich sein könnte und zum Wachstum der inneren Schicht beiträgt.

Tracer Untersuchungen in Kombination mit SNMS Techniken zeigten, dass in Gasen mit niedrigem pO_2 ein erheblicher Teil der Oxidschicht an der Metall/Oxid Grenzfläche geformt wird. Dies unterstützt die Theorie, dass kleinere Oxidkörner für verstärkten Transport von Sauerstoff nach innen sorgen könnten. Weiter konnte beobachtet werden, dass das innere Wachstum in Ar-H_2-H_2O höher war als in Ar-H_2O gasen. Dies könnte darauf hindeuten, dass der Sauerstoff- und der Wasserstoffpartialdruck des Gases ebenfalls Faktoren sind, die das Oxidationsverhalten in Gasen mit niedrigem pO_2 beeinflussen.

Auslagerungen in Ar-O_2-H_2O Mischungen zeigten, dass Wasserdampf die Haftung der Oxidschicht signifikant verbessern konnte. Es wird vermutet, dass dies zu H_2O Transport nach innen und damit zu verstärktem Oxidwachstum an der Metall/Oxid Grenzfläche führt. Es konnte gezeigt werden, dass Wasserdampf, wenn er in hinreichender Menge vorhandenen ist, in Multikomponenten Gasmischungen die Bildung von Nitriden und Karbiden unter der Oxidschicht verhindert. Dieser Effekt von Wasserdampf ist besonders deutlich in Gasen mit niedrigem Sauerstoffpartialdruck wie N_2-4%H_2-4%H_2O oder CO-2%CO_2-1%H_2O. Es wird angenommen, dass in diesen Atmosphären der niedrige Sauerstoffpartialdruck die Adsorption und Dissoziation von H_2O beschleunigt, und so die Dissozierung von Wasserdampf schneller ist.

Es konnte gezeigt werden, dass die Reinheit des Chromoxids einen erheblichen Effekt auf die Oxidationsrate und die Haftung der Oxidschicht hat. Dies könnte ein Schlüsselelement sein um die erhebliche Streuung in der Literatur zu interpretieren. Chromoxid Proben unterschiedlicher Reinheit wurden untersucht und es wurde festgestellt, dass reineres Chromoxid eine niedrigere Oxidationsrate hatte und eine weniger poröse Oxidschicht bildet. Dieses Verhalten war in Ar-O_2 Gasen besonders deutlich. Die Präsenz einiger Elemente könnte die Ursache für das höhere Oxidschichtwachstum sein, da diese die Defektkonzentrationen im Oxid beeinflussen. Die schlechtere Haftung ist wahrscheinlich auf Kohlenstoff zurückzuführen, welcher an der Oxid/Metall Grenzfläche das flüchtige CO mit einem Partialdruck von $4x10^{-5}$ atm bildet.

Abstract

The oxidation behaviour of chromium was studied in the temperature range 950 to 1050^{o}C. A number of atmospheres such as Ar-O_2, Ar-H_2-H_2O, and more complex N_2-O_2-H_2O and N_2-H_2-H_2O were used, to allow the effects of oxygen and water vapour partial pressures to be determined.

It was shown that the oxide scale formed in Ar-O_2 environments was dependent on the oxygen partial pressure. Decreasing the pO_2 in such gas mixtures lowered the oxidation rate and improved scale adherence. Different behaviour was found in Ar-H_2-H_2O. Scale adherence remained good in all low pO_2 gases and decreasing the pO_2 in the gas (this was done by using gases of higher H_2/H_2O ratio) led to an increase in the oxidation rate.

The main finding of the work was that the oxide scale formed on chromium in Ar-H_2O and Ar-H_2-H_2O gases significantly differs from that formed in Ar-O_2. It appeared that oxide grains were much smaller in low pO_2 gases containing water vapour than in dry high pO_2 gases. It is believed that this effect of water vapour on the oxide morphology development is due to the faster adsorption and dissociation of H_2O at the outer surface compared with O_2, which enhance the inward transport of oxygen ions to the metal/oxide interface. It is proposed that increased oxygen grain boundary diffusion is the dominant process but molecular transport of H_2 and H_2O through the scale could also operate and contribute to the inner scale growth.

The tracer study combined with SNMS techniques showed that in low pO_2 gases a significant amount of the scale was formed at the metal/oxide interface and this supports the observations that smaller oxide grains promote inward oxygen transport. It was also found that the extent of inward growth was higher in Ar-H_2-H_2O than in Ar-H_2O gas. This may indicate that the oxygen partial pressure of the gas or the hydrogen partial pressure were also factors determining the oxidation behaviour in low pO_2 gases.

Exposure in Ar-O_2-H_2O mixtures revealed that water vapour could markedly improve oxide scale adherence. This is believed to be a consequence of enhanced inward transport of H_2O, which promotes scale growth at the metal/oxide interface.

It was found that water vapour, when present in sufficient amounts in the multicomponent gas mixture could block the formation of nitrides and carbides beneath the oxide scale. The blocking effect of water vapour at the surface was especially pronounced in low pO_2 gases such as N_2-4%H_2-4%H_2O and CO-2%CO_2-1%H_2O. It is believed that in such atmospheres adsorption and dissociation of H_2O was enhanced by the low oxygen partial pressure and therefore dissociation of water vapour was faster.

The purity of chromium was shown to affect substantially both, the oxidation rate and the oxide scale adherence. This could be a key factor in the interpretation of the scatter found in the literature. Chromium specimens of different purity were investigated and it was observed that purer chromium had a lower oxidation rate and produced a less porous oxide scale. Such behaviour was particularly pronounced in Ar-O_2 gases. The presence of some elements could account for the enhanced oxidation rate due to modifications in defect concentrations in the oxide. Poor scale adherence was probably affected the most by carbon, which forms the volatile oxide CO at the chromium/chromia interface at pressure of $4x10^{-5}$ atm.

Table of Contents

Theory

Experimental

Theory Part

1. Introduction

High temperature alloys rely on the formation of protective surface scales for their resistance against gaseous corrosion. Most of the commonly used high temperature alloys form alumina or chromia scales, when exposed to oxygen containing atmospheres at high temperatures [1,2,3]. Comprehensive studies have been undertaken concerning oxide scaling reactions and the factors affecting the protective properties of such scales, especially with respect to their adherence and growth kinetics [4]. The vast majority of studies on the growth and adherence of oxide scales formed on pure chromium have been carried out in high-pO_2 atmospheres like air or oxygen [5-18]. A smaller number of papers have reported the oxidation behaviour of chromia formers in gases with low equilibrium oxygen partial pressures [19-24]. Such low-pO_2 environments, which frequently contain substantial amounts of water vapour, occur industrially in chemical processes, in energy conversion systems [25,26] and/or in solid oxide fuel cells [27,28]. Tveten and Hultquist [17-19] measured the effect of reactive element additions and hydrogen on the oxidation behaviour of Cr-base alloys in pure oxygen [17,18] and water vapour [19]. Upon oxidizing hydrogen-containing chromium the adherence of the scales formed in pure oxygen was poor and the authors attributed this to hydrogen induced cation transport in the oxide scale. In water vapour, higher oxide growth rates and improved oxide scale adherence were found. Similar experimental findings were made by Quadakkers et al. [22]. They observed oxide scales formed during exposure of Cr and various Cr-base alloys in Ar-H_2-H_2O to possess far better adherence than those formed during air exposure. Hänsel et al. [21] studied the role of water vapour on chromia scale growth in gases with low oxygen partial pressure. When molecular oxygen is a minority gas species, adsorption on the oxide surface of H_2O becomes an important process in the overall oxidation kinetics. This is reflected in an alteration of the oxide defect concentration in the oxide and hence the scaling rate. It also changes the oxide morphology at the oxide/gas interface.

The oxidation behaviour of pure chromium becomes more complicated when the reacting gas contains more than one oxidant. In that case a sublayer beneath the chromia scale can be formed. Zheng and Young studied the mechanism of the growth and breakdown of Cr_2O_3 scales in multicomponent environments with relatively low oxygen activities. Oxidation in CO-CO_2 or N_2-CO-CO_2 always led to the formation of carbides and in the latter case, a nitride sublayer beneath the

external chromia scale [29-31]. They suggested that permeation of carbon and nitrogen through the Cr_2O_3 might be due to molecular transport. Seybolt and Haman preoxidized chromium for 2.5h in oxygen and subsequently exposed it to nitrogen [32]. It was found that the previously established oxide film does not prevent nitrogen ingress. It is interesting, however, that chromium exposed to N_2-H_2-H_2O for the same time and the same temperature does not form any nitride sublayer [29]. Apparently the nature of the atmosphere affects the permeability of the oxide scale.

In the present work, the oxidation behaviour of pure chromium in low- and high-pO_2 environments has been studied in the temperature range of 950°-1050°C. In the experimental work the main emphasis was directed to the effect of the test environment on the adherence of the oxide scales. The high-pO_2 environments were Ar-O_2 mixtures, whereas the low-pO_2 gases were Ar (-H_2)-H_2O mixtures. Additionally studies in multicomponent gas systems were carried out in CO-CO_2-H_2O, N_2-O_2-H_2O and N_2-H_2-H_2O mixtures. In these cases, the investigations addressed the aspect of sublayer formation beneath the chromia scale related to the environment used and in particular, the effect of water vapour on the oxidation.

2. Metal - oxygen reactions

2.1 Thermodynamic aspects

The basic criteria for the prediction of oxide formation is knowledge of the free energy (ΔG) for the reaction:

$$M(s)+\frac{x}{2}O_2(g)=MO_x(s) \tag{1}$$

where the oxide MO_x is the product of the reaction between metal *M(s)* and oxygen *O_2(g).* ΔG can be written as an algebraic sum of chemical potentials of all components of the system:

$$\Delta G=\mu^o_{MO_x}-\mu^o_M-\frac{x}{2}\mu^o_{O_2}-\frac{x}{2}RT\ln p_{O_2} \tag{2}$$

In case of equilibrium $\Delta G=0$ and consequently

$$-\mu^o_{MO_x} + \mu^o_M + \frac{x}{2}\mu^o_{O_2} = -\frac{x}{2}RT \ln p_{O_2} \quad (3)$$

The left side of equation (3) is considered for the standard condition and equals ΔG^o_T; it can be written as:

$$\Delta G^o_T = -\frac{x}{2}RT \ln p_{O_2} \quad (4)$$

The value of ΔG^o_T can be derived from thermodynamic databases and thus the dissociation pressure p_{O_2} of the oxide MO_x can be calculated:

$$p_{O_2} = \exp\left(-\frac{2\Delta G^o_T}{xRT}\right) \quad (5)$$

If the oxygen pressure in the environment is higher than the dissociation pressure of the oxide MO_x, formation of oxide is possible. It corresponds to a negative value of ΔG. For example, in the chromium-oxygen system at 1000°C the ΔG^o_T - value for the formation of the oxide is given as [2]

$$Cr + \frac{3}{4}O_2 = \frac{1}{2}Cr_2O_3,\ \Delta G^o_T = -399.4\ kJ$$

According to equation (5) the dissociation pressure for chromium oxide at 1000°C equals 1.4×10^{-22} bars. This means that if the oxygen partial pressure in the atmosphere is higher than 1.4×10^{-22} bars chromium oxide will be formed [2].

In order to predict whether the oxidation process occurs under given conditions, the Ellingham/Richardson diagram can be useful. For example, at 650°C, all three oxides of iron can be formed if the oxygen partial pressure in the atmosphere is higher than $4.2 \times 10^{-14}\ bar$ (dissociation pressure of hematite), Fig.1, [2].

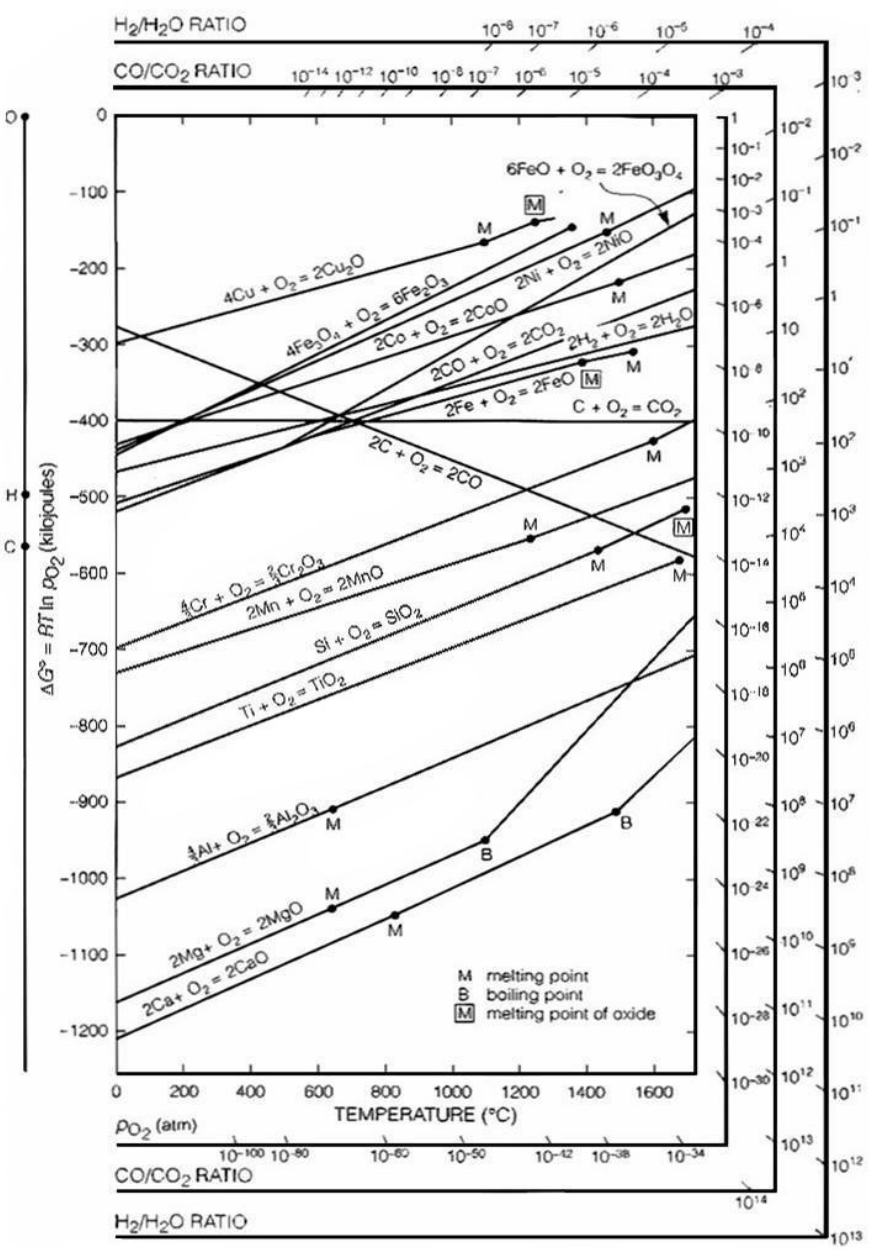

Fig. 1. *Ellingham diagram for metal oxide compounds, [2]*

It is also important to note that from the thermodynamical point of view increasing the temperature while maintaining constant oxygen pressure in the atmosphere can restrain the oxidation process of metals. This is schematically shown in Fig. 2, [33].

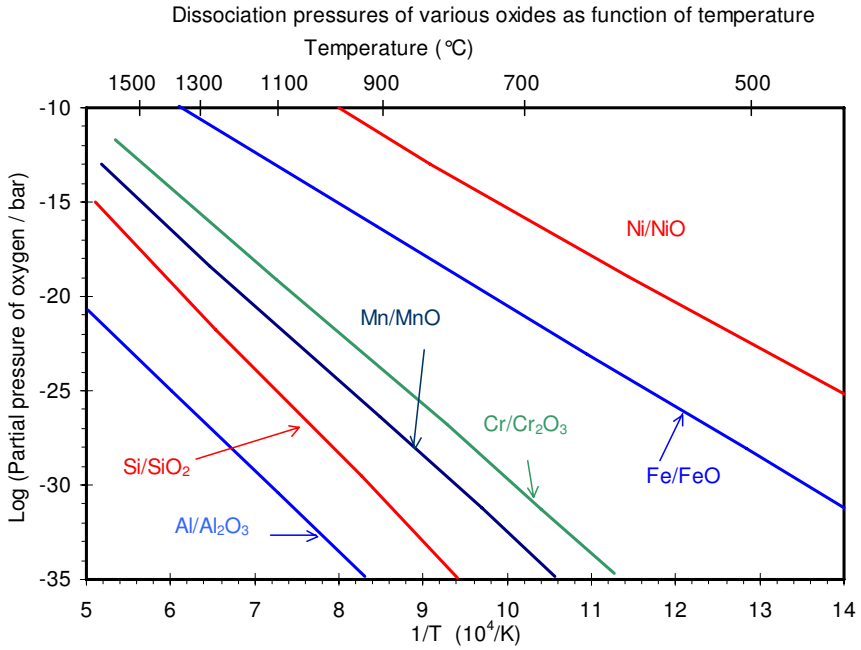

Fig. 2. *Dissociation pressures for several oxides as function of temperature for unit metal activities, [33]*

The coloured lines denote equilibrium between various metals and their respective oxides. Below the line the respective metal M is stable whereas above the line the corresponding oxide is stable.

To describe the oxidation behaviour of the metals at high temperature, knowledge of the oxidation kinetics is necessary in addition to the thermodynamics.

2.2 Kinetic aspects of metal oxidation

Based on thermodynamic calculations, it is possible to predict whether a reaction between a metal and oxygen can take place or not. In order to determine the rate of reaction the mechanism of the process is important. Reactions between a metal and an atmosphere lead to the formation of an oxide

scale if the oxygen partial pressure in the environment is higher than the dissociation pressure of the oxide. The reaction can be written by equation (1), however, the oxidation mechanisms depend on many factors that should be taken into account in order to obtain a full description of this process. The oxidation of metals can be divided into different steps during which a number of characteristic processes occur, Fig. 3, [1].

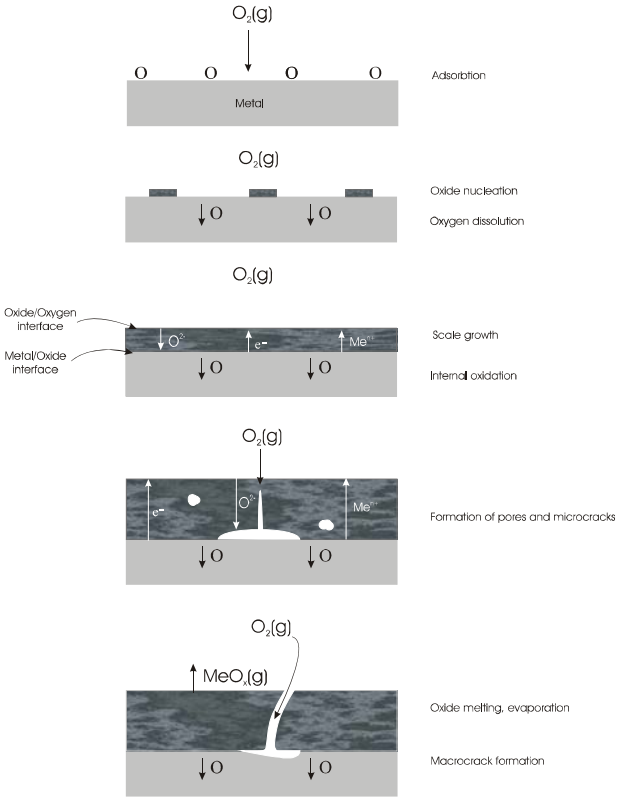

Fig. 3. *Schematic illustration of the various steps involved between oxygen and a metallic material reaction, [1]*

The initial step involves the adsorption of oxygen on the metal surface, formation of oxide nuclei, which are later developed into a dense oxide film, and finally the scale growth process. The initial oxidation reactions are often very fast and difficult to detect quantitatively. They mainly depend on oxygen partial pressure and temperature. In order to investigate these steps both low oxygen pressure and temperature should be applied. The further steps can be observed and analysed easier, however, care should be taken with the interpretation of this process as the oxidation mechanism may change with time depending on the conditions under which the metallic material is exposed.

2.2.1 Oxygen adsorption

The adsorption process is usually divided into physical and chemical adsorption. The main difference lies in the value of the bond force. In physisorption the enthalpy for the formation of a bond (van der Waals) is approximately 20 kJ/mol, whereas for chemisorption it is around 600kJ/mol [1]. Before oxygen from the ambient is chemically adsorbed on a metal surface it dissociates into atoms. Such an adsorbed gas can form different types of structures depending both on adsorbent and adsorbate, temperature, pressure etc. In the case of low oxygen content (e.g. in an $H_2 + H_2O$ *gas)* this layer can act as a barrier against chromium evaporation in the initial stage of oxidation, [1].

2.2.2 Oxide nucleation

When a metal surface saturated with adsorbed oxygen atoms is further exposed to oxygen gas, oxide nuclei are formed on the surface. This process is often preceded by the so-called incubation period. The nuclei can grow further forming a continuous thin film on the surface. Both the oxide nucleation and nuclei growth processes are temperature and pressure dependent. It is assumed that the growth of nuclei is governed by surface diffusion to the nuclei edges until a closed oxide layer is formed on the metal or alloy surface, Fig. 4, [1].

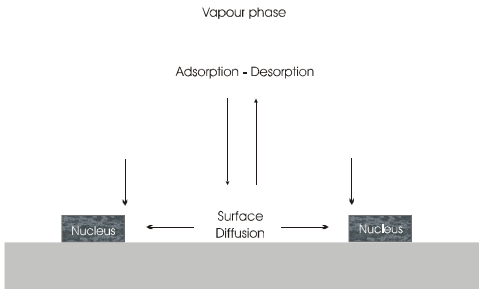

Fig. 4. *Schematic model for the nucleation and growth of oxide on a metal surface. The oxide nuclei grow laterally until the surface is covered with an oxide layer, [1]*

2.2.3 Growth of the oxide layer

The growth of oxide layer begins when the nuclei form a continuous film on the metal surface. Depending on the oxidation conditions and type of metal, the mechanism of oxide growth can differ

from case to case. At high temperatures most metals oxidize according to a power law type time dependency. The general law can be written:

$$\left(\frac{\Delta m}{q}\right)^n = k'' \cdot t + C \tag{6}$$

where Δm is mass gain,

q is surface area,

k'' is rate constant,

C is the integration constant,

n is the power exponent.

when n equals 1 the reaction is described by a linear rate equation

$$\frac{\Delta m}{q} = k_l\, t + C \tag{7}$$

with k_l the linear rate constant. This type of kinetics characterizes for instance the oxidation process where the reaction rate is determined by reactions at the scale/metal or scale/gas interfaces. Linear rate equations can also occur if the scales are porous due to macrodefects such that oxygen has continuous access to the metal/oxide interface. The oxidation rate does in such cases not depend on the scale thickness.

When n equals 2 the reaction is described by the parabolic rate equation

$$\left(\frac{\Delta m}{q}\right)^2 = k_p t + C \tag{8}$$

with k_p the parabolic rate constant and C the integration constant.

This type of time-dependence was described by Tammann as well as Pilling and Bedworth who observed that the oxidation rate is often inversely proportional to the scale thickness [34,35]. This type of rate equation prevails if the diffusion process of one or both reactants through the scale, is rate determining:

$$\frac{dx}{dt} = \frac{k_p'}{x} \tag{9}$$

where x is the scale thickness

Integrating equation (9) gives a time dependence of the form shown in equation (8)

3. Oxidation of chromium

The oxidation of pure chromium has been widely investigated, as it is one of the main alloying elements in steels and alloys used in high temperature applications such as power plants or solid oxide fuel cells.

3.1 Properties of Cr_2O_3

Cr_2O_3 is the only solid chromium oxide that is thermodynamically stable at high temperature. Cr_2O_3 has the corundum structure and can be grouped with oxides such as $\alpha - Al_2O_3$ or Fe_2O_3. This structure can be considered to consist of hexagonally close-packed oxygen atoms (ions) where the chromium atoms (cations) occupy two-thirds of the octahedral sites [1,13].

3.1.1 Nonstoichiometry and defect dependent properties

Although much research has been done, there is no unequivocal opinion of the chromia defect structure. It is often accepted that chromia at low-pO_2 gases behaves as an n-conductor and at high-pO_2 as a p-type conductor [1,12-14,36,37]. Measurements of Young and co. on bulk chromium oxide indicated that the oxide had a metal deficient defect structure [36]. Therefore it was assumed that during thermal oxidation of chromium, the oxide layer grew by diffusion of chromium vacancies. Kofstad and Lillerud concluded that at low oxygen partial pressures, chromium interstitials are predominant point defects in Cr_2O_3, Fig. 5, [13,14]. This means that Cr_2O_3 should behave as an n-type material at low oxygen partial pressures. It is important to note that the sintering procedure has a major influence on the electronic properties of the samples. All air-sintered samples show p-type behaviour. Samples sintered in an atmosphere with a low oxygen partial pressure (H_2/H_2O) are n-type [36]. These samples are n-type also in air below 850^oC. It is interpreted that the n-type behaviour in air at low temperatures for the compact Cr_2O_3 (sintered in an atmosphere with low oxygen partial pressure) is the result of “frozen in state”. The observed n-type behaviour of chromia confirms the interstitial cation model of Kofstad and Lillerud. These authors based their interstitial model on an overall consideration of many defect depending properities, (the sintering behaviour of Cr_2O_3 while additional evidence was obtained from oxidation experiments). The conductivity measurements by Matsui and Naito also suggest n-type behaviour at low oxygen partial pressures [37]. Their measurements were carried out on chromia powder sintered to 78% of the

theoretical density. The electrical conductivity measurements were carried out at different oxygen partial pressure, which were achieved by mixing Ar and O_2 or H_2 and CO_2. The authors found that the electrical conductivity decreases with increasing pO_2 in the range from 10^{-23} to 10^{-13} atm until the conductivity goes through a minimum, and then increases with increasing pO_2. At the minimum, the conduction changes from n-to p-type behaviour.

Data on self-diffusion of chromium and oxygen in Cr_2O_3 suggests that chromium self-diffusion goes through a minimum with decreasing oxygen activity and then increases rapidly as the Cr/Cr_2O_3 boundary is approached, Fig. 6, [1].

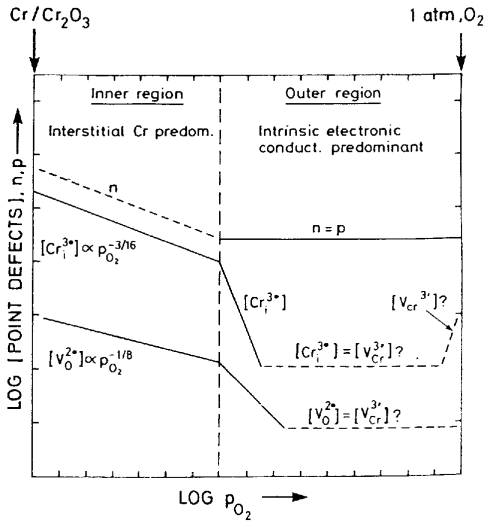

Fig. 5. *Possible defect structure model for Cr_2O_3, [12]*

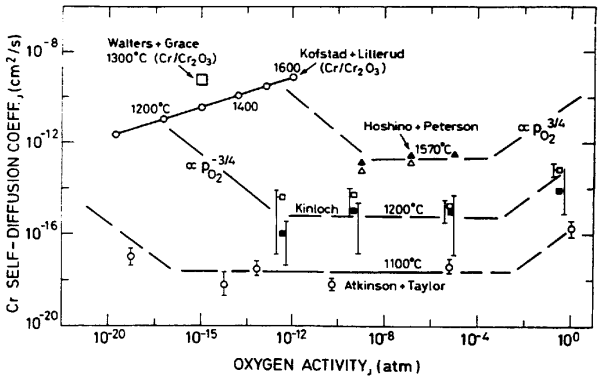

Fig. 6. *Chromium self-diffusion coefficient in Cr_2O_3 as a function of oxygen activity, [1].*

3.2 Oxidation of Cr in high pO_2

It is broadly accepted that the oxidation kinetics of chromium in oxygen or air above 700°C are generally interpreted as parabolic [1-3,12-14]. However reported results of k_p values vary by more than four orders of magnitude in the temperatures range 1000°-1400°C, Fig. 7, [13].

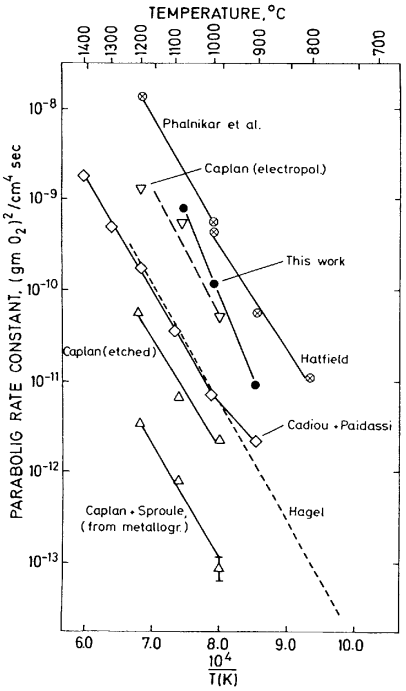

Fig. 7. *Summary of reported parabolic rate constants for oxidation of chromium in oxygen in the temperature range 700°-1400°C, [13]*

The important factor to explain the large discrepancies in oxidation rates is the purity of chromium used in the experiment. Even small amounts of contaminants such as carbon, sulphur or hydrogen may change the defect structure of the oxide and/or segregate at the metal/oxide interface [1,10,17,38]. Specimen preparation can play an important role as well. It was found that electropolished specimens oxidized more rapidly than samples which were etched; for etched chromium some orientations oxidized rapidly, while others oxidized much slower, Fig. 8, [10]. Another reason for the large difference is that at temperatures around 1000°C and higher, periodic increases in the reaction rate often occur, which can influence the k_p estimation, Fig. 9, [1,13,39].

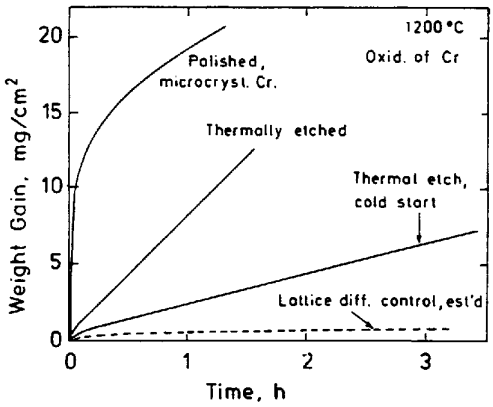

Fig. 8. *Influence of specimen pre-treatment on oxidation of chromium, [1]*

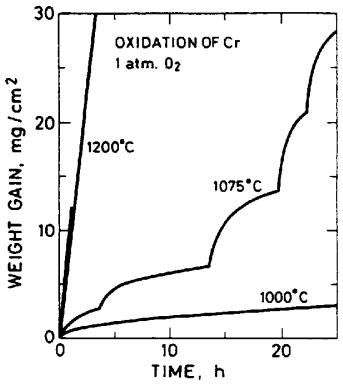

Fig. 9. *Repeated cracking of scales during isothermal oxidation of chromium leading to a sequence of protective stages in the overall oxidation process, [1]*

Scale morphology formed in oxygen or air is reported to be highly porous exhibiting nodule growth, blistering, wrinkling, and multilayered ballooning. The scale adherence is poor and even complete detachment of the oxide from the metal can occur after cooling. High compressive stresses occurring during oxidation are often suggested to be a reason for such characteristic buckles in oxide scale formation. Studies by Hultquist and Tveten showed, that the presence of hydrogen in chromium prior to oxidation affects kinetics and scale morphology [17,18]. After oxidation of hydrogen-free chromium in 20 mbar O_2, the oxide scale was adherent to the metal and there was no sign of wrinkling. In experiments using oxygen labelling the authors estimated the scale fraction of oxide growth taking place at the metal/oxide interface to exceed 25%. In contrast to this, upon oxidizing

hydrogen-containing chromium, the fraction of growth taking place at the metal/oxide interface was significantly less. The oxide scale was wrinkled and spalled off upon cooling to room temperature. Based on these findings, it was concluded that oxide growth at the metal/oxide interface was beneficial for the adherence of the oxide. Another significant effect of hydrogen content in the metal was an initially increased oxidation rate. The oxide growth at the oxide/gas surface was due to the transport of cations through the oxide scale and the oxide growth at the metal/oxide interface was due to transport of oxygen by some short-circuit mechanism, such as grain-boundary diffusion. Based on these findings, the authors suggested that hydrogen present in the metal could influence the defect structure of the scale. Hydrogen is probably being dissolved in the scale as interstitial protons $H^{\bullet}$ and the latter are compensated by defect electrons or metal vacancies. The proposed defect concentration as a function of the concentration of interstitial protons is shown in Fig. 10, [17]. At higher proton concentrations, the protons become dominant and are compensated by electrons and eventually by metal vacancies. This in turn enhances the metal transport. At the same time, the concentration of oxygen vacancies decreases and oxygen transport is slower.

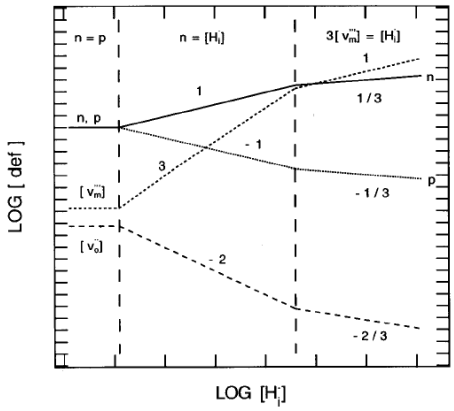

Fig. 10. *Schematic diagram of possible defect structure in Cr_2O_3 . The diagram illustrates the concentration of native defects as a function of the concentration of interstitial protons in the oxide at constant temperature and oxygen partial pressure. Numbers along lines denote the respective slopes, [17]*

3.3 Oxidation of Cr in low pO_2

There are only a few papers concerning chromium oxidation in low oxygen partial pressures. The study of Kofstad and Lillerud shows that the oxidation rate is higher in lower pO_2 gases than in high pO_2 gases. However, no obvious dependency of the oxidation rate on the pO_2 can be derived, Fig.

11, [13,14]. General features are that the scale was buckled and deformed with numerous cracks, always occurring in the inside of the layer. The authors suggested that the approximately linear kinetics is probably due to penetration of oxygen gas through the cracks before they are healed. It was also found that the oxide grew detached from the larger, plane surfaces of the specimens, however, as the oxygen pressure is further decreased the ability of the oxide to deform plastically becomes sufficiently large that the scale no longer cracks or breaks down. In such atmospheres chromium metal was observed on the inner surface of the oxide scale. This illustrated the importance of chromium vapour transport across the gap between the metal and the oxide scale. It was noted that the chromium crystals are located at one end (lower end) of the specimen. This feature, and the large amount of chromium crystals, suggests that there has been a vapour transport of chromium as a result of a temperature gradient along the specimen. The amount of chromium crystals is too large to be explained by the condensation and crystallization of the chromium metal vapour present in the cavity between the metal and the oxide scale during cooling of the specimen to room temperature when the oxidation run was discontinued. Other authors have shown that chromia scales formed in H_2-H_2O atmospheres can also be cracked and/or buckled but it usually occurs to a far less extent [24,29,40-50]. Quadakkers et al. studied the oxidation behaviour of pure Cr and a Cr-ODS alloy in air and in Ar-H_2-H_2O at 950°C, Fig. 12, [23]. Long time exposures showed that whereas in the low pO_2 gas stable oxide growth occurs, a slight weight loss was observed during air oxidation. Metallographic analyses revealed well adherent scale formation in reducing gases and indication of spalling was found in air. Similar to the study of Kofstad in low pO_2 gases, in some cases formation of chromium crystals on the inner surface of the oxide was observed [23]. On top of the oxide surface, a number of whiskers and blades are reported and are usually well adherent to the metal.

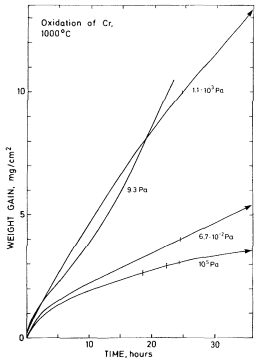

Fig. 11. *Oxidation of chromium at 1075°C at different oxygen partial pressures, [13]*

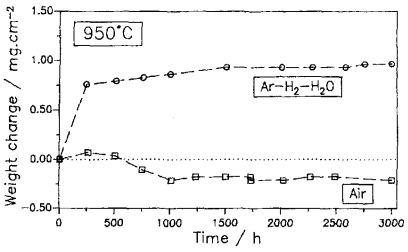

Fig. 12. *Weight change during long time oxidation of Cr5Fe1Y_2O_3 at 950°C in air and Ar-4%H_2-2%H_2O, [23]*

The study of Polman et al. also showed that oxidation rates of chromium are faster in H_2-H_2O or CO-CO_2 gas mixtures than in O_2, Fig. 13, [41]. The experiments were carried out at 900°C. Characteristic whisker type morphology on top of the oxide surface and a better adhering oxide scale in low pO_2 gases was reported. The authors explained formation of whiskers on chromium in a similar way as proposed by Raynaud and Rapp for NiO in moist oxygen, [42]. According to them, whiskers grow by surface diffusion of cations along a tunnel centred around the core of a screw dislocation. Surface diffusion D_s is very fast and the dissociation of the molecular oxidant is the rate-limiting step for whiskers grown in high pO_2 gases, Fig. 14. Unfortunately there are no experimental data for the activation energy of the chemisorption or dissociation of O_2, H_2O and CO_2 on chromium.

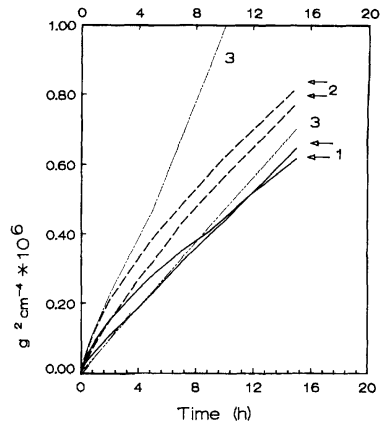

Fig. 13. *Oxidation of chromium at 900°C, 1) O_2, 2) 1.5%H_2O-H_2, 3) 1%CO-CO_2, [41]*

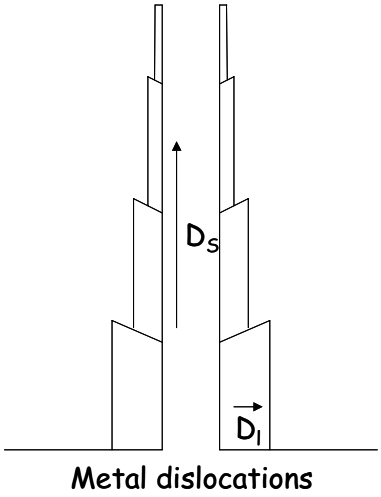

Fig. 14. *Proposed model for whisker formation. D_s is surface diffusion in the tunnel, and D_l the lattice diffusion, [41]*

In analysing the behaviour of chromium in low-pO_2 gases, the way of establishing the oxygen pressure of the gas is essential. Mixing hydrogen with water vapour or carbon monoxide with carbon dioxide in different ratio generates a low-pO_2 and very often such mixtures are used. However, the presence of hydrogen and/or water vapour in the first case and carbon in the second might have an important impact on the oxidation behaviour of chromium in such gases [3]. Hydrogen causes in appropriate conditions decarburisation of alloys, and, dissolution in the metallic phase. It causes as a rule, negative changes in the physical properties of the metallic materials. It is also considered that hydrogen exhibits a detrimental influence on the oxide scale growth. The H_2 is formed on the scale surface in the reaction (10):

$$Me + H_2O = MeO + H_2 \tag{10}$$

Atomic hydrogen dissolves immediately in the scale and can diffuse to the metallic core, the effect of this phenomena is the catalytic action of this gas in the process of formation of the reaction product in the metal consumption zone [3]. Hulquist measured the hydrogen concentration in the chromium core before and after oxidation in water vapour at 900^{o}C. The uptake of hydrogen was found to correspond to 1.5 wt. ppm. after 1600 min and 7 wt. ppm. after 220h [18]. It was also found out that chromium samples, which contained hydrogen in the metal core prior to oxidation, oxidized faster, than hydrogen-free samples.

3.4 Oxidation mechanism of Cr in H_2O-containing gases

In previous chapters it was shown that differences in oxidation rate and scale morphology exist when pure chromium was exposed to high and low-pO_2 gases. Since high pO_2 gases were composed of molecular oxygen and low pO_2 gases frequently of H_2-H_2O mixtures, the question arises whether these differences are related to the absolute value of the oxygen partial pressure or the presence of water vapour. Thus, a study of the oxidation behaviour of chromium in mixed O_2-H_2O is very important. To describe the prevailing oxidation mechanisms few authors investigated the oxidation of chromium in molecular oxygen containing addition of water vapour, [18,40,43]. Tveten et al. oxidized pure chromium with different hydrogen contents in oxygen and oxygen containing water vapour. They recorded a higher oxygen consumption when chromium was exposed to wet oxygen, Fig. 15, [18].

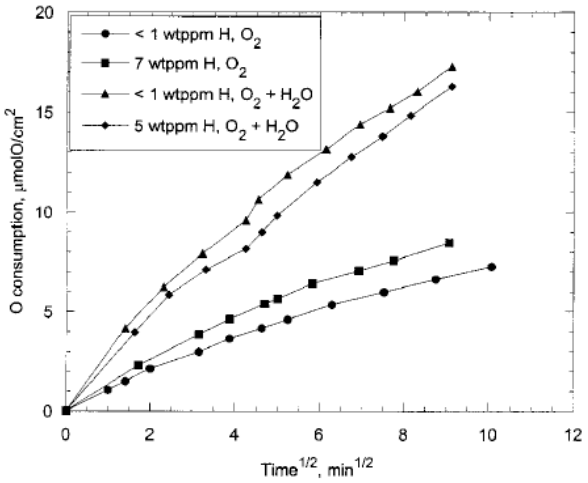

Fig. 15. *Oxygen consumption in exposure of Alfa Cr with <1 wt. ppm H at 900°C in 20 mbar O_2 and in 10 mbar H_2O - 10 mbar O_2, [18]*

The authors also carried out 1 stage oxidation in labelled mixed O_2-H_2O gas, (10mbar $^{16}O_2$ and 10mbar $H_2{}^{18}O$) gas. Interesting to note is that in such an atmosphere no H_2 is relieved until all O_2 is consumed, equations (11-14) and Fig. 16, [18]. The authors suggested that surface reactions at the oxide/gas interface could play an important role in the oxidation process.

$$2Cr + 3H_2{}^{18}O = Cr_2{}^{18}O_3 + 6H \tag{11}$$

$$6H + 3/2\,{}^{16}O_2 = 3H_2{}^{16}O \tag{12}$$

$$2Cr + 3H_2{}^{16}O = Cr_2{}^{16}O_3 + 6H \tag{13}$$

$$6H + 3/2{}^{16}O_2 = 3H_2{}^{16}O \tag{14}$$

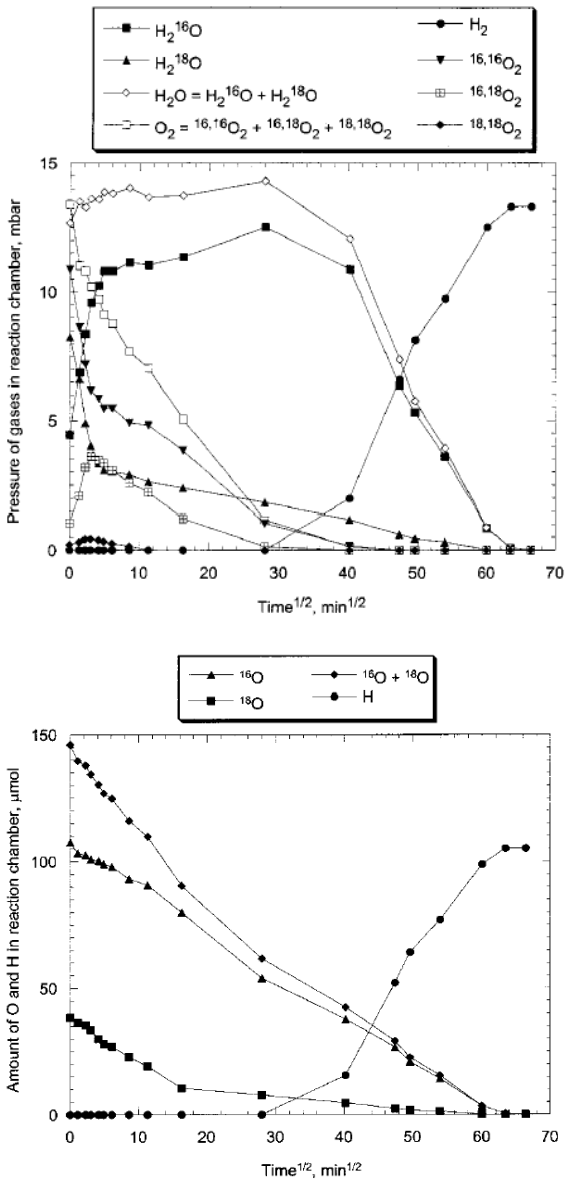

Fig. 16. *Oxidation of Alfa Cr with <1 wt. ppm H at 900°C in 10 mbar $^{16}O_2$ -10 mbar $H_2{}^{18}O$. Mass-spectrometer data versus square root of time. Data of amounts in the lower graph are calculated from the measured partial pressures in the upper graph, [18]*

3.5 Volatile species in the Cr-O system

Chromium exposed to high temperatures forms volatile species. This process is strongly dependent on the oxygen partial pressure in the system [2]. At high oxygen pressures such as dry air the main volatile species is CrO_3(g). It evaporates from Cr_2O_3 in oxygen atmospheres:

$$\frac{1}{2}Cr_2O_3 + \frac{3}{4}O_2 = CrO_3(g) \tag{15}$$

The reaction of Cr_2O_3 with O_2 to form a gaseous species affects the oxidation kinetics of alloys which form protective Cr_2O_3 scales. Gravimetric measurements show negative departures from parabolic kinetics, which may result in linear steady-state weight loss kinetics [10]. A study by Kofstad revealed that the linear rates of weight loss at 1atm O_2 were equal $2.2 \cdot 10^{-2}\ mg/cm^2 hr$ at 1100°C, $6.7 \cdot 10^{-3}\ mg/cm^2\ hr$ at 990°C, and $2.1 \cdot 10^{-3}\ mg/cm^2$ at 900°C [13]. The partial pressure of volatile CrO_3(g) formed can be calculated quantitatively, [10]. The pO_2 dependence can be easily determined from equation (15). According to the mass action law for the reaction, the partial pressure of CrO_3(g) in equilibrium with Cr_2O_3 is given by:

$$p_{CrO_3} = K_{eq}^{1/2} p_{O_2}^{3/4} \tag{16}$$

where and p_{CrO_3} and p_{O_2} are the equilibrium partial pressures of CrO_3(g) and O_2, respectively and K_{eq} is the equilibrium constant for reaction (15). Belton and Kim obtained an expression for K_{eq} of reaction (15), [44]. It is given as,

$$\log K_{eq} = \frac{-2.46x10^4}{T} + 6.16 \tag{17}$$

The Kellog-type diagram describes the dependencies on O_2 activity of the equilibrium partial pressures of the predominant vapour species, Fig. 17, [2]. It is clearly seen that in high pO_2 gases CrO_3(g) is the dominant and Cr(g) becomes more important at low pO_2 gases. It is important to note that the absolute values of gaseous partial pressures predicted thermodynamically can differ depending on data taken and hence discrepancies can be found in various reports [45-49].

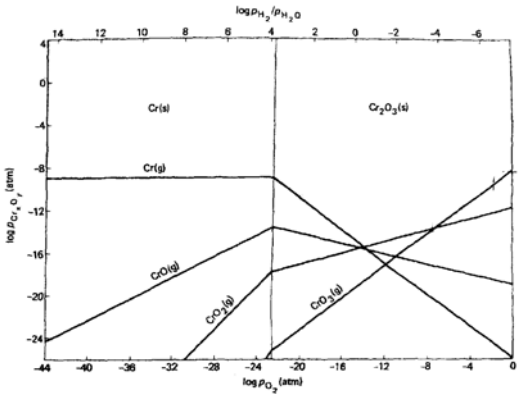

Fig. 17. *Cr-O system volatile species at 1250K, [2]*

It has been known for some time that the evaporation rate increases when water vapour is present in the reaction gas [9,43,50]. The study by Caplan and Cohen indicated that the weight loss of Cr_2O_3 exposed to high pO_2 gases containing water vapour was higher, [9]. Authors suggested that moisture increases the evaporation rate and hence a higher mass loss of chromium is observed.

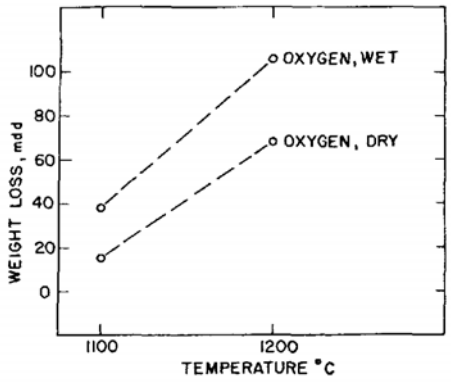

Fig. 18. *Weight loss of Cr_2O_3 in wet and dry oxygen at 1000^o and 1200^{o}C, [9]*

The study by Hänsel revealed that adding water vapour to air increases the evaporation rates [50]. A number of TG tests were carried out under the gas flow conditions used in all TG experiments. For this purpose two types of specimens were used, i.e. dense, hot isostatically pressed chromia and specimens of a chromium based oxide dispersion strengthened (Cr-ODS) alloy. The latter material is known to form excellent adhering, dense chromia scales, which exhibit substantially lower growth

rates than non-dispersed pure chromium. For this reason, the ODS alloy allows the estimation of the increase in vaporisation rates in the presence of water vapour by comparing the oxidation kinetics in dry and wet environments. Details of the experimental methods used are described elsewhere [50]. Evaporation rates measured in dry and wet high pO_2 environments under the experimental conditions prevailing in the TG tests used in the present study are shown in Fig. 19. It is seen that water vapour enhances the evaporation rates, i.e. evaporation increases with increasing water vapour addition. The slight differences in evaporation rates measured for different materials could be attributed to differences in oxide scale roughness and microporosity.

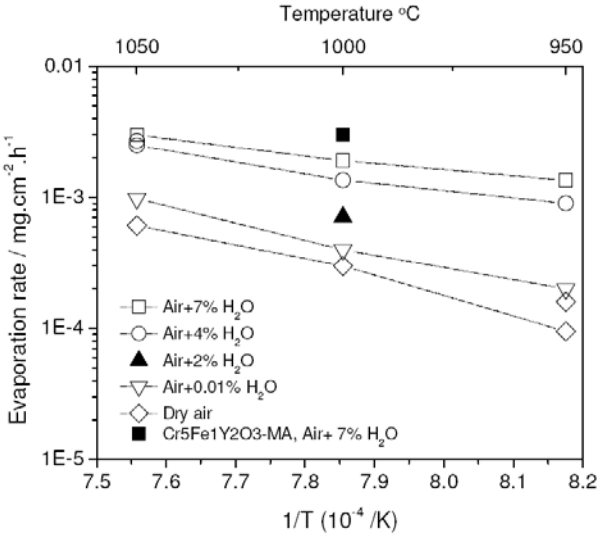

Fig. 19. *Evaporation rates under the flow condition used in the prevailing TG-tests, measured for compact, sintered chromia and a Cr-ODS alloy, [50]*

Recent studies of several authors indicated that the formation of $CrO_2(OH)_2$ can be possible when the reacting gas contains water vapour [51-56]. Yamauchi et al. investigated the effect of H_2O on the deterioration of a Cr_2O_3 scale in N_2-O_2-H_2O atmospheres [43]. The rate of mass loss in N_2-2.4%O_2-19.7%H_2O atmospheres was found to be one order of magnitude higher than the rates in N_2-O_2 and N_2-H_2O. More oxygen additions to fixed N_2-H_2O atmospheres resulted in higher evaporation rates. Formation of $CrO_2(OH)_2$ gaseous species was suggested to be the main volatile species. Hilpert investigated the formation of volatile species including $CrO_2(OH)_2$ by thermochemical modelling, Fig. 20, [55]. It appeared that the formation of $CrO_2(OH)_2$ increases with increasing water vapour content in the gas. The recent work of Opila allows a more exact estimation of the volatile

$CrO_2(OH)_2$ formation [56]. The equilibrium for the reaction (18) for which the constant K equals (19) is described by (20), [56].

$$\frac{1}{2}Cr_2O_3 + \frac{3}{4}O_2 + H_2O = CrO_2(OH)_2 \tag{18}$$

$$K = \frac{p_{CrO_2(OH)_2}}{p_{O_2}^{3/4} p_{H_2O}} = \exp\left(\frac{-\Delta G^o}{RT}\right) \tag{19}$$

$$\Delta G^o = 53{,}500 + 45.5T \ \text{(J)} \tag{20}$$

Comparing values of $pCrO_2(OH)_2$ for both studies, some difference can be seen, an example is given in Tab.1. The source of thermodynamic data taken for the calculations seems to be very important and further investigations are needed to enlighten the mutual effect of water vapour and oxygen on the formation of $CrO_2(OH)_2$.

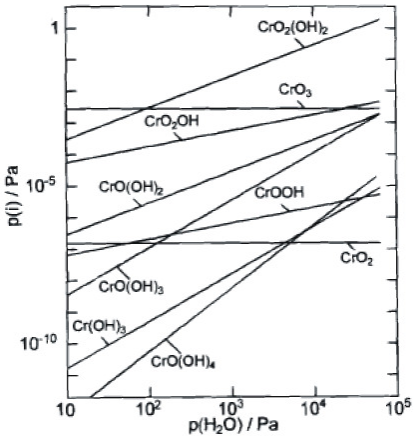

Fig. 20. *Calculated partial pressures over Cr_2O_3 at 1223 K in humid air, pO_2=2.13x10^{4}Pa with different H_2O partial pressures, [55]*

Table 1. *Comparison of $pCrO_2(OH)_2$ over Cr_2O_3 at 1223 K in 200mbar O_2 – 100mbar H_2O derived from studies of Hilpert and Opila [55,56]*

Author	Hilpert	Opila
$pCrO_2(OH)_2$	5x10^{-6}atm	7x10^{-7}atm

4. Oxidation of Cr in multicomponent gas mixtures

Oxidation of chromium becomes more complex when more than one oxidant is present in the reacting gas. It is because the chemical reaction between chromium and gas mixture components is determined by a series of factors among which the most important include compactness of the scale and its permeability for the atmospheric components, the rate of formation of individual compounds and properties of the reaction products [1-3].

4.1. Phase stability diagram for Cr-O-N and Cr-O-C

Fig. 21 a) and b) show the phase stability diagrams for the Cr-O-N and Cr-O-C systems respectively. It is commonly considered that they can only be formed when the chromia scale is permeable to carbon or/and nitrogen containing gas species [29,31]. This in turn may be a very important factor in understanding the oxidation mechanisms of chromium in different types of environment.

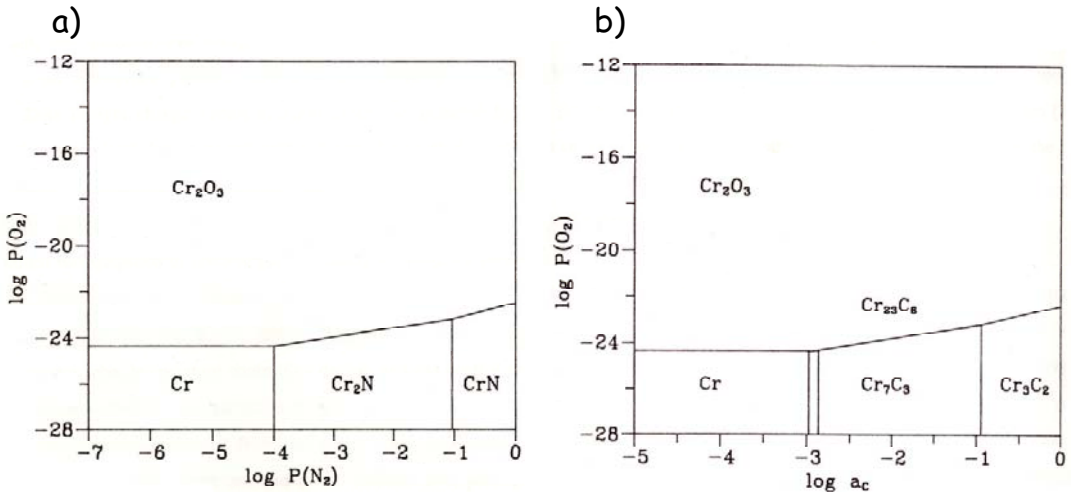

Fig. 21. *a) Phase stability diagram Cr-O-N at 900°C and b) phase stability diagram Cr-O-C at 900°C, [30]*

4.2 Oxidation in Air and N_2-O_2 gas mixtures

The often-investigated example of a multicomponent gas system is air, [57-62]. During oxidation of chromium in air, the inner scale layer usually contains the nitride Cr_2N and the outer layer consists of Cr_2O_3, [59]. It is observed that the outer scale is porous, which is considered to be the reason for nitrogen penetration towards the metal/scale interface. Since nitrogen has a lower chemical affinity to chromium than oxygen, it only reacts with chromium at the scale/metal interface, and as a result the inner scale layer is composed mainly of chromium nitride.

Hagel studied the behaviour of chromium in oxygen, air and nitrogen in the temperature range between 650^o and 1350^{o}C, Fig. 22, [58]. It was found that the reaction rate increases with nitrogen present in the gas. Wilms and Rea studied chromium oxidation in air at 950^{o}C [59]. They observed a substantial variation in the thickness of nitride layers including the complete absence in certain areas of the specimen. After oxidation the authors carried out chemical analysis on the specimens in order to find out whether or not nitrogen contaminated the metal. It was found out that nitrogen had penetrated chromium to a depth of approximately 6.3mm, Fig. 23.

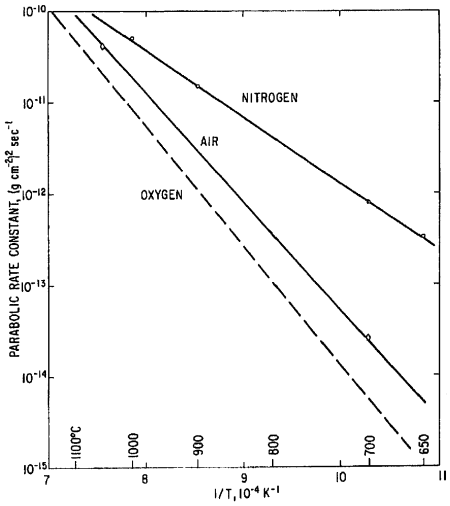

Fig. 22. *Parabolic rate constants for exposure of chromium to oxygen, nitrogen and air at 0.1 atm, [58]*

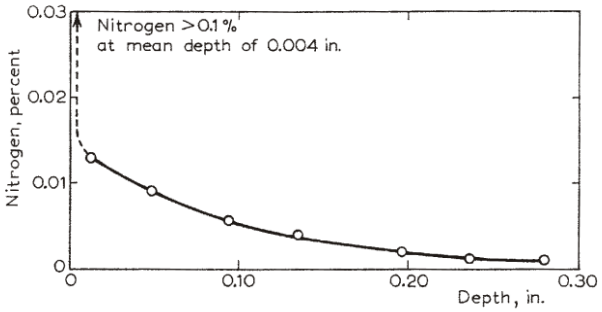

Fig. 23. *Penetration of nitrogen in chromium after heating in air at 950°C for 200h, [59]*

4.3 Oxidation in N_2-CO-CO_2 gas mixtures

Zheng and Young investigated the oxidation behaviour of chromium in multicomponent environments with relatively low oxygen activities [29-31]. Isothermal oxidation of chromium in N_2-CO-CO_2 leads to a formation of three layers. The outer layer was pure Cr_2O_3, the intermediate layers consisted of a mixture of Cr_7C_3, chromia and a small amount of Cr_2N, Fig. 24. The inner layer was pure, compact Cr_2N. The formation of carbide and nitride beneath the chromia clearly indicates that carbon- and nitride-containing species penetrate the Cr_2O_3 grown in this gas. The sequence of reaction products is in accordance with local equilibrium. Thus at the surface, where the chromium activity is lowest, the most stable product, oxide, is formed. At the scale/metal interface, where the chromium activity is highest and oxygen activity lowest, the least stable product, nitride, forms. The intermediate stability phase Cr_7C_3 is formed in the centre of the scale.

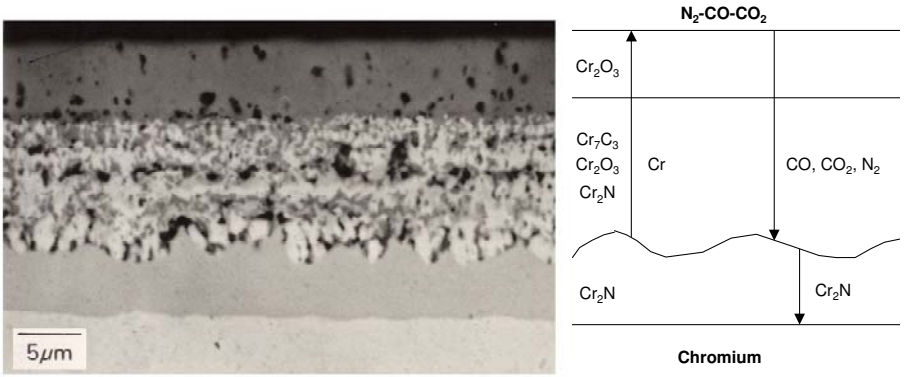

Fig. 24. *SEM micrograph of the scale formed on chromium after 22h reaction in N_2-62%CO-2%CO_2 at 900°C and schematic representation of the scaling process, [29]*

The continued growth of carbide and nitride beneath the oxide shows that the secondary oxidants continue to penetrate the Cr_2O_3 throughout the reaction. Thus the chromia scale is not an effective barrier to nitridation/carburization. Since the carbon solubility in chromia is negligible and it seems likely that the same would be true for nitrogen, atomic diffusion through the oxide scale can be excluded and molecular transport via scale imperfections might be indicated. Penetration into the chromia scale probably occurs via scale imperfection such as pores, voids or grain boundaries.

4.4 Oxidation in N_2-H_2-H_2O gas mixtures

An interesting finding is that a chromia scale grown in low pO_2, N_2-H_2-H_2O mixtures is composed of only Cr_2O_3 with no underlying Cr_2N, Fig. 25, [29,30]. It is interesting to note that the scale formed in such conditions consists of a substantial amount of long whiskers and blades. Comparison of the chromia morphology formed in N_2-H_2-H_2O and in air revealed physical differences and apparently the scale formed in low pO_2 gases is able to hamper the ability of N_2 to penetrate the scale or at least delay this, since after 72h of oxidation hardly any nitrides were found. Another possibility could be that H_2O is preferentially adsorbed on the internal oxide surfaces, preventing N access.

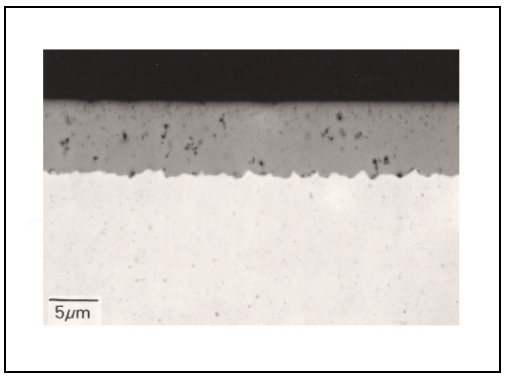

Fig. 25. *SEM micrograph of the scale formed on chromium after 22h reaction in N_2-57%H_2-2%H_2O at 900°C, [29]*

5. Aim of present investigation

The oxidation behaviour of pure Cr at high temperature has been studied extensively for a few decades. These studies have necessitated from both scientific understanding of observed physical phenomena and from constantly growing technological importance of corrosion resistant materials based on formation of chromia scale.

Up to now oxidation behaviour of chromium was studied mostly in high pO_2 gases such as air or Ar-O_2 mixtures and only a few researches were carried out in wet or/and low pO_2 gas mixtures. Little is known about the effect of water vapour on the oxidation mechanism and among results reported there are substantial scatter. Although chromia forming alloys are used not only in high-pO_2 gases such as air or combustion gases but also in H_2-H_2O based gases prevailing e.g. in chemical processes, gasification environment or fuel cells up to day the way of mass transport through the chromium oxide and the effect on oxide scale properties in different type of environment has not been completely clarified.

This work is meant to provide comprehensive analysis of oxidation behaviour of chromium at high temperature in different oxygen partial pressures using chromium of different purity. The main aim of the work was to understand effect of water vapour on adherence, volatilization and mass transport through the oxide scale. Another aspect of the study was to determine the effect of contamination, especially of carbon, on oxidation behaviour in different test environments.

Experimental

6. Experimental description

6.1 Materials characterization

The ultra high pure chromium and ODS alloy studied were supplied by Plansee (Reutte, Austria), batch JUG, DUR and DDB, Table 2 and 3. Goodfellow supplied commercial chromium, KER.

Table 2. *Compositions of the materials used in experiments.*

		Mass %					
Alloy	Batch	Cr	Fe	Al	Y	Ti	Ni
Cr (5N)	JUG	99.99	-	-	-	-	-
Cr (5N)	DUR	99.99	-	-	-	-	-
Cr (commercial)	KER	99.1	-	-	-	-	-
Cr5Fe1.0Y_2O_3-MA	DDB	95.1	5.4	-	0.76	-	0.15

Table 3. *Trace contamination of the materials used in experiments.*

	Mass %			
Batch	C	S	O	N
JUG	0.007	<0.001	0.0032	0.0018
DUR	<0.001	<0.001	0.002	0.0005
KER	<0.012	<0.023	0.360	0.011
DDB	0.005	0.001	0.4262	0.0285

6.2 Specimen preparation

From the prevailing materials, samples with 20x10x2 mm dimensions were machined. For the oxidation studies the specimens were ground to 1200 grit surface and ultrasonically cleaned in ethanol immediately before use. Only a few samples were ground to 240 grit and a few were polished to $1\mu m$ surface finish using diamond paste. This was performed to examine whether or not surface preparation has an influence on the oxidation behaviour.

6.3 Experimental setup

Thermogravimetric measurements for up to 72 hours exposure in the temperature range of 950^{o} to 1050ºC were carried out using a Setaram Thermobalance TG92, Fig. 26 and a few experiments at 950^{o}C were carried out in a Thermobalance Cahn D200, Fig. 27. The sets were similar, the main difference between the apparatus was that in the Thermobalance Cahn D200, the sample was placed in a silica reactor and then lifted into the furnace reaction zone. In the Setaram Thermobalance, the furnace was always at one position and it was the sample which was inserted into the hot zone. In both cases the samples were suspended on an alumina hook and gravimetric data were recorded continuously during each single experiment including the cooling of the sample after the isothermal exposure. This procedure allowed not only measurement of the oxidation rate but also of any oxide scale spallation. The TG-results were corrected to account for buoyancy effects, using data measured for samples of the same geometry as the specimens used in the oxidation experiments, Fig. 28. For this purpose a chromium based oxide dispersion strengthened (ODS) alloy was used. The material is known to form excellently adhering, dense chromia scales, which exhibit substantially lower growth rates than the pure chromium used in the present study [23,24]. The oxidation time was always counted from the moment at which the sample was placed inside the hot zone. Approximately 30 min was needed for the sample to reach the reaction temperature.

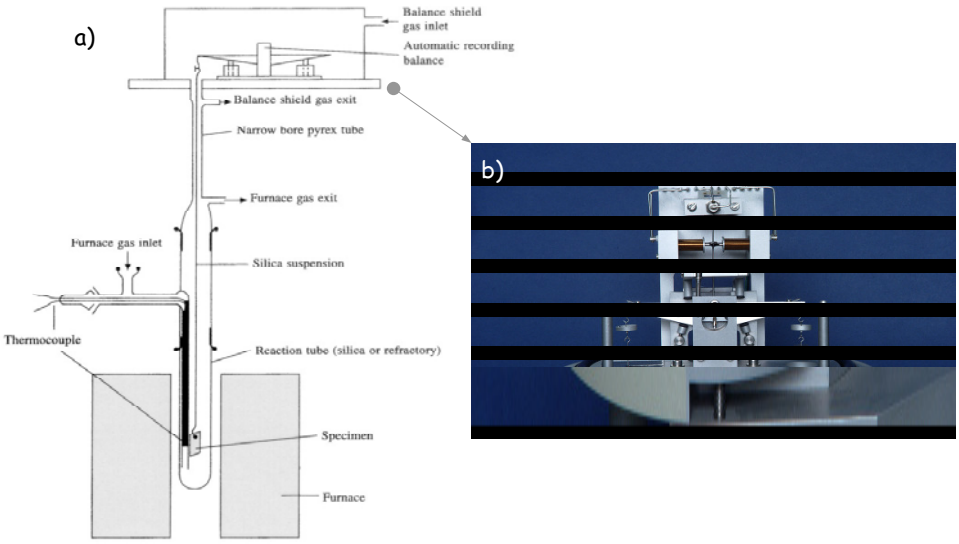

Fig. 26. *a) Schematic of the Setaram Thermobalance TG92 equipment used for investigation, b) photograph of the balance head*

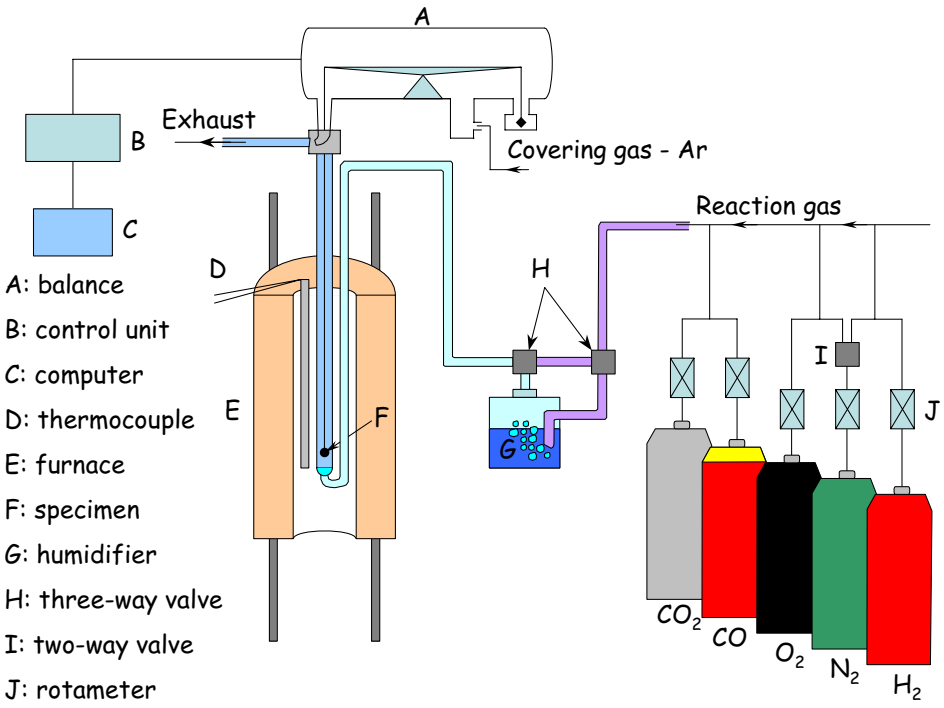

Fig. 27. *Schematic of the TG Cahn D200 equipment used for investigation*

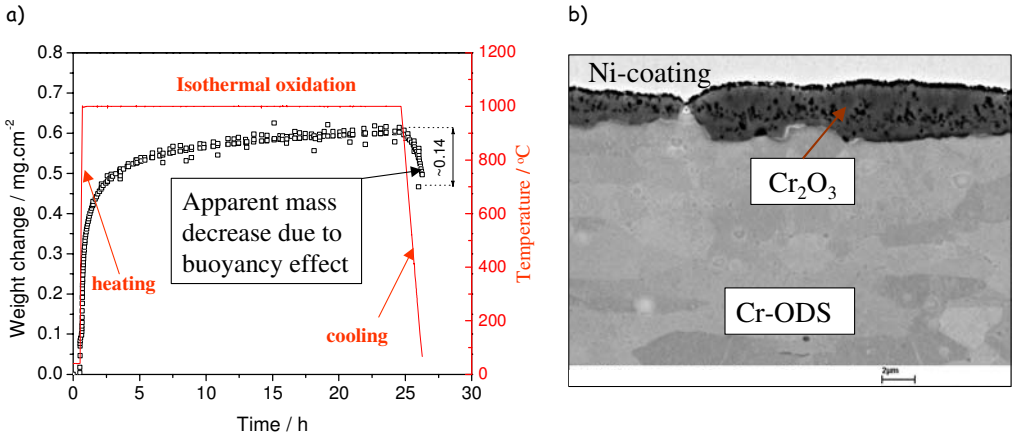

Fig. 28. *Isothermal oxidation of Cr5Fe1Y$_2$O$_3$ in Ar-4%H$_2$-7%H$_2$O at 1000°C, a) recorded weight change, b) SEM cross-section photograph of the oxide scale*

6.4 Conditions of reacting gases

Individual samples were oxidized in the temperature range of 950° and 1050°C in flowing gas mixtures with varying water vapour contents. The water vapour content was established by bubbling Ar, N_2 or Ar-H_2 mixtures of ultra-high purity through deionised water or LiCl solution at controlled temperatures. The total gas flow rates for the Setaram Thermobalance were 2 l/hr, corresponding to linear flows in the tubular reactor of 0.77 cm/sec, at a total pressure of 1 bar and 0.71 cm/s for Thermobalance Cahn D200. The compositions of the gases used are given in Table 4 and 5 and schematically illustrated in Fig. 29. Oxidation tests were carried out in high and low oxygen pressures and some in the mixtures of molecular oxygen and water vapour. Therefore, the partial pressures of the most dominant volatile species that could be formed are also listed in the tables [56, 63].

Table 4. *Gas compositions with respective equilibrium oxygen partial pressures at 1000°C, left part of Table, [63]. The volatile species at highest pressure in equilibrium with Cr_2O_3(s), right part of Table, [56,63]*

Gas no.	Starting gas composition [vol. %]				Equilibrium oxygen partial pressure, [atm]	Partial pressures of volatile species [atm]		
	Ar	O_2	H_2O	H_2	pO_2	$pCrO_2(OH)_2$	$pCrO_3$	pCr
1	99.99	0.01			1×10^{-4}		1.9×10^{-11}	
2	99.9	0.1			1×10^{-3}		6.1×10^{-11}	
3	99	1			1×10^{-2}		3.4×10^{-10}	
4	80	20			2×10^{-1}		3.3×10^{-9}	
5	98.9	0.1	1		1×10^{-3}	1.5×10^{-9}		
6	97.9	0.1	2		1×10^{-3}	3.0×10^{-9}		
7	92.9	0.1	7		1×10^{-3}	1.1×10^{-8}		
9	92	1	7		1×10^{-2}	5.9×10^{-8}		
10	89	1	10		1×10^{-2}	8.5×10^{-8}		
11	73	20	7		2×10^{-1}	5.6×10^{-7}		
12	93		7		1.4×10^{-6}	7.8×10^{-11}		
13	92.99		7	0.01	1.4×10^{-9}	4.2×10^{-13}		
14	92.9		7	0.1	1.4×10^{-11}	1.3×10^{-14}		
15	92		7	1	1.4×10^{-13}	4.2×10^{-16}		
16	89		7	4	8.5×10^{-15}			2.0×10^{-15}
17	94		2	4	6.9×10^{-16}			1.3×10^{-14}
18	67		30	3	3×10^{-13}	3.3×10^{-15}		

Table 5. *Gas compositions with respective equilibrium oxygen partial pressures and carbon activities at 950°C, left part of Table, [63]. The volatile species at highest pressure in equilibrium with Cr_2O_3(s), right part of Table, [56,63]*

Gas no.	Starting gas composition [vol. %]						Equilibrium oxygen partial pressure, [atm]	Carbon activity	Partial pressures of volatile species [atm]		
	N_2	O_2	H_2O	H_2	CO	CO_2	pO_2	a_c	$pCrO_2(OH)_2$	$pCrO_3$	pCr
1	99	1					0.01			$1.3x10^{-10}$	
2	98.5	1	0.5				0.01		3.5×10^{-9}		
3	98	1	1				0.01		6.9×10^{-9}		
4	97	1	2				0.01		1.4×10^{-8}		
5	96	1	3				0.01		2.1×10^{-8}		
6	94	1	5				0.01		3.5×10^{-8}		
7	92	1	7				0.01		4.8×10^{-8}		
8	89	1	10				0.01		6.9×10^{-8}		
9	70	20	10				0.2		6.5×10^{-7}		
10	50	40	10				0.4		1.1×10^{-6}		
11	78	20	2				0.2		1.3×10^{-7}		
12	99		1				1.4×10^{-7}		1.6×10^{-12}		
13	95		5				4.8×10^{-7}		2.0×10^{-11}		
14	92		4	4			4.6×10^{-16}				5.1×10^{-16}
15	88		2	10			1.6×10^{-17}				5.7×10^{-15}
16					100		1.7×10^{-19}	1.00			1.8×10^{-13}
17					98	2	3.6×10^{-19}	0.72			1.3×10^{-13}
18			1		97	2	8.0×10^{-19}	0.46			5.4×10^{-14}

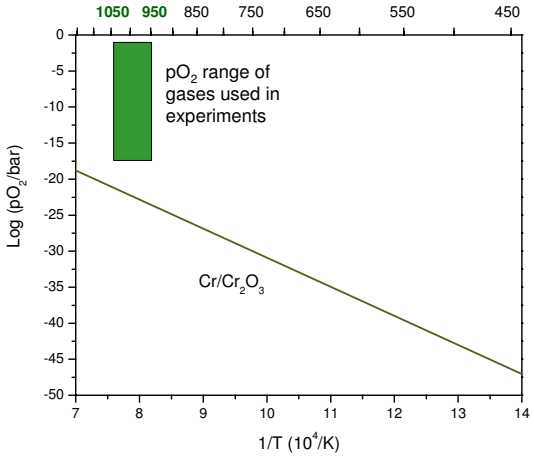

Fig. 29. *Range of pO_2 for test atmospheres compared with dissociation pressure of Cr_2O_3 as function of temperature, [63]*

6.5 Methods used for post oxidation analysis

The oxidized samples were cross-sectioned and prepared using the conventional metallographic route i.e., grinding, polishing and fine polishing or by fracturing the samples. In the latter case, it was possible to access the metal/oxide interface directly and also the oxide grain structure. Analysis of scale composition and morphologies was carried out using X-ray diffraction, optical metallography and field emission scanning electron microscopy (FESEM) as well as TEM coupled with FIB.

Some samples were chosen for examination using Sputtered Neutrals Mass Spectroscopy. In such cases samples were oxidized in atmospheres contained labelled oxygen, e.g. one stage oxidation in Ar-$^{16}O_2$-$H_2{}^{18}O$ or two-stage oxidation which first stage was carried out in Ar-$H_2{}^{16}O_2$ and second in Ar-$H_2{}^{18}O_2$ or Ar-H_2-$H_2{}^{16}O$ / Ar-H_2-$H_2{}^{18}O$. The ^{18}O enrichment in Ar-O_2 gases was 20% and in Ar-H_2O it was 50%. Immediately after oxidation the formed scales were analysed by SNMS to determine ion intensities which after quantification allowed to obtain depth profiles of measured isotopes. The quantification method was described in detail elsewhere, [64-66]. The quantification of the data was carried out for the major element, i.e. Cr, ^{16}O and ^{18}O. The data for trace elements were treated only in qualitative way because no accurate sensitivity factors were available. As the amount of these elements in the alloy and scale were only tenth of percentage they did not significantly affect the quantification of the elements profile.

Because the ^{18}O enrichment in the gas was 20% and 50% respectively the concentrations were recalculated to data which would have been obtained if a gas with 100% ^{18}O enrichment had been used. For example in the case of 50% enrichment, the double ^{18}O concentration was subtracted from ^{16}O values and the ^{18}O concentrations were multiplied by factor of 2. An analogous procedure was used in case of 20% enrichment.

7. Study of oxidation behaviour of high purity chromium, batch JUG

7.1 Oxidation in Ar-O_2 gas mixtures

Pure chromium, batch JUG, was exposed to various dry Ar-O_2 atmospheres, (Ar-0.01%O_2, Ar-0.1%O_2 and Ar-1%O_2) for 72h at 1000^{o}C, Fig. 30. It was observed that lowering the oxygen partial pressure in such gas mixtures affects both oxidation rate and scale adherence. Chromium exposed to relatively high oxygen pressure i.e. Ar-1%O_2 oxidized the fastest and oxide scale spalled off completely after cooling to room temperature. Samples oxidized in oxygen-reduced atmospheres i.e. Ar-0.1%O_2 and especially Ar-0.01%O_2 adhered better to the metal and the oxidation rate was substantially lower. In the latter atmosphere the supply of oxygen from the gas could be the reaction limiting step, however considering gas compositions and oxidation conditions it comes out that *4* $mg \cdot cm^{-2}$ of oxygen was supplied during the process and it was enough to form a scale as thick as was formed in the Ar-1%O_2. Therefore it is believed that oxygen supply from the gas could be the rate-limiting step only in the early stages of oxidation. Morphologies of latter scales are shown in Fig. 31. The oxide scale formed in Ar-0.01%O_2 was dense and minor pores were randomly distributed in the bulk oxide. The scale formed in Ar-0.1%O_2 seems also to be dense but contrary to Ar-0.01%O_2 extensive porosity was formed at the metal/oxide scale. Apparently by increasing the oxygen partial pressure, formation of the interfacial voidage became more severe and this in turn led to oxide spallation during cooling to room temperature as occurred in Ar-1%O_2.

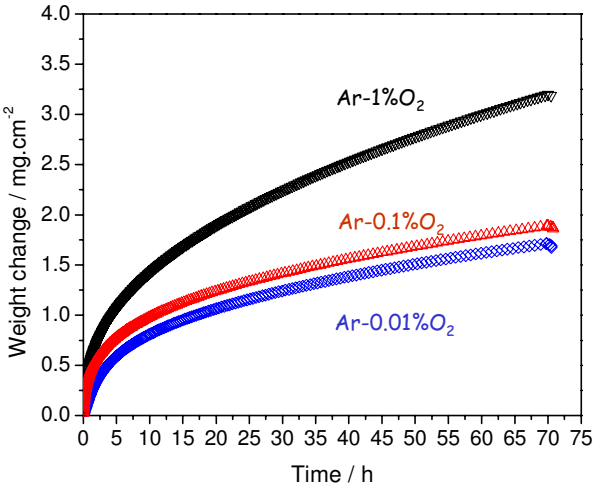

Fig. 30. *Weight change during isothermal oxidation of chromium, batch JUG in various, Ar-O_2 atmospheres at 1000^{o}C*

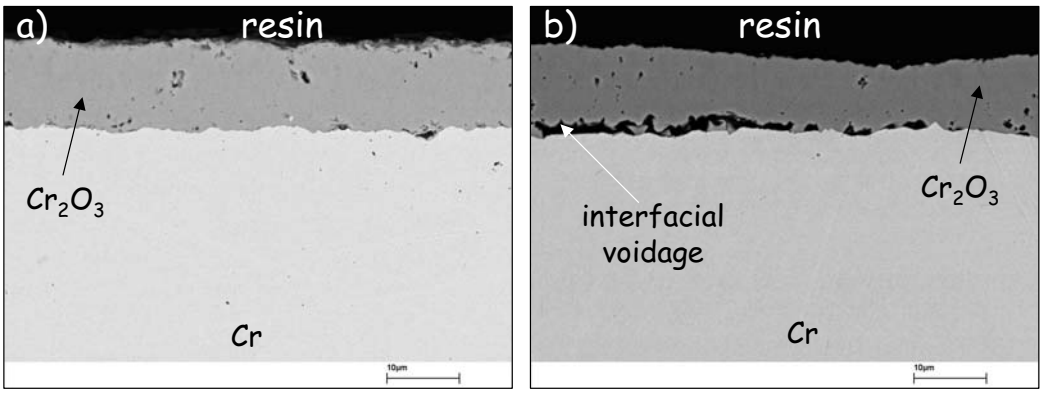

Fig. 31. *SEM polished cross-sections of oxide scales formed on chromium, batch JUG at 1000°C after 72h oxidation in a) Ar-0.01%O_2 and b) Ar-0.1%O_2. Scale formed in Ar-1%O_2 spalled off completely after cooling to room temperature*

To explain such behaviour, knowledge of the defect structure of chromia and mass transport throughout the oxide scale is desirable. As was discussed in the theory part, opinions of the defect structure in Cr_2O_3 are equivocal, however the most accepted is that chromia behaves as a p-conductor in the high pO_2 environments i.e. oxide scale grows mainly due to outward transport of chromium, [1,12-14,36,37]. Therefore the cations migrate with electrons from the metal/scale interface towards the scale/gas interface to react with the oxygen adsorbed at the surface [1-3]. At the same time in the opposite direction there must be flow of cation vacancies and electron holes. Consequently the driving force for the reaction will be reflected by the concentration gradient of cation vacancies across the scale. The chromium vacancies are formed according to

$$\frac{3}{4}O_2 = \frac{3}{2}O_O + \alpha h^{\bullet} + V_{Cr}^{\alpha'} \tag{21}$$

where α is the effective charge on the chromium vacancies. If the vacancies are triple charged the electroneutrality condition is

$$3\left[V_{Cr}^{'''}\right] - \left[h^{\bullet}\right] = 0 \tag{22}$$

then the corresponding defect equilibria may be written as

$$K_s = \frac{\left[V_{Cr}^{'''}\right]^4}{p_{O_2}^{3/4}} \tag{23}$$

from which

$$V_{Cr}^{'''} = const \cdot p_{O_2}^{3/16} \tag{24}$$

The concentration gradient of cation vacancies across the scale depends on the oxygen partial pressure of the atmosphere as it is shown schematically in Fig. 32, [2]. Therefore the oxidation rate

constant is expected to increase as the oxygen partial pressure of the gas increases. Such oxidation behaviour was observed during oxidation of chromium of various oxygen partial pressures in Ar-O_2 gases shown in Fig. 30. The gradient of cation vacancies building up in the scale also has another implication. Probably the most significant is that vacancies diffusing inwardly tend to precipitate as voids at the metal/scale interface and further condensate to form larger pores and even interfacial gaps decreasing the contact area between scale and metal. This in turn leads to lowering cohesion forces between metal and oxide, and when the system is cooling down to room temperature and thermal stresses are generated, the oxide scale of such morphologies often spalls off. Clearly, the higher the cation vacancy gradient across the scale, the higher the flow of vacancies and the faster the precipitation of the voids and condensation at the metal/oxide interface. Similarly, it was the case in Ar-O_2 gases. In Ar-0.01%O_2 only minor pores were present at the metal/oxide interface, in Ar-0.1%O_2 a number of pores were formed and in Ar-1%O_2 atmosphere, the oxide scale completely spalled off during cooling, Fig. 31. It is important to note that the above considerations of chromium oxidation are directed to the dry Ar-O_2 atmosphere. As will be shown in further chapters, the oxidation behaviour in low pO_2 gases generated by mixing H_2-H_2O is different.

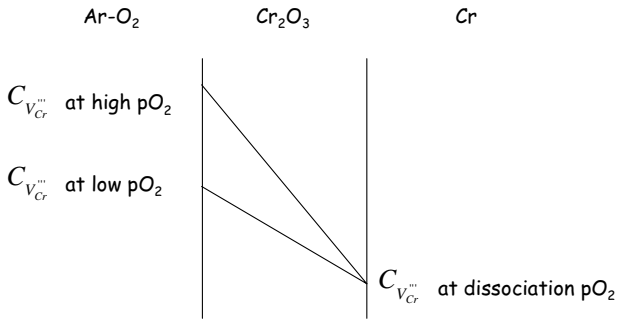

Fig. 32. *Concentration of cation vacancies built up across a Cr_2O_3 scale in high and low oxygen partial pressures in Ar-O_2 atmosphere, [2]*

The question arises how chromium was transported through the voidages which form at the metal/oxide interface. As oxidation proceeded and contact between scale and the metal was being lost, the area across which cations could be supplied decreased [2]. This means that to supply the scale/gas interface over the separated areas, the cations have had a longer diffusion distance and hence reaction rate was expected to fall. As it is shown in Fig. 30 the oxidation rate of chromium exposed to Ar-1%O_2 was still high, even after longer times. The most likely explanation is that vaporization of the metal, i.e. Cr(g) across the void could keep up with scale growth, continuously

supplying the oxide with chromium cations, Fig. 33. To estimate chromium supply to the scale due to gaseous transport the Hertz-Langmuir equation can be used, (25), [1].

$$k_i = \frac{\alpha_i p_i}{(2\pi m_i kT)^{1/2}} \tag{25}$$

where k_i - evaporation rate, p_i - the vapour pressure, α_i - evaporation coefficient. For p_i expressed in atm and k_i in $g \cdot cm^{-2} \cdot s^{-1}$, equation (25) takes the form

$$k_i = 44.3\alpha_i p_i \left(\frac{M_i}{T}\right)^{1/2} \tag{26}$$

The α_i vary depending on the evaporation condition and compound. When the solid and gaseous species contain the same molecules it often found to be unity or close to unity. Considering that at the metal/oxide interface the oxygen partial pressure equals the dissociation pressure of chromia, which is approximately $1.4 \cdot 10^{-22}\, atm$ at 1000°C it can be found that the partial pressure of gaseous chromium, $p_{Cr(g)}$, was approximately $1.4 \cdot 10^{-9}\, atm$, equations (27-29).

$$Cr(s) = Cr(g) \qquad \Delta G_{27} = 216kJ \tag{27}$$

$$K_{27} = \exp\left(\frac{-\Delta G_{27}}{RT}\right) = p_{Cr} \tag{28}$$

$$p_{Cr(g)} = 1.4 \cdot 10^{-9}\, atm \tag{29}$$

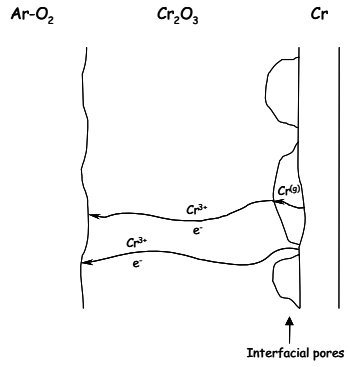

Fig. 33. *Schematic illustration of chromium transport in scale formed in Ar-O_2 gases in cases of voidage formation at the metal/oxide interface*

Inserting the data into equation (26) and taking into account reaction (30), the uptake of oxygen in the range of approximately 1.5 $mg \cdot cm^{-2}$ was estimated after 72h. This value would be too low to explain observed weight change, Fig. 30, if the interfacial gap were formed at the beginning of the oxidation process along entire metal interface. However it could not be the case because the pore formation at the metal/oxide interface required time and in the very early stages of exposures when the oxidation rate was high the chromium could be supplied by solid cations diffusion. As the oxidation proceeded and the pores were developed at the metal/oxide interface the oxidation rate slowed down and even if larger voids developed the evaporation of chromium across the void could keep up with scale growth.

$$2Cr + \frac{3}{2}O_2 = Cr_2O_3 \tag{30}$$

Table 6. *Estimated evaporation rate of gaseous chromium and measured weigh change after 72h oxidation in Ar-1%O_2 at 1000^{o}C*

α	$M_{Cr(g)}$, $g \cdot mol^{-1}$	$p_{Cr(g)}$, atm	$k_{Cr(g)}$, $g \cdot cm^{-2} \cdot s^{-1}$	Estimated weigh change after 72h, $mg \cdot cm^{-2}$	Measured weigh change after 72h oxidation in Ar-1%O_2, $mg \cdot cm^{-2}$
1	52	$1.4x10^{-9}$	$1.3x10^{-8}$	1.5	3.2

7.1.1 Effect of surface preparation

Specimen surfaces were ground to different finishes using grinding papers of different grit or polished using diamond paste and exposed to Ar-1%O_2 gas, Fig. 34. In all cases oxide adherence was poor and the scale spalled off during cooling to room temperature. No significant differences between samples were found.

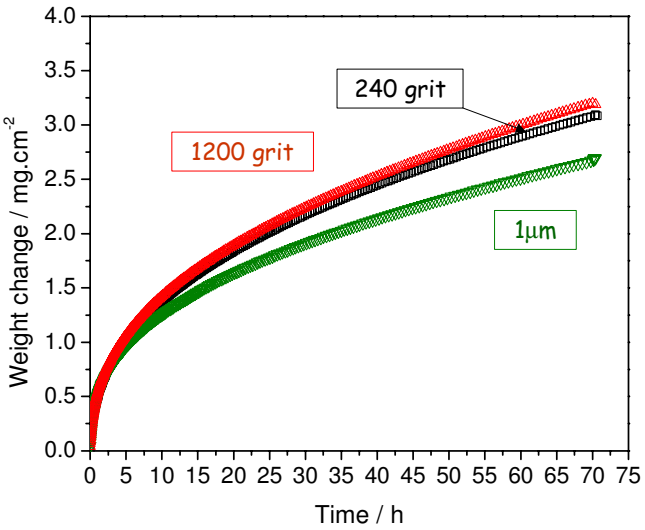

Fig. 34. *Isothermal oxidation of chromium, batch JUG prepared in various ways prior to oxidation in Ar-1%O_2 atmospheres at 1000°C*

7.1.2 Volatilization of Cr-bearing species in Ar-O_2 gas mixtures

During the high temperature exposure of metals to oxygen bearing atmospheres not only solid but also volatile oxides are formed. The partial pressure of these species is strongly related to the pO_2 and the pH_2O. In Ar-O_2 atmospheres when contamination with H_2O is neglected the volatile species of highest pressure is CrO_3(g). According to the Cr-O system, the partial pressure of CrO_3(g) in Ar-1%O_2 gas at 1000°C is approximately 10^{-9} atm, [2]. The evaporation of CrO_3 results in continuous thinning of the Cr_2O_3 scale. Thus, the instantaneous change in scale thickness (x) is the sum of two contributions, thickening due to oxide growth and thinning due to evaporation.

$$\frac{dx}{dt} = \frac{k_d'}{x} - k_s' \qquad (31)$$

where k_d' and k_s' are constants describing the diffusive process and rate of volatilization respectively [2]. Initially, when diffusion through the thin scale is rapid, the effect of CrO_3 volatilization is not significant but, as the scale thickens, the effect of volatilization increases, this is schematically shown in Fig. 35.

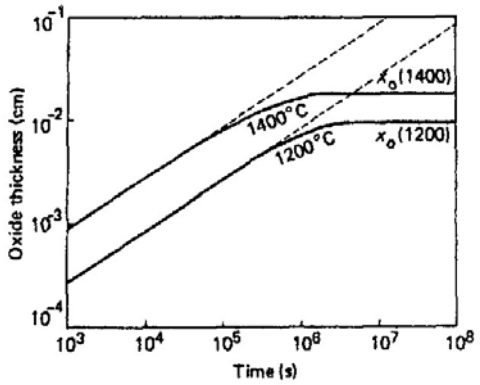

Fig. 35. *Scale thickness versus time for the oxidation of Cr, [2]*

A study by Kofstad revealed that the linear rates of weight loss at 1 atm O_2 were approximately $6.7 \cdot 10^{-3} mg \cdot cm^{-2} \cdot h^{-1}$ at 990°C, [13]. In the present study the oxygen partial pressure was not higher than 0.01 atm and temperature was 1000°C. Assuming to a first approximation that the evaporation rate is proportional to $pCrO_3$ and neglecting temperature difference, one would find that evaporation of chromium in this study was approximately $2.1 \cdot 10^{-4} mg \cdot cm^{-2} \cdot h^{-1}$, equations (32-34) and Table 7.

$$Cr_2O_3 + \frac{3}{2} O_2 = 2CrO_3 \tag{32}$$

$$k = \frac{p^2_{CrO_3}}{p^{3/2}_{O_2}} \tag{33}$$

$$p_{CrO_3} \sim p^{3/4}_{O_2} \tag{34}$$

Table 7. Estimation of evaporation rate based on Kofstad data, 990°C, [13]

	pO_2, *atm*	evaporation rate, $mg \cdot cm^{-2} \cdot h^{-1}$
Kofstad study	1	6.7×10^{-3}
Calculation for Ar-1%O_2	0.01	**2.1×10^{-4}**

Taking data of Hänsel who studied evaporation rates on chromia in Ar-20%O_2 using the same gas flow rate and temperature as in the present study and applying the similar approximations as described above one would find even lower values of evaporation rate, Table 8, [50].

Table 8. Estimation of evaporation rate based on Hänsel data, 1000°C, [50]

	pO_2, *atm*	evaporation rate, $mg \cdot cm^{-2} \cdot h^{-1}$
Hänsel study	0.2	$3.4x10^{-4}$
Calculation for Ar-1%O_2	0.01	**$3.6x10^{-5}$**

Comparison of estimated values of evaporation rate with the weight changes recorded during oxidation shows that evaporation of CrO_3 could be neglected without introducing essential error to the measured weight change.

7.2 Oxidation in Ar-H_2O gas mixtures

7.2.1 Effect of surface preparation

The chromium surface was prepared in various ways prior to oxidation. Specimen surfaces were ground to different finish using grinding papers of different grit or polished using diamond paste and exposed to Ar-7%H_2O at 1000°C. There were no substantial changes in the oxidation rate observed, Fig. 36. The mass gain after 72h of oxidation was higher than in dry Ar-1%O_2. In all cases, the scale adhered well to the metal surface. In the sample ground to 1200 grit, some spallation was observed, probably due to local formation of larger pores near metal/oxide interface. The most significant difference between samples was found in the morphology of the metal/oxide interface. The sample polished prior to oxidation had a uniform interface after the exposure whereas in specimens which were ground to 240 or 1200 grit finish, the interface was irregular and ragged. In the latter case, the local formation of large voids, a sort of inner ”buckles” was also formed.

The morphologies showed that the adherence of the scale to the metal was better in Ar-H_2O gases than in Ar-O_2 and this was due to the lack of voidage at the metal/oxide interface observed in Ar-O_2 atmospheres. It was shown in section 7.1 that lowering the oxygen partial pressure in Ar-O_2 gases hampers the formation of interfacial pores and in turn improves scale adherence. Thus, if the oxidation mechanism of chromium proceeded in the same way in Ar-H_2O as it did in Ar-O_2 one would expect fewer pores at the metal/oxide interface and thus good oxide scale adherence as the partial pressure in Ar-H_2O was lower than in Ar-O_2, Table 4. However, comparing oxidation rates in

dry and wet gases, it appeared that scale thickening in Ar-H_2O did not decrease as was to be expected but was even higher than in any tested dry Ar-O_2 atmosphere, Fig. 30 and Fig. 36.

Also, the scale formed in dry Ar-O_2 gases seemed to become denser when oxygen was reduced, and in Ar-H_2O although no pores were formed at the metal/oxide interface, extensive porosity was found inside the scale. This suggests that it was water vapour that had the greater impact on the oxidation behaviour of chromium than the lower oxygen partial pressure. It must be considered that during oxidation in Ar-H_2O, formation of oxide proceeds by the reaction of chromium with the oxygen originating from the water vapour. Such reactions are known to be much faster than in the case of reaction between chromium and molecular oxygen, [1-3]. It is due to the energy of chemisorption being much smaller for H_2O than for O_2. Little is known about adsorption processes on chromia at high temperature, but work by a few authors seemed to give similar indications [41,67-74]. Probably the most relevant is the work of Anghel who studied the adsorption of N_2, H_2, CO and H_2O on oxidized chromium and zirconium in the temperature range 400°-600°C, [67]. Based on that study, the following tendency of adsorption was proposed: N_2<H_2<CO<H_2O.

Similar indications of the adsorption processes in different gases can be found in the work of Polman et al [41]. The author investigated morphological phenomena occurring during oxidation of chromium in a similar temperature range as in this work and proposed that the activation energy of chemisorption for chromium should be according to the order $E^{act}_{H_2O} < E^{act}_{CO_2} < E^{act}_{O_2}$.

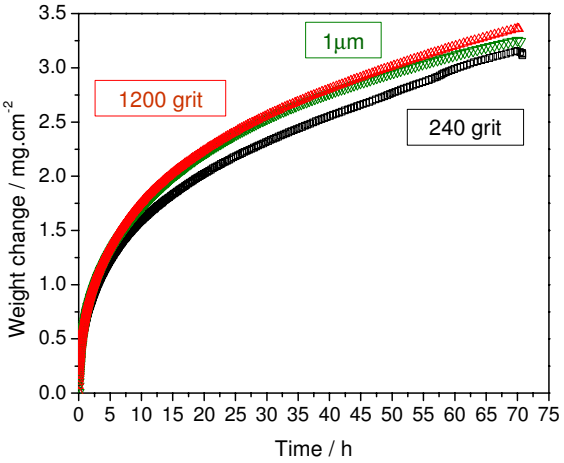

Fig. 36. *Isothermal oxidation of chromium, batch JUG prepared in various ways prior oxidation in Ar-7%H_2O atmospheres at 1000°C*

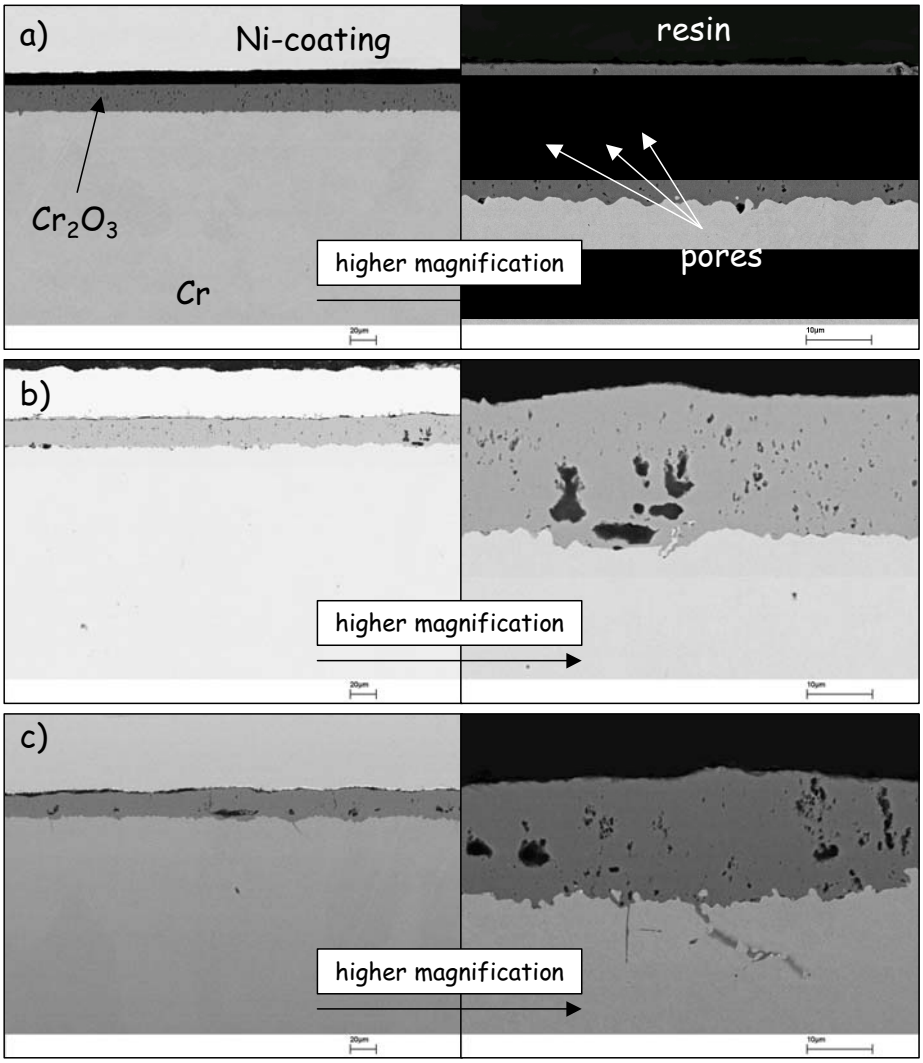

Fig. 37. *SEM polished cross-sections of oxide scales formed on chromium, batch JUG after 72h oxidation in Ar-7%H_2O at 1000^{o}C, prior oxidation specimen surface was a) polished b) ground to 1200 grit, c) ground to 240 grit*

Differences in adsorption suggested that surface reactions might be a key factor in understanding the overall oxidation behaviour of chromium. One could speculate that at least in the early stages of oxidation when the scale was thin and surface reactions were rate controlling instead of diffusing chromium cations, the enhanced oxidation rate in Ar-H_2O occurred due to faster reactions of Cr with H_2O than O_2. The surface reaction with water vapour could also affect the morphology of the scale, especially the grain size.

During oxidation processes competition between nucleation of new oxide sites and oxide growth could be an important factor, [1]. If reactions on the surface are fast it is most likely that the tendency for nucleation will be higher than for grain growth and as a result a number of small crystals will form. This could be the case during oxidation in Ar-H_2O gases. On the contrary, if reactions on the surface were slow, the oxide grains would tend to grow rather than form new nucleation sites and this could be the situation in Ar-O_2 systems. This aspect will be discussed in detail in section 7.3. Obviously, morphological differences have a great impact on the mass transport through the oxide and therefore in the subsequent studies, the main attention is devoted to these aspects.

7.2.2 Two-stage oxidation in Ar-2%$H_2{}^{16}O$/Ar-2%$H_2{}^{18}O$

To get more information about scale growth processes in the Ar-H_2O atmospheres, a chromium sample was exposed at 1000°C to Ar-2%$H_2{}^{16}O$ for 3 hours and then the atmosphere was changed in-situ to Ar-2%$H_2{}^{18}O$ for another 3h. After that the specimen was analysed by Sputtered Neutrals Mass Spectroscopy to determine the tracer distribution in the scale, Fig. 38. The procedure was described in section 6.4.

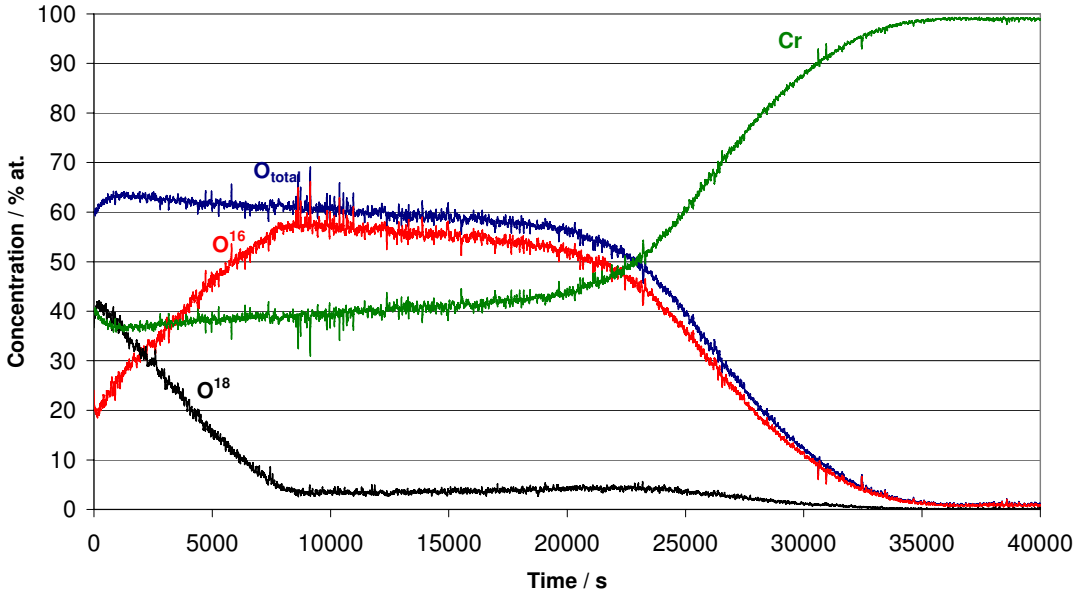

Fig. 38. *SNMS depth profile after two-stage oxidation of chromium, batch JUG for 3h in Ar-2%$H_2{}^{16}O$ / 3h in Ar-2%$H_2{}^{18}O$ at 1000°C*

It can be seen that the concentration of the ^{18}O isotope was high in the outer part of the scale suggesting that outward cation diffusion was the main transport mode. It must, however, be noted that the ^{18}O concentration did not gradually decrease to zero in the outer part of the scale but was also present in the inner part of the oxide and showed a minor enrichment near the scale/metal interface. This is more clearly seen in semi-logarithmic plot of the as-measured data in Fig. 39. This could be an indication that the oxide growth occurred not only at the gas/oxide interface but to some extent also at the metal/oxide interface.

As will be shown in section 7.3 the oxide scale consists of much finer grains in Ar-H_2O gas, Fig. 42, compared to the Ar-O_2, Fig. 41 and this fact might suggest that the scale growth in the Ar-H_2O gas proceeded to a large extent through inward oxygen transport via rapid diffusion paths, i.e. oxide grain boundaries.

Zurek et al studied the oxidation behaviour of a binary Ni-Cr alloy in Ar-4%H_2-7%H_2O and Ar-20%O_2 gases at 1000°C, [75]. The authors found the grains of the oxide formed in the Ar-4%H_2-7%H_2O were substantially finer compared to those formed in the Ar-20%O_2 and thus inward grain boundary diffusion was suggested to be the predominant transport mode. The authors considered also that in the oxide scale composed of fine grains isotope exchange could result in a decreasing intensity of the inner ^{18}O peak and higher intensity of the "exchange-branch" in the outer scale. This is schematically shown in Fig. 40.

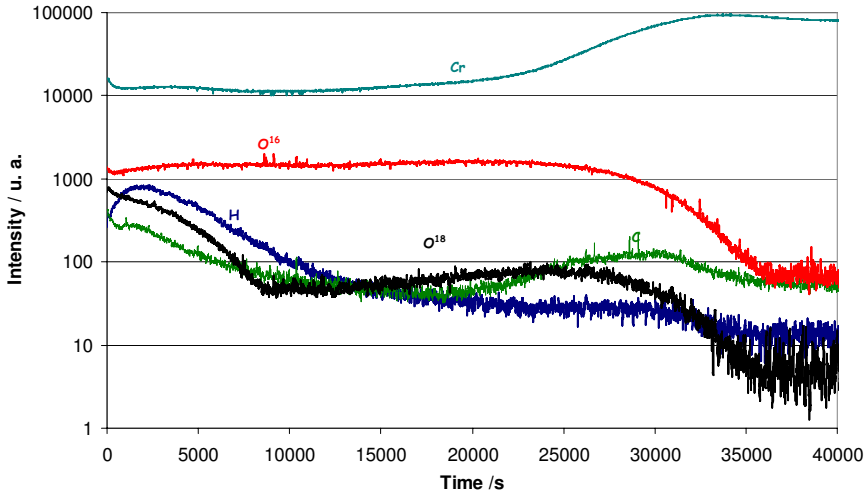

Fig. 39. *SNMS-profile before quantification after two-stage oxidation of chromium, batch JUG for 3h in Ar-2%$H_2{}^{16}O$ / 3h in Ar-2%$H_2{}^{18}O$ at 1000°C*

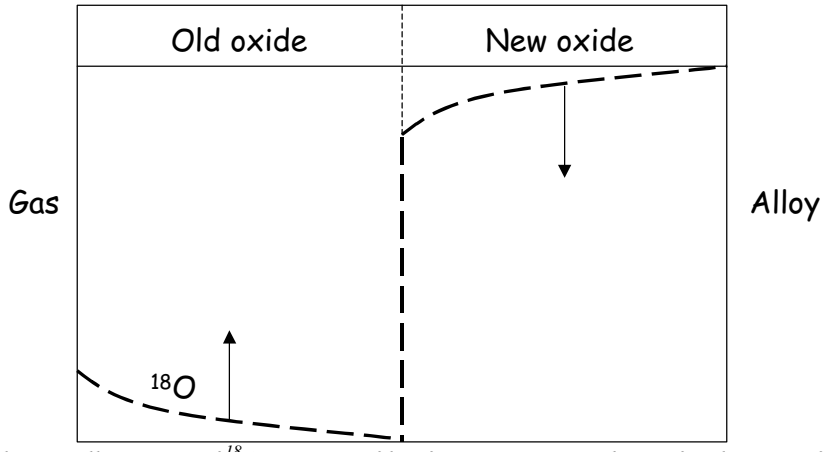

Fig. 40. *Qualitative illustration of ^{18}O tracer profile after two-stage oxidation for the case of scale growth proceeding via grain boundary oxygen transport taking isotope exchange into account, [75]. Dashed line shows profile in coarse-grained oxide. The arrows indicate the change in the profile in case of a fine-grained oxide*

Considering fine oxide grain microstructure to be the reason of enhanced inward transport the questions arise how the H_2O alters the chromia grain size and whether or not the inward grain boundary diffusion was the only way of oxygen transport to the metal/oxide interface. Possible answers to these questions will be discussed in section 7.4 after the differences in scale morphologies formed in the Ar-H_2O and in the Ar-O_2 have been illustrated.

7.2.3 Volatilization of Cr-bearing species in Ar-H_2O gas mixtures

The oxygen partial pressure in the atmosphere containing water vapour without addition of molecular oxygen is approximately 10^{-6} atm. According to the Cr-O system presented in Fig. 17, the partial pressures of the volatile species formed are low and for $CrO_2(g)$ and $CrO_3(g)$ at 1000°C they are approximately 10^{-12} atm. It has been known for some time that volatilization can strongly be enhanced in the presence of water vapour molecules by the formation of the volatile chromium oxy-hydroxide $CrO_2(OH)_2$, [55,56]. Such species are formed according to reaction (18). The free energy of formation of this species has recently been estimated by Opila, reviewed in section 3.5, [56]. Equation (18) shows that the partial pressure of $CrO_2(OH)_2$ depends on both the oxygen and water vapour partial pressure in the gas. Consequently the evaporation rate in the environment containing water vapour without addition of molecular oxygen is extremely low and can be neglected.

7.3 Comparative TEM study on the early stages of oxidation

Applying the FIB technique coupled with a TEM analysis shows further evidence of different scale morphologies formed in Ar-O_2 and Ar-H_2O gases. For testing, chromium specimens were exposed for 30min to Ar-20%O_2 and Ar-2%H_2O at 950°C, Fig. 41 and Fig. 42 respectively. TEM sections of the oxidized samples demonstrated clearly that even after very short exposure time to the dry gas, voids and pores were formed at the Cr/Cr_2O_3 interface and a very compact and adherent oxide scale was present when chromium was oxidized in the Ar-H_2O. Comparing the scale thicknesses, it appeared that oxidation in the Ar-H_2O gas was faster than in Ar-O_2. Another important feature of the scale morphologies was the size of the oxide grains. In the dry gas the grains were generally large and columnar in shape. Only at the metal/oxide interface did the grains become smaller in size. On the contrary, in the wet gas the oxide grains were very small and more evenly distributed within the scale than in case of the Ar-O_2 exposed specimen. Hardly any pores were observed at the metal/oxide interface and some were present in the scale.

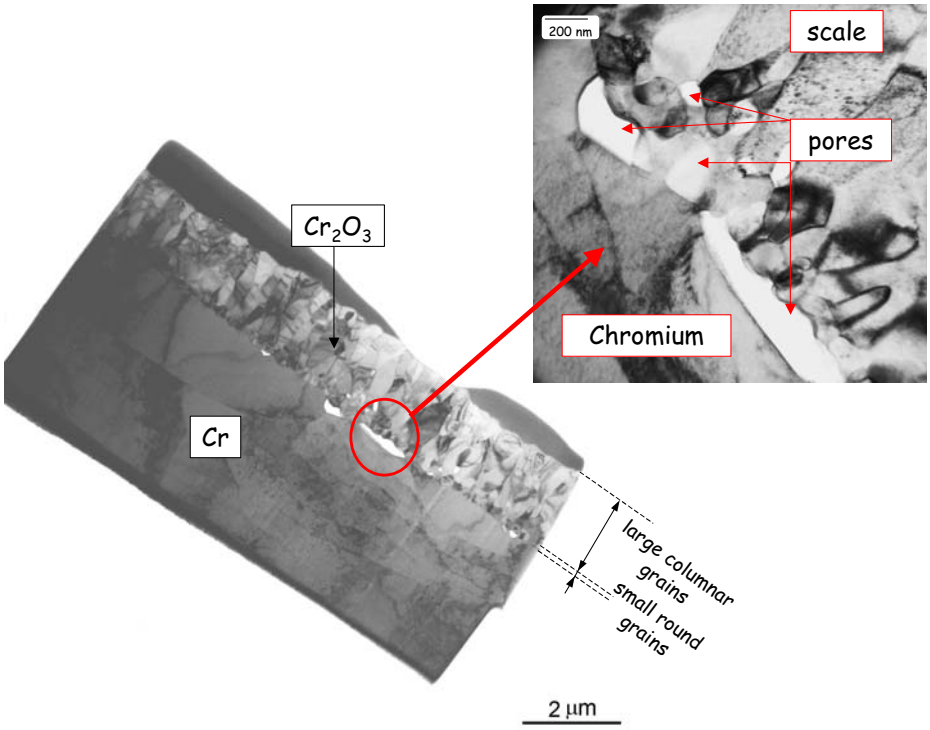

Fig. 41. *TEM cross section of chromium, batch JUG after 30min oxidation in Ar-20%O_2 at 950°C*

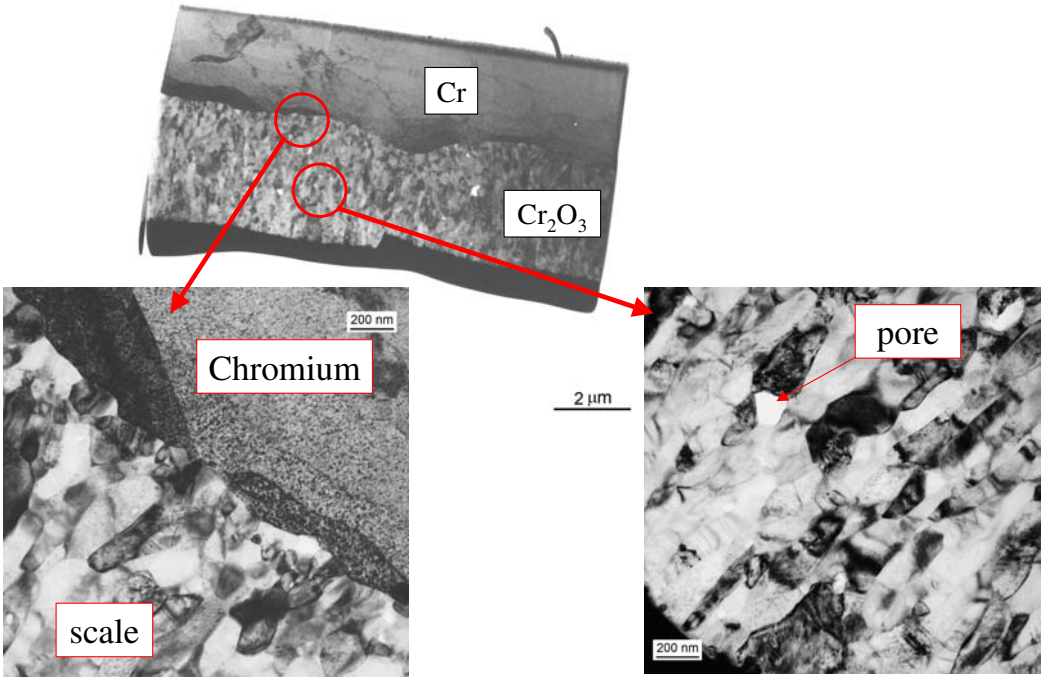

Fig. 42. *TEM cross section of chromium, batch JUG after 30min oxidation in Ar-2%H_2O at 950°C*

Little is known about the influence of water vapour on the grain size of the oxide scale but work by Jacob et al gives similar indications to those found in the present study, [68]. The authors reported that chromia formed at 800°C and 1000°C in dry N_2/O_2 mixtures had a larger grain size than when formed in the wet N_2-20%O_2-1%H_2O gases. This suggests that water vapour must have an important influence on the microstructure of the oxide scale. It is believed that adsorption, grain growth and pore distribution in the scale were most affected by water vapour. Therefore these aspects are considered below in detail.

- Adsorption -

It has been known for some time that adsorption of H_2O is much faster on the oxides surface than O_2 or N_2. This was discussed in section 7.2.1 and confirming examples were given. In the Ar-H_2O in which adsorption was fast the tendency for nucleation of new oxide grains was higher than for grain growth. This could be one of the important factors for the scale to be composed of many small oxide

grains. Such a structure provides fast diffusion paths to the metal/oxide interface because of the high grain boundary density, [76]. In the Ar-O_2 contrary to the Ar-H_2O fewer, but larger grains were formed during oxidation. Adsorption of molecular oxygen to the metal surface was slow and similarly nucleation of new oxide sites was also slow. In turn the growth of oxide grains was favoured and large columnar grains were formed during the process.

It must be noted that adsorption and reaction at the gas/oxide interface are related to the surface condition, [76]. Therefore, surface tension of the oxide should also be considered because it could have an impact on the reactivity of the surface. Unfortunately, little is known about the influence of external atmospheres on the surface tension of chromium oxide at high temperature, but it is known that gases can affect the surface tension of various metals and oxides. Fig. 43 represents an example of the oxygen pressure effect on the surface tension of solid silver.

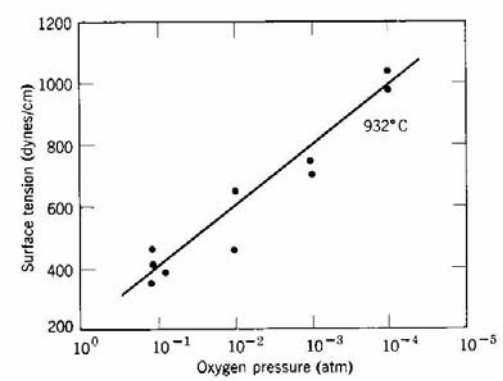

Fig. 43. *Effect of oxygen partial pressure on the surface energy of solid silver at 932^{o}C, [76]*

- Grain growth and porosity -

Grain growth is an essential aspect of oxidation processes of metals and alloys and is commonly observed during sintering of ceramics [76,77]. The driving force for grain growth is the reduction of grain boundary area per unit volume, which is proportional to the inverse of the average grain size. The total energy of the system is decreased by the elimination of grain boundary area and therefore grains migrate toward their centres of curvature with some grains growing and some shrinking. The interface energy is associated with the boundary between individual grains. In addition, there is a free energy difference across a curved grain boundary which is given by

$$\Delta G = \gamma \bar{V}\left(\frac{1}{r_1}+\frac{1}{r_2}\right) \tag{35}$$

where ΔG is the change in free energy going across the curved interface, γ is the boundary energy, $\bar{V}$ is the molar volume and r_1 and r_2 are the principle radii of curvature. This difference in free energy of the materials on two sides of a grain boundary makes the boundary move toward its centre of curvature. The rate at which a boundary moves is proportional to its curvature and to the rate at which atoms jump across the boundary. The change in energy with an atom position change is shown in Fig. 44, [76].

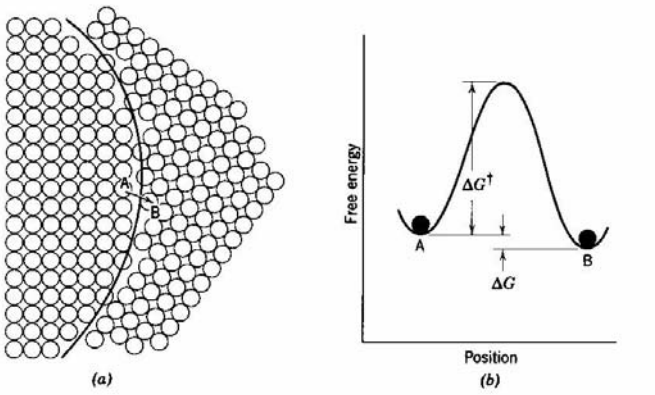

Fig. 44. *a) Structure of boundary and b) energy change for atom jump, [76]*

It was shown that water vapour affects grain size and the overall oxide microstructure. In that sense grain growth must have been affected and as was illustrated, boundary motion slowed down. The question arises as to what the action of water vapour was. A few possible explanations will be presented and it is believed that all of the factors could work at the same time and contribute to the overall behaviour. One of the reasons could be seen in the molecular transport of water vapour across the scale to the metal/oxide interface. During inward diffusion of water vapour it is very likely that molecules are being adsorbed at the grain boundaries slowing boundary motion and in effect grain growth, [76]. Additionally, because of the dipole character of H_2O, the molecules could polarize themselves and repel as schematically illustrated in Fig. 45, [76].

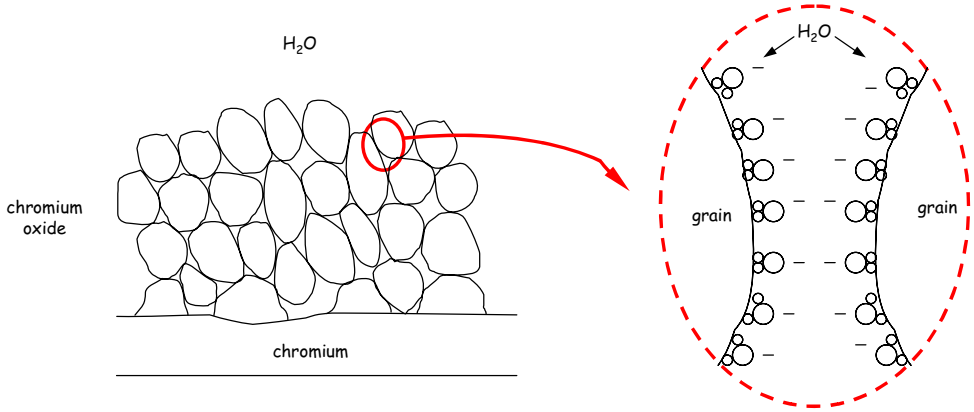

Fig. 45. *Schematic illustration of adsorption and polarization of H_2O on to the grain boundary*

Molecular transport of water vapour to the metal/oxide interface could have other consequences. Continuous dissociation of the inner oxide and filling of the interfacial porosity resulted in outward movement of pores. It has been reported that the effect of pores in fairly dense compacts is to slow down grain growth, [76]. It is known that inclusions increase the energy necessary for the movement of grain boundaries and inhibit grain growth. Such inclusions can be particles of another phase but also pores. If we consider a boundary such as the one illustrated in Fig. 46, the boundary energy is decreased when it reaches a pore proportional to the cross sectional area of the pore. The boundary energy must be increased again to pull it away from the pore. Consequently when numbers of pores are present in a grain boundary its normal curvature becomes insufficient for continued grain growth after some limiting size is reached. It has been found that the size is given by

$$d_l = \frac{d_i}{f_{d_i}} \tag{36}$$

where d_l is the limiting grain size, d_i is the particle size of the inclusion, and f_{d_i} is the volume fraction of pores, [76]. Although this relationship is only approximate it indicates the effectiveness of pores increases as their size is lowered and volume fraction increases. The process is schematically illustrated in Fig. 46.

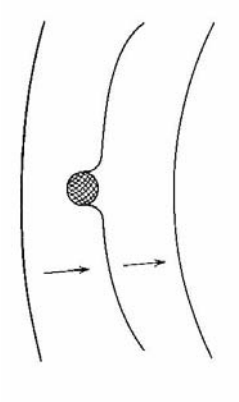

Fig. 46. *Changing configuration of a boundary while passing a pore, [76]*

Another possibility is that the grain boundary drags the particle along, which remains attached to the boundary as it moves. The inclusion particle moves along with the boundary gradually becoming concentrated at boundary intersections agglomerating into larger particles as grain growth proceeds. This is illustrated in Fig. 47.

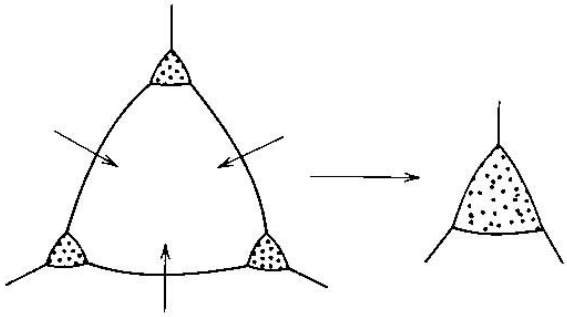

Fig. 47. *Pore agglomeration during grain growth, [76]*

As grain growth proceeds the driving force diminishes and any pore dragged along by the boundary increases in size so that their mobility decreases. As a result the exact way in which pores inhibit grain growth changes during the grain growth process. It is also important to note that in systems composed of larger grains, pores tend to disappear and in systems composed of a number of small grains, pores would rather grow. This is schematically illustrated in Fig. 48, [78].

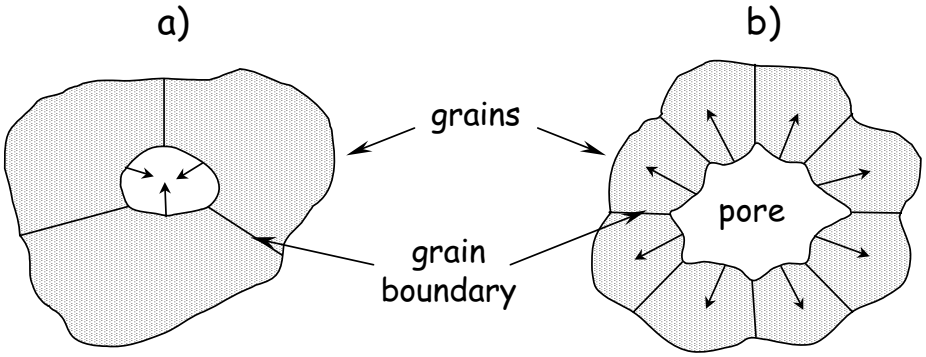

Fig. 48. *Schematic illustration of mass transfer tendency in systems composed of a) large grains and b) small grains, [78]*

Indications for such a behaviour were found in the present experimental results. In the Ar-O_2 large grains were formed and only minor porosity was found in the bulk scale, even after longer oxidation time. In Ar-H_2O gases, pores were seen in the scale and apparently they became larger as the exposure time was extended.

It must be noticed that also vacancy condensation played a role in the process of pore formation. In dry Ar-O_2 gases grains were large and because of inward transport being insignificant, the voids were concentrated mainly at the metal/oxide interface. Therefore, vacancies condensated at that interface to form larger pores. In Ar-H_2O gases the grains were smaller, inward transport enhanced and consequently interfacial voids were "pushed" outward, Fig. 51. Therefore vacancies could condensate at the chromia/pore interface contributing to the pore growth. This is schematically illustrated in Fig. 49.

Another important aspect of the different oxide grain morphology is related to the plasticity of the scale. Oxides composed of fine grains have a larger number of grain boundaries than oxides with large grains and considering dislocation sliding as the main mechanism of oxide deformation, the scale formed in the first listed case, should be more plastic, [1].

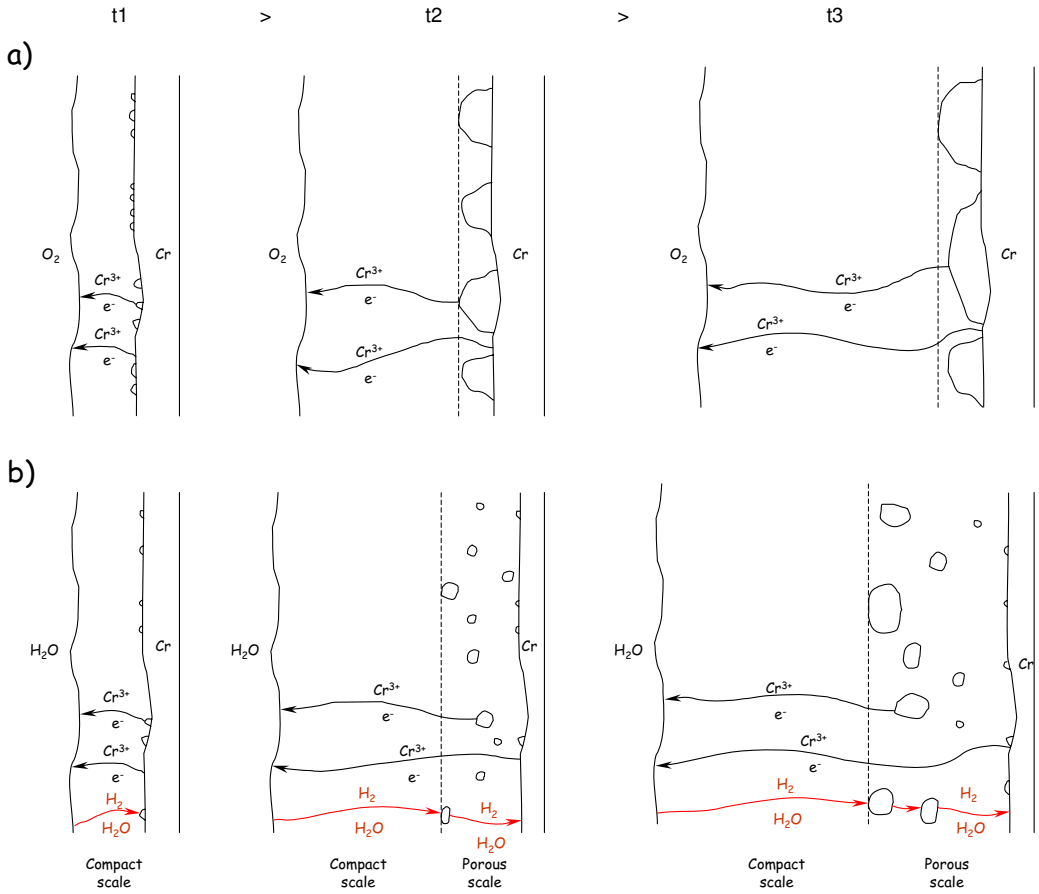

Fig. 49. *Schematic illustration of void formation in a) Ar-O_2 and b) Ar-H_2O gases, where oxidation time $t_1<t_2<t_3$*

7.4 Mass transport in scale formed in Ar-H_2O gas mixtures

It was shown in section 7.3 that oxide scales grown in the Ar-H_2O form a finer grained microstructure compared to those formed in the Ar-O_2. Different factors were considered and the possible explanation of the behaviour was proposed. In section 7.2.2, applying tracer studies and SNMS analysis it was shown that the inward oxygen diffusion constitutes an important part of the oxide growth in Ar-H_2O gas. The remaining question concerns the way of oxygen transport to the metal/oxide interface. It is believed that a higher grain boundary density in the scales formed in the

Ar-H_2O than in the Ar-O_2 could markedly enhance oxygen grain boundary diffusion, however, it should also be considered that H_2 and H_2O diffused throughout the scale to the metal/oxide interface in the form of molecules and at this interface reacted with the metal to form oxide. During oxidation in Ar-H_2O gases, as the oxygen activity in the scale decreases in the direction of the scale/metal interface, the pH_2 would gradually increase and the pH_2O decrease. The thermodynamic estimation for Ar-7%H_2O is shown in Fig. 50. It can be seen that the pH_2O at the metal/oxide interface would be still high, i.e. $3.8 \cdot 10^{-6}$ atm and as such should be considered as a potential carrier of oxygen. In voids which might form at the scale/oxide interface using the Hertz-Langmuir equation in a similar way as described in section 7.1, equation (26), but inserting relevant values, the rate of water vapour transport to the metal/oxide interface can be estimated and the possible oxygen uptake calculated, Table 9.

Comparing the calculated values with measured weight changes it can be seen that water vapour could supply the metal/oxide interface with oxygen and in such cases, the inward growing oxide could continuously fill the pores formed at the metal/oxide interface preventing their growth at that interface. Therefore the growth of interfacial voidage would be suppressed and in turn a well adherent scale will grow which was observed experimentally.

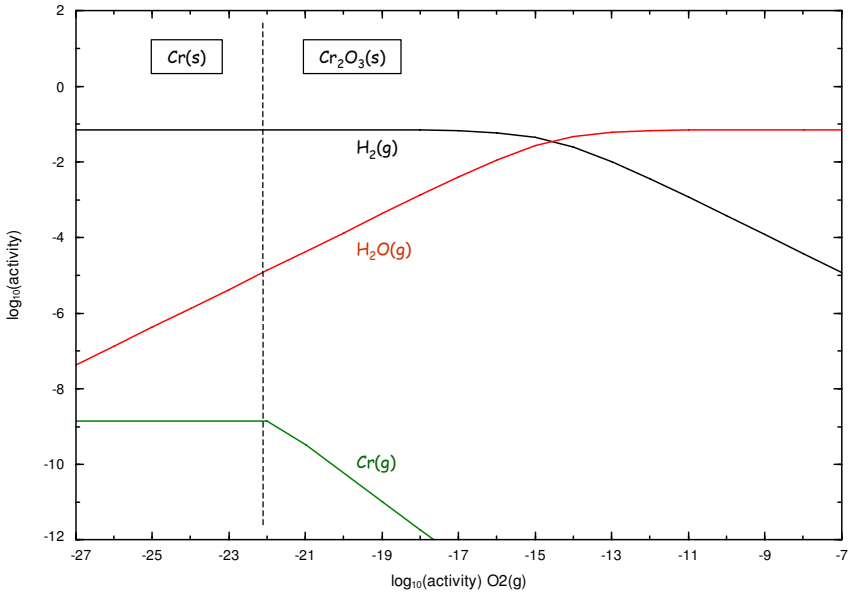

Fig. 50. *Thermodynamic estimation of the pH_2 and the pH_2O as function of oxygen activity illustrating partial pressures of various species in the Cr_2O_3 scale during oxidation of chromium in Ar-7%H_2O at 1000°C assuming local thermodynamic equilibria, [63]*

Table 9. *Calculated and measured oxygen uptake after 72h oxidation in Ar-7%H_2O at 1000°C occurring in gas using the Hertz-Langmuir equation (26)*

α	M_{H_2O}, $g \cdot mol^{-1}$	p_{H_2O}, *atm*	k_{H_2O}, $g \cdot cm^{-2} \cdot s^{-1}$	*Calculated oxygen uptake after 72h,* $mg \cdot cm^{-2}$	*Measured oxygen uptake after 72h oxidation in Ar-7%H_2O,* $mg \cdot cm^{-2}$
1	18	3.8×10^{-6}	2.4×10^{-6}	548	3.4

It should be noted that water vapour could also be formed in the interfacial pore even if only hydrogen would diffuse inwards. Since the partial pressure of oxygen in the inner pore is very low and approximately equals the dissociation pressure of chromia, ($1.4 \cdot 10^{-22}$ atm), the inner oxide at the pore can dissociate and form chromium cations and water vapour. The latter subsequently diffuse to the pore/metal interface and forms oxide, which fills the pore. This is schematically illustrated in Fig. 51. Rahmel and Tobolski as well as Fuji and Meussner proposed a similar mechanism to explain the oxidation behaviour of Fe and Fe-Cr alloys respectively in water vapour containing environments [79,80].

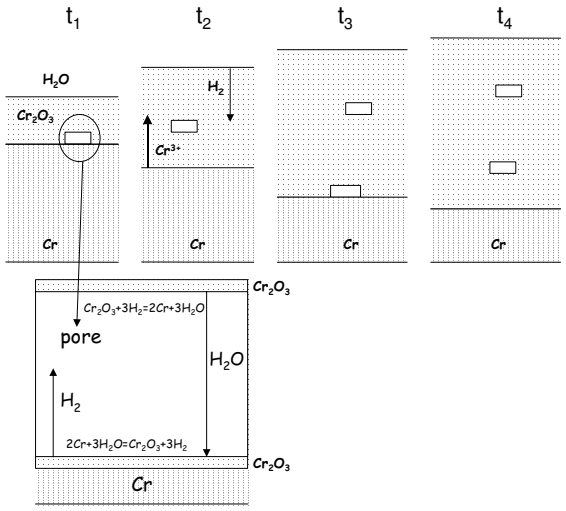

Fig. 51. *Schematic development of the oxide scaling process on pure Cr in H_2O, [40]*

It is interesting to note that the SNMS results indicate that the concentration of hydrogen seems to increase within the scale. Fig. 39 shows the intensity of the measured elements by SNMS before quantification. Enrichment of hydrogen was found in the growing oxide and carbon was seen to increase in the metal in regions close to the metal/oxide interface. It must be noted that great care

should be taken in interpreting fluctuations in hydrogen intensity because due to the low mass number, this element was at the detection limit of the mass spectroscopy used and therefore it could not be excluded that such a peak was recorded due to the contaminations. However, similar indications were given by Yamauchi et al during the high temperature oxidation of a Fe-Cr steel in different N_2-O_2-H_2O atmospheres using glow discharge spectroscopy [81]. They also found that the hydrogen intensity increased upon increasing the concentration of water vapour in the gas which could be an indication that the presence of hydrogen in the scale is related to the atmosphere and not to hydrogen diffusion from the metal as proposed by different authors.

7.5 Oxidation during in-situ gas changes

To obtain further insight into the mechanisms which are responsible for the differences in adherence of the oxide scale formed in wet and in dry gases, two-stage oxidation experiments with an in-situ gas change i.e., without intermediate cooling, were carried out. Chromium specimens were exposed at 1050°C to wet gas, Ar-7%H_2O for 16h and changed to dry gas, Ar-20%O_2 for a further 56h oxidation. In the second experiment the gases were utilized in the reverse order. Another set of experiments was carried out using the same method, however a time of 56h was chosen for the first stage and 16h for the second. Details together with the measured relative amount of spalled oxide scale after cooling to room temperature are shown in Table 10.

Table 10. *Relative amount of spalled oxide after cooling to room temperature*

Gas combination **wet = Ar-7%H_2O** **dry =Ar-20%O_2**	**1 stage**	**2 stage**	Relative amount of spalled oxide after cooling (% of total oxide)
dry / wet	16h	56h	1.8
wet / dry	16h	56h	11.0
	1 stage	**2 stage**	
dry / wet	56h	16h	14.3
wet / dry	56h	16h	6.3

Fig. 52 shows the scale growth kinetics and Fig. 53 compares the weight change after isothermal oxidation with the weight change after cooling for both test procedures. In these sets, gas was changed in situ after a relatively short time, 16h. It can be seen that the combination wet/dry results in higher scale spallation during cooling than combination dry/wet. This observation is in agreement with the metallographic cross sections taken after the two stage exposures, Fig. 54. The combination

wet/dry results in an oxide scale microstructure, which seems to be governed by the first wet stage, but the oxide is detached from the metal substrate. In turn, the combination dry/wet shows that in the second stage, in which the gas was changed to wet gas, new oxide was also being formed at the metal/oxide interface and a large gap at the metal/oxide interface was filled in.

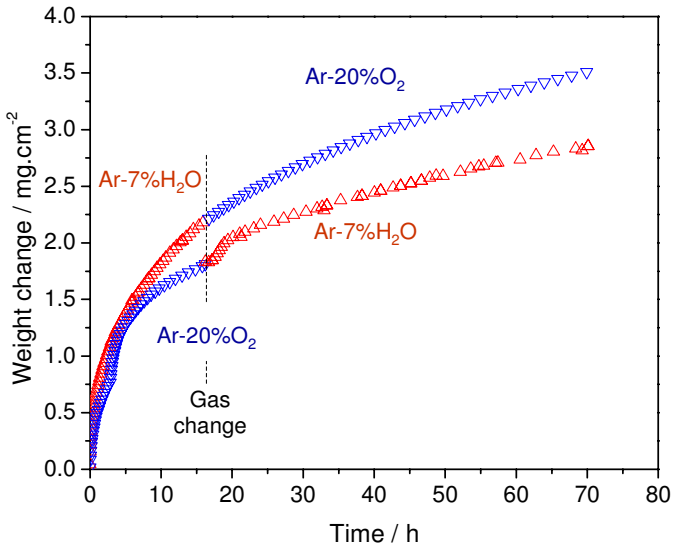

Fig. 52. *Effect of in-situ gas changes on oxidation of chromium, batch JUG at 1050°C*

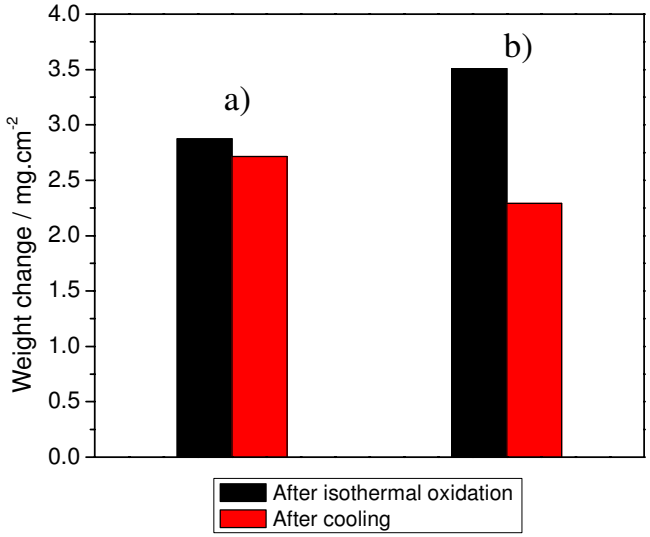

Fig. 53. *Weight change after isothermal oxidation of chromium, batch JUG at 1050°C with in-situ gas change, a) 16h in Ar-20%O_2 and subsequently 56h in Ar-7%H_2O, b) 16h in Ar-7%H_2O and subsequently 56h in Ar-20%O_2*

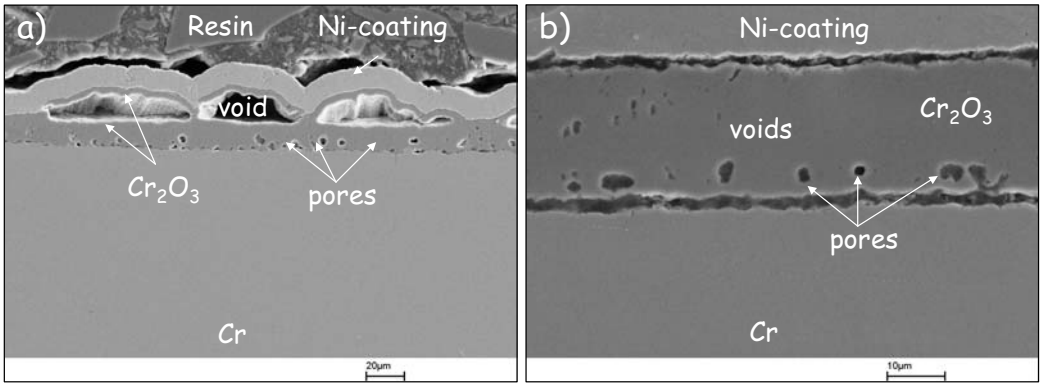

Fig. 54. *SEM cross sections of oxide formed on chromium, batch JUG after isothermal oxidation at 1050°C with in-situ gas change, a) 16h in Ar-20%O_2 and subsequently 56h in Ar-7%H_2O, b) 16h in Ar-7%H_2O and subsequently 56h in Ar-20%O_2*

In a second set of experiments the gas was changed in-situ after 56h, Fig. 55 and Fig. 56. These experiments showed primarily that the influence of the gas, which is introduced in the second stage, is time dependent. The combination dry/wet revealed that healing of the gap at the metal/oxide interface must have also occurred, however the amount of spalled oxide is higher than for the case where the gas was changed after a shorter time, i.e. 16h, compare Fig. 53 and Fig. 56. The combination wet/dry shows that the oxide still adheres well to the metal. It is probable that voids and/or gaps could not be formed at the metal/oxide interface in great number because there was simply not enough time.

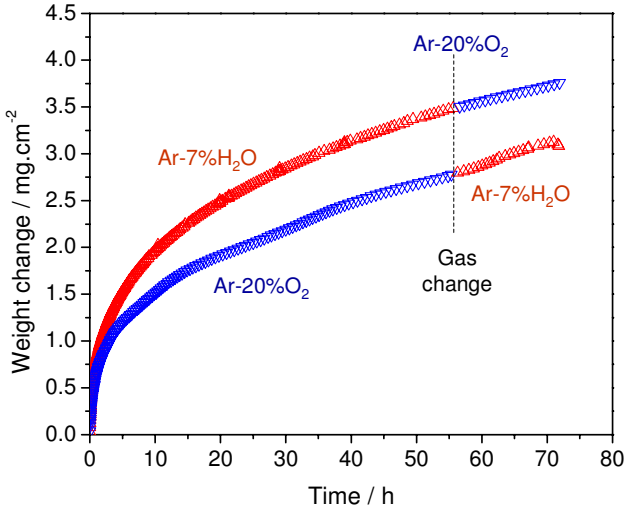

Fig. 55. *Effect of in-situ gas changes on isothermal oxidation of chromium, batch JUG at 1050°C*

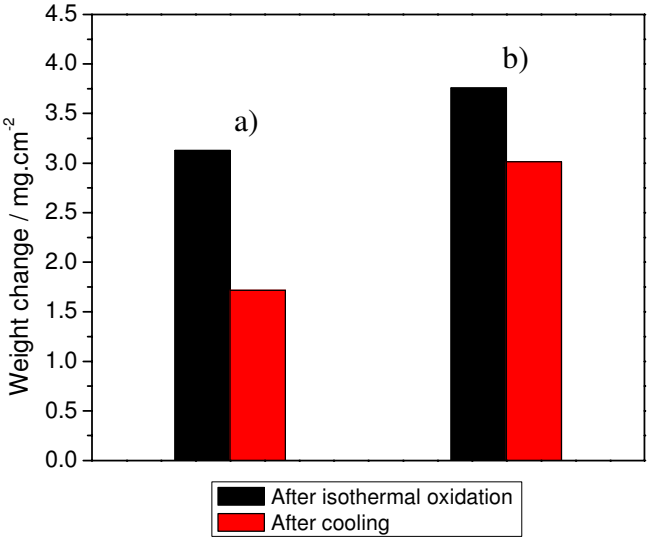

Fig. 56. *Weight change after isothermal oxidation of chromium, batch JUG at 1050°C with in-situ gas change, a) 56h in Ar-20%O_2 and subsequently 16h in Ar-7%H_2O, b) 56h in Ar-7%H_2O and subsequently 16h in Ar-20%O_2*

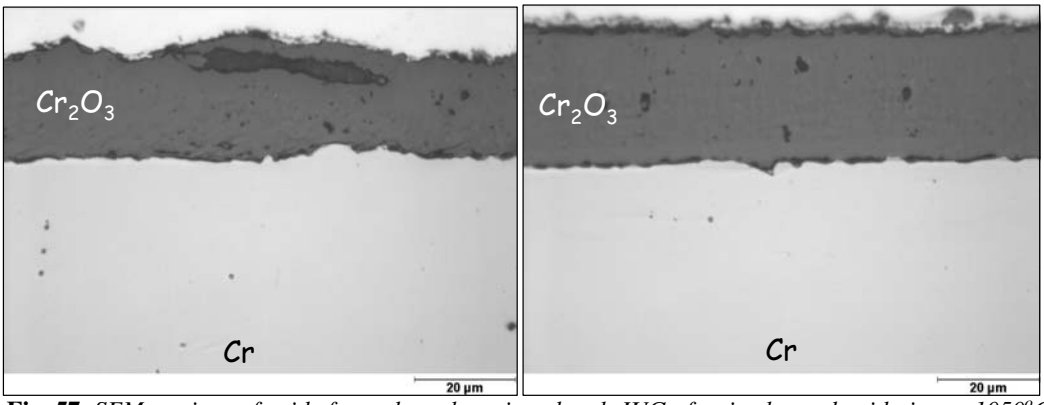

Fig. 57. *SEM sections of oxide formed on chromium, batch JUG after isothermal oxidation at 1050°C with in-situ gas change, a) 56h in Ar-20%O_2 and 16h in Ar-7%H_2O, b) 56h in Ar-7%H_2O and 16h in Ar-20%O_2*

- Key differences in oxidation behaviour in (dry) Ar-O_2 and (wet) Ar-H_2O gases, Summary -

It was shown that oxidation rate in the Ar-H_2O was faster than in the dry Ar-O_2 and at the same time oxide adhered much better to the metal after cooling to room temperature. Similarly, good oxide adherence was found in tests with in-situ gas changes if the test gas in the second stage was wet. The good adherence of the scale was also maintained when the gas in the second stage was dry but the exposure time was short. The oxidation rate in Ar-O_2 gases was dependent on the pO_2 and oxide scaling was faster when oxygen pressure was increased in the gas. It was proposed that chromium vacancies condensed at the meta/oxide interface and formed larger pores. Therefore increasing the pO_2 in the gas generated a higher flux of chromium vacancies resulting in more significant interfacial voidage. After early stages of oxidation in Ar-O_2 gas relatively large grains in the range of 1μm were formed.

Oxide scales were found to be compact. It must be noted however that such founding is based on observation of scale morphology formed only in Ar-0.01%O_2 and Ar-0.1%O_2 gases. As will be shown in chapter 8.1 increasing further the pO_2 in Ar-O_2 gases trigger development of compressive stresses and in turn formation of convoluted and badly damaged scale.

In Ar-H_2O atmosphere no voids were found at the metal/oxide interface but a number of pores of different sizes were present in the scale. The oxide grains were much smaller than in Ar-O_2 gas, around few hundreds of nanometres. Such morphology was suggested to be the effect of H_2O presence rather than the low pO_2 because it is mainly the fast adsorption of water vapour at the surface that enhanced the nucleation rate and in turn promoted the formation of new oxide grains. This resulted in higher oxidation rate comparing to Ar-O_2 gases. The scale morphology was in turn composed of many small oxide grains. The higher number of grain boundaries enhanced inward transport by providing fast diffusion paths. Inward oxygen grain boundaries diffusion and molecular diffusion of H_2 or/and H_2O to the metal/oxide interface were suggested to be important part of that transport. Dissociation at the inner oxide/pore interface and oxide growth at the pore/metal interface hampered pore condensation at the metal/oxide interface and markedly improved scale adherence. The consequence of such reactions was a virtual outward movement of pores. Because vacancies condensed at the oxide grain boundaries/pores interfaces, scales developed a number of pores in the scale, increasing their size with oxidation time.

7.6 Oxidation behaviour of chromium in Ar-O_2-H_2O gas mixtures

It was discussed in previous sections that the oxidation behaviour in the Ar-O_2 and in the Ar-H_2O seemed to be governed by different mechanisms. Therefore studies in Ar-O_2-H_2O gases might be an important element for better understanding the effect of the pH_2O and the pO_2 on the oxidation of chromium. It has been known for some time that in such gas mixtures enhanced evaporation of $CrO_2(OH)_2$ becomes significant and this aspect is considered first, [51-56].

7.6.1 Volatilization of Cr-bearing species in Ar-O_2-H_2O gas mixtures

It was shown in section 3.5 that evaporation of $CrO_2(OH)_2$ in mixed O_2-H_2O atmospheres can markedly increased. The partial pressure of this species was calculated according to recent thermodynamic data obtained by Opila and is shown in Tab. 2, [56]. The changes in partial pressures of $Cr_2O(OH)_2$ with the addition of H_2O for a few representative atmospheres are additionally shown in Fig. 58. It is clearly seen that the formation of this species is particularly essential in atmospheres containing both high amounts of molecular oxygen and water vapour.

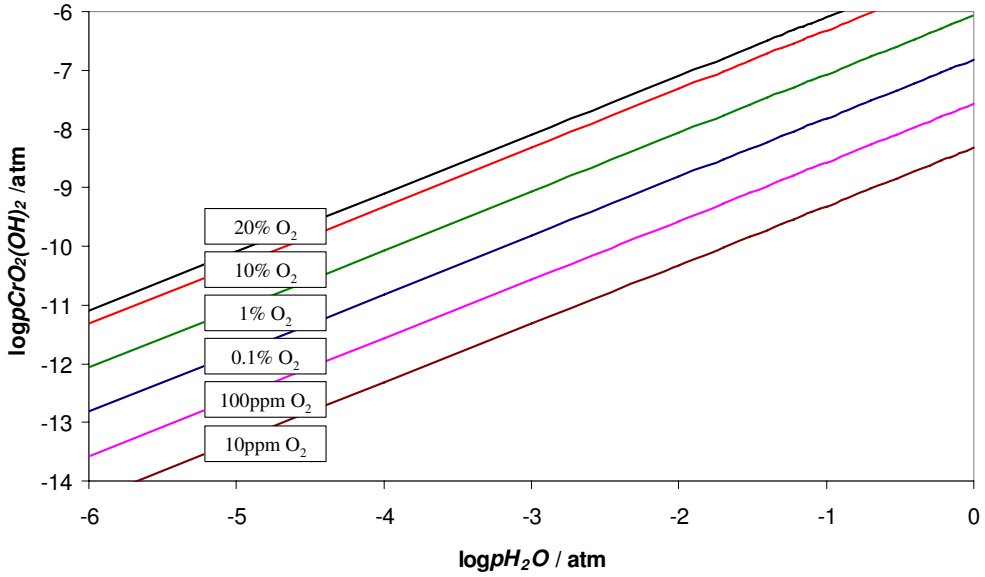

Fig. 58. *Partial pressure of $Cr_2O(OH)_2$ formed in various atmosphere at 1000°C, calculated using data from Opila, [56]*

7.6.2 Oxidation in Ar-0.1%O_2-x%H_2O gas mixtures

Various experiments in Ar-0.1%O_2 with different concentrations of water vapour were carried out. Fig. 59 shows that the oxidation rate in Ar-0.1%O_2-x%H_2O increased with increasing water vapour content. This trend however was altered when 7%H_2O was present in the gas. Then, the mass change was low and very similar to the dry Ar-0.1%O_2. Although some spallation of oxide was recorded during cooling to room temperature the general improvement in oxide adherence was observed in the presence of water vapour. It is seen in the morphologies of the metal/oxide interface shown in Fig. 60.

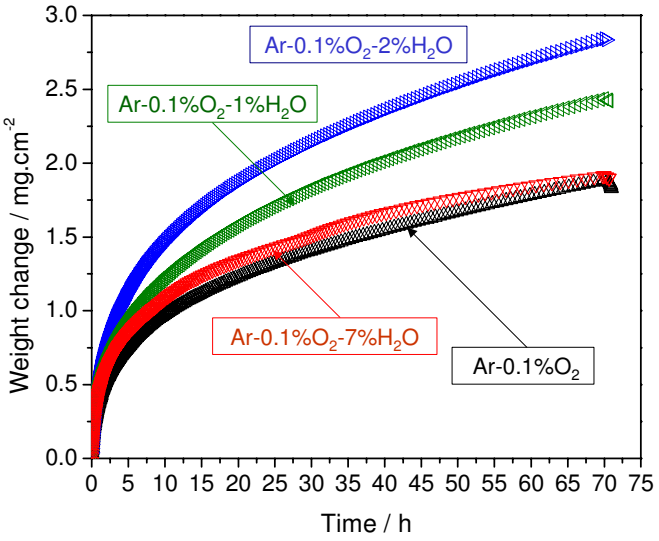

Fig. 59. *Isothermal oxidation of chromium, batch JUG in various, Ar-O_2-H_2O atmospheres at 1000^{o}C*

In Ar-0.1%O_2 gas, the scale was compact and most of the voidages were concentrated at the metal/oxide interface and only minor porosity was found inside the oxide scale, Fig. 60a. Addition of water vapour to Ar-0.1%O_2 gas healed the metal/oxide interface from the pores and the scale became more intact to the metal surface, Fig. 60b-d. Pores, however tended to precipitate in the bulk oxide and their size seemed to be dependent on the amount of water vapour in the gas.

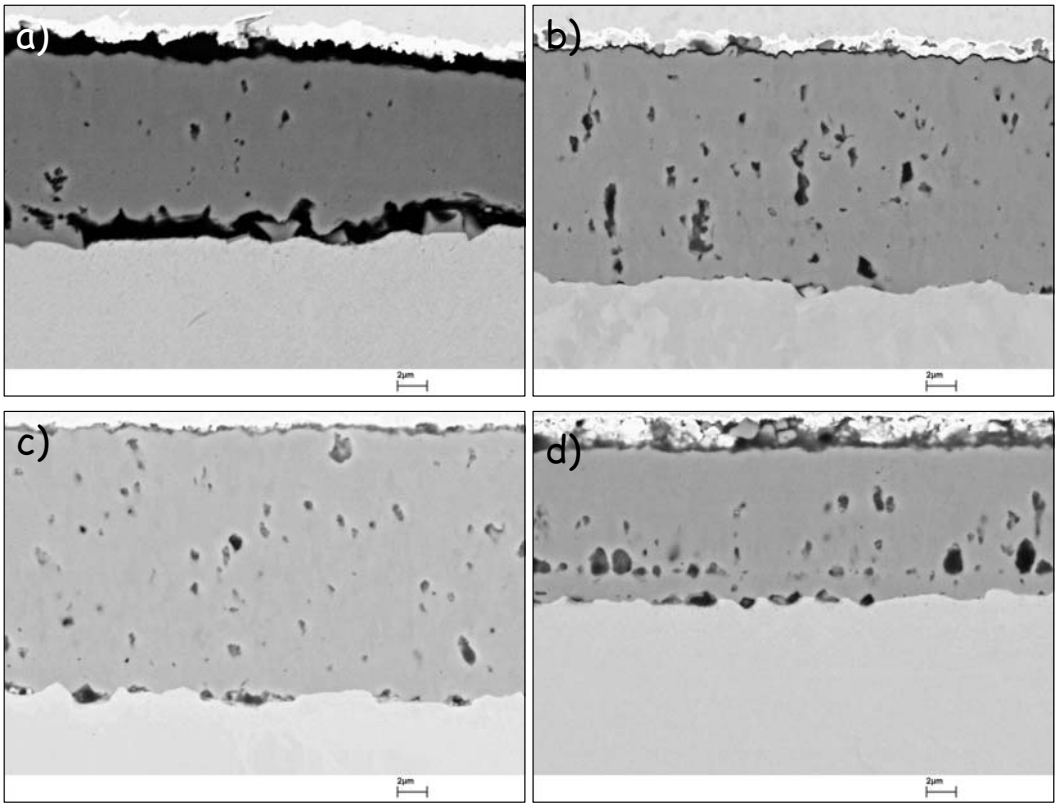

Fig. 60. *SEM images of polished cross-sections of oxide scales formed on chromium, batch JUG after 72h oxidation at 1000°C in a) Ar-0.1%O_2, b) Ar-0.1%O_2-1%H_2O, c) Ar-0.1%O_2-2%H_2O, d) Ar-0.1%O_2-7%H_2O*

The mechanism responsible for the interfacial porosity healing must have been related to the presence of water vapour in the atmosphere and it is believed that enhanced grain boundary diffusion and molecular transport of H_2O and/or H_2 to the metal/oxide interface were the prime reasons for such behaviour. This aspect was discussed in detail in section 7.4, Fig. 51.

Morphologies of the scales confirmed thermogravimetric studies shown in Fig. 59. Thickness of the oxide increased upon addition of a small amount of water vapour and decreased when higher amounts (7%H_2O) of water vapour were present. Such behaviour could be explained when evaporation of Cr-bearing species was high and this case was very likely in the studied atmospheres because it is known that adding H_2O to Ar-O_2 increases the evaporation, Fig. 58, [56]. As was shown in previous chapters, the oxidation rate in Ar-H_2O gas was higher than in any tested Ar-O_2, and one would expect that the addition of water vapour to the Ar-O_2 gas increase the oxidation rate. This was

observed when low amounts of H_2O were added. However with further increase of the water vapour content in the gas, formation of volatile oxy-hydroxides became significant and mass was lost due to enhanced evaporation. In this sense, the effect of water vapour on the oxidation behaviour in Ar-O_2-H_2O gases could be understood as a competitive influence on oxidation and evaporation rates at the same time. The quantitative estimation of evaporation rate will be given in section 7.6.3.

7.6.3 Oxidation in Ar-1%O_2-x%H_2O gas mixtures

In this set of experiments 7% and 10%vol H_2O were added to Ar-1%O_2, Fig. 61. In both cases a reduction in weight change by H_2O addition was observed and again enhanced evaporation was suggested to be the reason of such behaviour. Water vapour additions again improved oxide adherence and the scale did not spall off during cooling to room temperature, as it was the case in dry Ar-1%O_2. Interestingly, extensive in-scale void formation was found in Ar-1%O_2-10%H_2O and only minor in Ar-1%O_2-7%H_2O, Fig. 62b and c. If water vapour improves oxide adherence to the metal, one would not expect such pore formation in Ar-1%O_2-10%H_2O gas. To explain such behaviour, the overall effect of water vapour must be considered. It was proposed that when water vapour is added to the dry Ar-O_2-H_2O gas, the inward transport increases and this is due to enhanced oxygen grain boundary diffusion and molecular transport of H_2O and/or H_2 to the metal/oxide interface where pore formation take place. Therefore increasing the partial pressure of H_2O in the gas should increase the concentration of H_2O at the oxide/metal interface and enhance pore healing. However in Ar-O_2-H_2O mixtures increasing water vapour significantly enhances formation of the $CrO_2(OH)_2$ Tab. 2, and consequently the thin scale formed. This promotes continuous outward transport of chromium from the metal/oxide interface at the same time increasing chromium vacancy flow in the opposite direction. Consequently the competition between formation of interfacial voidage due to fast vacancy condensation and filling of the pores by the inward reaction of H_2O and metal occurs.

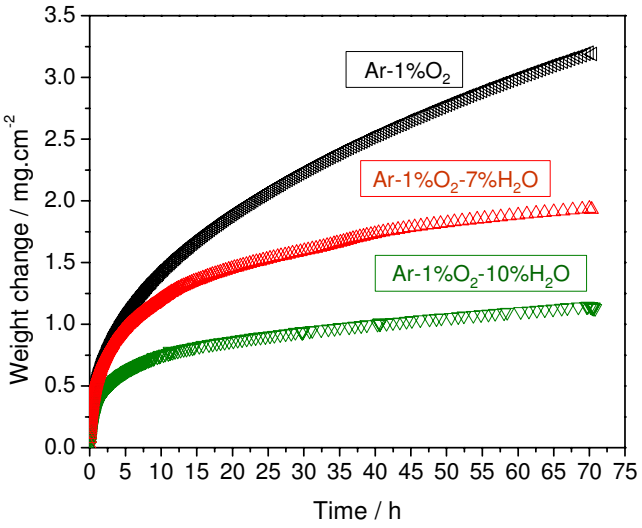

Fig. 61. *Isothermal oxidation of chromium, batch JUG in various Ar-1%O_2-x%H_2O atmospheres at 1000°C*

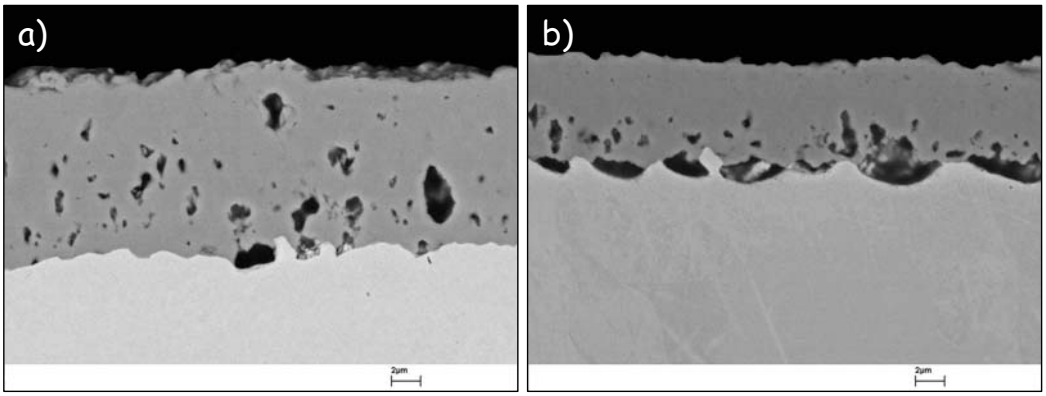

Fig. 62. *SEM images of polished cross-sections of oxide scales formed on chromium, batch JUG after 72h oxidation in a) Ar-1%O_2-7%H_2O, b) Ar-1%O_2-10%H_2O. Scale formed in the Ar-1%O_2 spalled off completely after cooling to room temperature*

It was proposed that the lower weight change recorded in gases containing higher amount of water in combination with 1%O_2 was due to enhanced evaporation rate. Below an attempt for evaporation rate estimation is presented. To simplify it was assumed that $CrO_2(OH)_2$ was only volatile species formed at the outer surface. The partial pressures of that species formed in tested gases are included

in Table 2. Knowing the values of partial pressures enabled to estimate chromium mass transfer from solid oxide to flowing gas. Theory of gas transport in viscous flow regime was applied and required gas properties were used, [82-85]. Similar approach was recently proposed to predict Cr evaporation fluxes during oxidation of Fe-Cr alloy in temperature range 650°-800°C, [86]. The molar flux J of a species is given by

$$J = \frac{k_m}{RT}\left(p^{(i)} - p^{(0)}\right) \tag{37}$$

where: k_m - mass transfer coefficient, $p^{(i)}$ and $p^{(0)}$ - partial pressure of the gas species at the solid surface and in the bulk respectively, R and T - gas constant and temperature.

The value of k_m is given by

$$k_m = 0.664\left(\frac{D_{AB}^4}{\upsilon}\right)^{1/6}\left(\frac{v}{l}\right)^{1/2} \tag{38}$$

where: D_{AB} - binary gas diffusion coefficient, υ - kinematics viscosity, v - the bulk gas linear velocity and l - the sample length. The value of $p^{(0)}$ is approximate as zero and D_{AB} and υ are evaluated from kinetic theory of gases using Chapman-Enskog description. The modelled gases are Ar-x%H_2O, which x is in the range of 1-10. Calculation of the diffusion coefficient is based on simplified model of the gas as a binary mixture, taken here as Ar-$CrO_2(OH)_2$. The required parameter are the collision diameters, σ, of the two gaseous species and the characteristic energy of the interaction, ε, between molecules. Relevant values, together with calculated parameters are listed in Table 11. Data are not available for $CrO_2(OH)_2$ and the values were estimated, [86].

$$\sigma_{AB} = \frac{\sigma_{Ar} + \sigma_{CrO_2(OH)_2}}{2} \tag{39}$$

$$\frac{\varepsilon_{AB}}{k} = \left(\frac{\varepsilon_{Ar}}{k} + \frac{\varepsilon_{CrO_2(OH)_2}}{k}\right)^{1/2} \tag{40}$$

where k - Boltzmann's constant. D_{AB} is calculated from Chapman-Enskog expression:

$$D_{AB} = \frac{1.858\cdot 10^{-3}\sqrt{T^3\left(\frac{1}{M_{Ar}} + \frac{1}{M_{CrO_2(OH)_2}}\right)}}{p\sigma_{AB}^2\Omega_{AB}} \tag{41}$$

where M_{Ar} and $M_{CrO_2(OH)_2}$ denote molecular weight of Ar and $CrO_2(OH)_2$ respectively, p - the total pressure and Ω_{AB} - collision integral, value of which are tabulated as functions of $\frac{kT}{\varepsilon}$. At p =1atm, the ranges of values adopted for σ_{AB} and $\frac{\varepsilon}{k}$ lead to the estimates of D_{AB}.

The viscosity of gaseous species, here it was assumed to be Ar-x%H_2O, η_{mix} is given by

$$\eta = \frac{2.6693 \cdot 10^{-5} \sqrt{MT}}{\sigma \cdot \Omega} \tag{42}$$

the viscosity of a gas mixture is found from:

$$\eta_{mix} = \frac{X_{Ar}\eta_{Ar}M_{Ar}^{1/2} + X_{H_2O}\eta_{H_2O}M_{H_2O}^{1/2}}{X_{Ar}\eta_{Ar} + X_{H_2O}\eta_{H_2O}} \tag{43}$$

where X_{Ar} and X_{H_2O} denote the mole fraction of Ar and H_2O. Values of the kinematics viscosity equals:

$$\upsilon = \frac{\eta_{mix}}{\rho_{mix}} \tag{44}$$

with ρ_{mix} the gas mixture density. The applicability of the equation is related with Schmidt number S_c, which can be estimated by

$$S_c = \frac{v}{D_{AB}} \tag{45}$$

and should be in the range of 0.6-50. This condition was satisfied. The remaining term, $(v/l)^{1/2}$, varies with experimental design and for the present study it was approximately $0.6s^{-1}$ for all gases. The estimated chromium flux is shown in Table 12.

Table 11. *Gas molecular interaction parameters, [86]*

Species	$\sigma, \overset{o}{A}$	ε/k
Ar	3.681	91.5
H_2O	2.641	809
$CrO_2(OH)_2$	4	400

The values of k_m, D_{AB}, υ, v, l, are nearly the same for all modelling gases and are listed below. $k_m = 0.42\ cm \cdot s^{-1}$, $D_{AB} = 1.28\ cm^2 \cdot s^{-1}$, $\upsilon = 2\ cm^2 \cdot s^{-1}$, $v = 0.71\ cm \cdot s^{-1}$, $l = 2\ cm$

Table 12. *Partial pressure of $CrO_2(OH)_2$ and estimated flux of chromium, T=1000°C*

Atmosphere	$p_{CrO_2(OH)_2(g)}$ *atm*	J_{Cr} $g \cdot cm^{-2} \cdot s^{-1}$	*Chromium mass loss after 72h oxidation* $mg \cdot cm^{-2}$
Ar-0.1%O_2-1%H_2O	$3.5x10^{-9}$	$4.1x10^{-13}$	$3.5x10^{-5}$
Ar-0.1%O_2-2%H_2O	$6.9x10^{-9}$	$8.1x10^{-13}$	$7.0x10^{-5}$
Ar-0.1%O_2-7%H_2O	$2.1x10^{-8}$	$2.4x10^{-12}$	$2.1x10^{-4}$
Ar-1%O_2-7%H_2O	$3.4x10^{-8}$	$4.1x10^{-12}$	$3.5x10^{-4}$
Ar-1%O_2-10%H_2O	$4.8x10^{-8}$	$5.7x10^{-12}$	$4.9x10^{-4}$

The calculated values of the chromium loss due to evaporation are far too low to explain the weight change observed in Ar-O_2-H_2O gases containing high amount of water vapour, Fig. 59 and Fig. 61. One could consider that another effect different than the evaporation operated and led to observed weight change reduction or the evaporation rate was dependent on another factor not included in the mass flux estimation. First case is rather unlikely because it was clearly shown that oxidation rate in Ar-H_2O were higher than in Ar-O_2 gases and indeed oxidation rate increased when small amount of water vapour was added to dry Ar-O_2 gas. Therefore it is more probable that another parameter should be taken into account for correct evaporation prediction. For example the model described above assumed that evaporation surface was flat and this was not a real case because the scale roughness increased that surface. It was also shown that oxide scale formed on pure chromium in Ar-O_2-H_2O was porous and if some of the pores were open the evaporation surface could highly increased. This is schematically shown in Fig. 63.

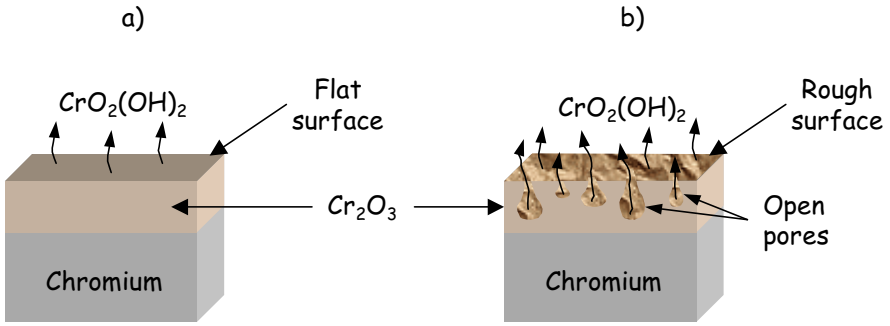

Fig. 63. *Schematic comparison of evaporation rate due to formation of $CrO_2(OH)_2$ in Ar-O_2-H_2O gas in case of a) flat surface of the scale, b) rough surface of the scale with open pores*

Also the value of $CrO_2(OH)_2$ partial pressure is an important parameter because it is proportional to the estimated flux. Substantial scatter in reported values has already been pointed out in section 3.5,

Table 1. And for example estimating the chromium flux in Ar-20%O_2-10%H_2O gas at 950^{o}C using data obtained by Hilpert [55] instead of Opila [56] shows higher values, Table 13.

Table 13. *Estimated evaporation rate due to formation of $CrO_2(OH)_2$ in Ar-20%O_2-10%H_2O at 950^{o}C using data from Opila,* [56] *and Hilpert,* [55]

Data	$J_{Cr},\ g \cdot cm^{-2} \cdot s^{-1}$
Oplia	$7.7x10^{-11}$
Hilpert	$5.9x10^{-10}$

Finally one might also consider that the rate of oxide growth could enhance evaporation kinetics in some way and therefore estimated evaporation rate was lower than in real system. Hänsel studied evaporation rate in Air-7%H_2O at 1000^{o}C under the same gas flow conditions as in this work, [50]. Review was shown in chapter 3.5. Two types of specimens were used, i.e. dense, hot isostatically pressed chromia and specimens of a chromium based oxide dispersion strengthened (ODS) alloy. It was found that in the system when chromia was continuously growing, i.e. Cr-ODS the value of evaporation rate was higher, Table 14.

Table 14. *Evaporation rate and expected mass loss during exposure of sintered Cr_2O_3 and Cr-ODS to Air-7%H_2O at 1000^{o}C, [50]*

Specimen	$J_{Cr},\ g \cdot cm^{-2} \cdot s^{-1}$	Weight loss after 72h of oxidation, $g \cdot cm^{-2}$
Sintered Cr_2O_3	$5.6x10^{-10}$	0.14
Cr-ODS	$1.1x10^{-9}$	0.28

Therefore although presented estimation of chromium flux due to evaporation of $CrO_2(OH)_2$ did not fit with experimental findings it is believed that evaporation of that species was the main reason of reducing the weight change in Ar-0.1%O_2 and Ar-1%O_2 atmospheres containing higher, i.e. 7% and 10% H_2O.

7.6.4 One-stage oxidation in Ar-1%$^{16}O_2$-2%$H_2{}^{18}O$

In previous sections it was shown that oxidation rate was higher in the Ar-H_2O than in the Ar-O_2 atmospheres. It was also found that weight change increased when small amount of H_2O, i.e. 1% or 2%vol were added into in Ar-1%O_2 gas. To learn more about such behaviour the one stage oxidation studies were carried out in the Ar-O_2-H_2O using labelled oxygen isotope. For testing the Ar-1%$^{16}O_2$-2%$H_2{}^{18}O$ gas was chosen and different exposure times, i.e. 0.5h, 1h, 3h, 8h and 24h were applied. Oxidized specimens were analysed subsequently by Sputtered Neutrals Mass Spectroscopy in the similar way as described in section 6.4. Since the same tendency was observed for all experiments only three profiles are presented below, Fig. 64-Fig. 66.

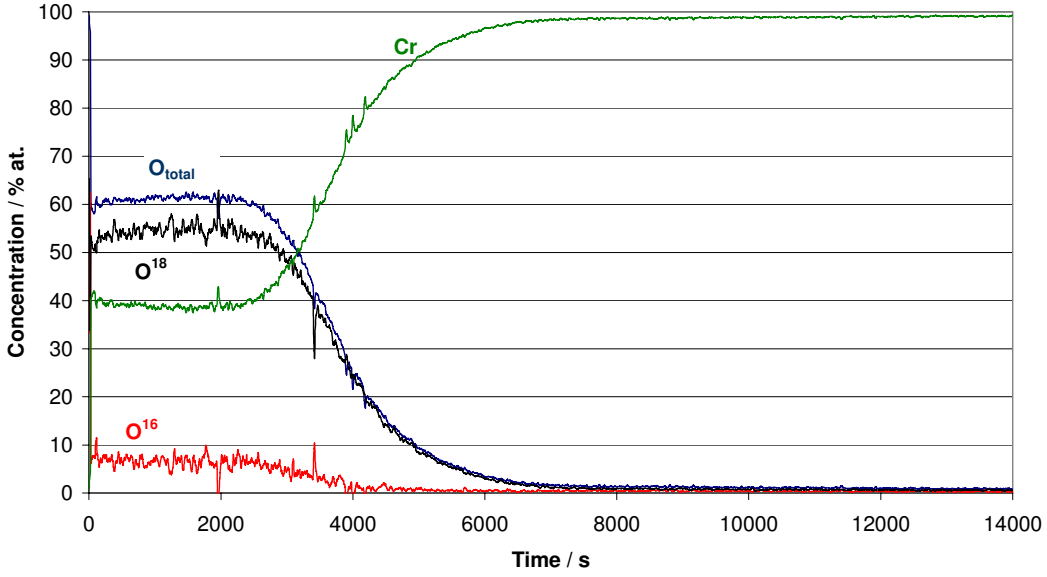

Fig. 64. *SNMS depth profile after one-stage oxidation of chromium, batch JUG, for 0.5h in Ar-1%$^{16}O_2$-2%$H_2{}^{18}O$ at 1000^{o}C*

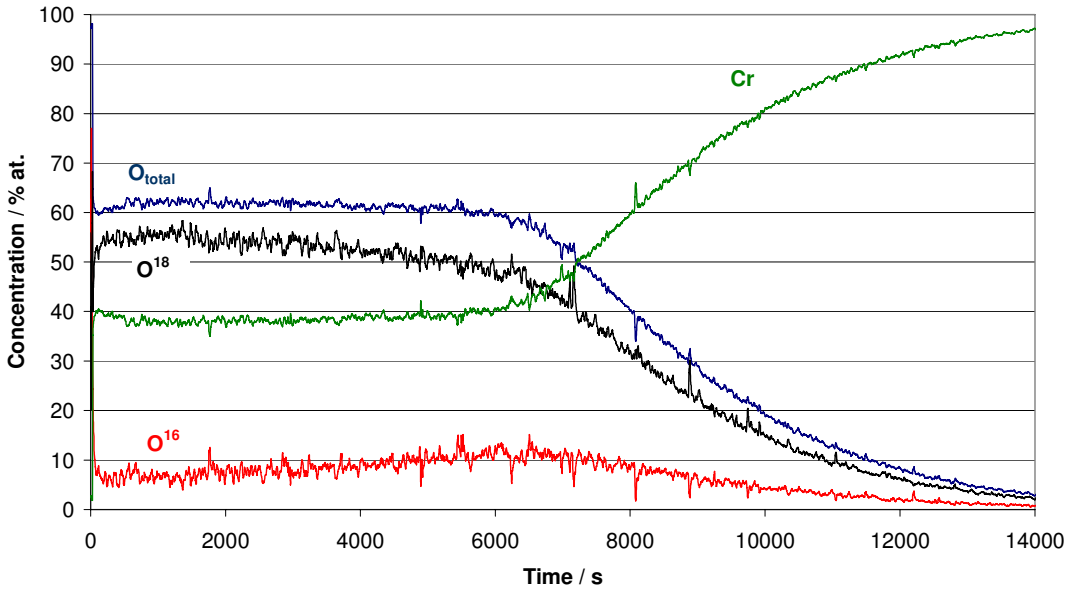

Fig. 65. *SNMS depth profile after one-stage oxidation of chromium, batch JUG, for 3h in Ar-1%$^{16}O_2$-2%$H_2{}^{18}O$ at 1000^{o}C*

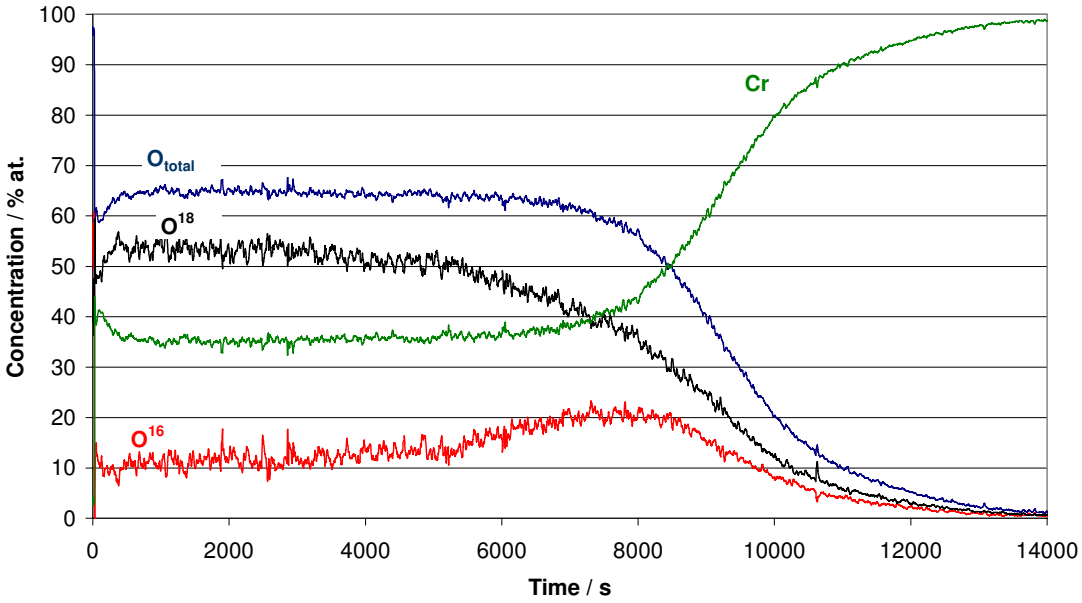

Fig. 66. *SNMS depth profile after one-stage oxidation of chromium, batch JUG, for 8h in Ar-1%$^{16}O_2$-2%$H_2{}^{18}O$ at 1000^{o}C*

It was found that the oxidation process proceeded mainly due to reaction of chromium with oxygen derived from water vapour. This could be attributed that adsorption of H_2O was much faster onto the oxide surface than O_2. In all studied specimens an increase in hydrogen and carbon intensity was found in the scale. This is shown in Fig. 67. The first effect could be related to inward molecular transport of H_2O and/or H_2 to the metal/oxide interface and second with diffusion of carbon from the metal to the metal/oxide interface. Similar findings were observed in Ar-H_2O gas discussed in section 7.2.2. This suggested that water vapour even in small amounts could strongly affect oxidation behaviour of chromium and change the mechanism of oxidation.

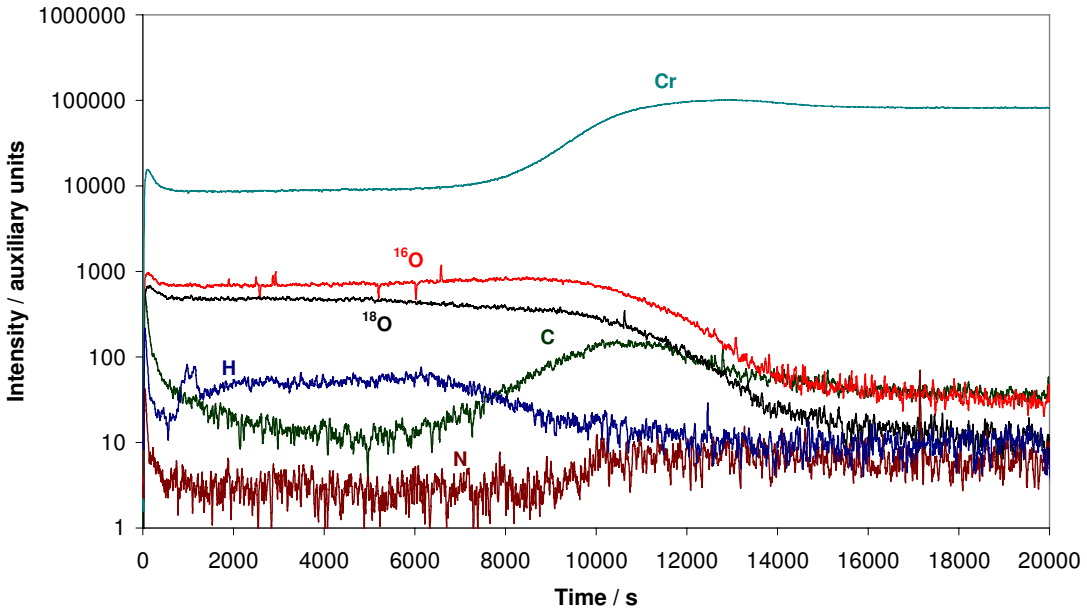

Fig. 67. *SNMS-profile before quantification after one-stage oxidation of chromium, batch JUG for 8h in Ar-1%$^{16}O_2$-2%$H_2{}^{18}O$ at 1000^{o}C*

It must be also noted that after longer oxidation times, (3h), the concentration of ^{16}O increased near the metal/oxide interface. This effect is not completely clear, however a likely explanation is proposed below. At first, based on the two-stage oxidation test in Ar-H_2O presented in Fig. 38 it could be assumed that also in Ar-O_2-H_2O gases the scale growth took place at the gas/oxide interface and to some extent at the oxide/metal interface. Consequently chromium reacted with $H_2{}^{18}O$ and $^{16}O_2$ from the gas at the gas/oxide interface and formed the oxide.

$$2Cr + 3H_2{}^{18}O = Cr_2{}^{18}O_3 + 6H \qquad (46)$$

$$2Cr + \frac{3}{2}{}^{16}O_2 = Cr_2{}^{16}O_3 \quad (47)$$

Fig. 64-Fig. 66 show that in the Ar-1%O_2-2%H_2O reaction of Cr with $H_2{}^{18}O$ and $^{16}O_2$ was approximately in the ratio of 10:2. Therefore formation of the oxide proceeded mainly by the reaction of chromium with oxygen originating from water vapour. However, since the gas also contained molecular oxygen, $^{16}O_2$ was present, the hydrogen revealed from reaction (45) could form $H_2{}^{16}O$ molecules.

$$6H + \frac{3}{2}{}^{16}O_2 = 3H_2{}^{16}O \quad (48)$$

It is believed that the water vapour not only reacted at the gas/oxide interface but also was transferred to the metal/oxide interface and contributed to the inward growth of the oxide. Fig. 38 shows the indication of inward transport in Ar-H_2O gas so very likely that it was also the case in Ar-O_2-H_2O gases. Therefore the concentration profile is the sum of reactions at the gas/oxide and metal/oxide interface. In the early stages of exposure the oxidation rate was fast and surface reactions were the rate-limiting step. Chromium reacted with adsorbed ^{18}O and ^{16}O forming an oxide and some $H_2{}^{18}O$ molecules penetrated the scale and reacted at the metal/oxide interface. As the scale became thicker it was diffusion of chromium that limited the oxidation rate so there were more chances for $H_2{}^{16}O$ to be formed and enter the oxide scale. In such a case concentration of $H_2{}^{16}O$ and in turn ^{16}O increased at the metal/oxide interface and this was observed in the study.

Water vapour affected the oxidation behaviour of chromium when added to O_2 containing gas systems. Two effects were suggested to play a major role. First, it was to enhance the oxidation rate due to faster adsorption of H_2O on to the growing oxide surface than O_2. Second, it was to increase the evaporation rate due to extensive formation of $CrO_2(OH)_2$. Apparently the influence of H_2O on both processes depends on the partial pressure of H_2O and O_2 in the gas. Fig. 64-Fig. 66 showed that the oxide scale formed in Ar-1%$^{16}O_2$-2%$H_2{}^{18}O$ was composed approximately 80% of oxygen derived from water vapour. It could be seen that the possible increase in oxidation rate was met by this 80%. Therefore, a further increase of H_2O in the gas would probably not significantly affect the oxidation rate. But it would have a important influence on the formation of $CrO_2(OH)_2$ and in turn on evaporation rate. Consequently the dominating factor at low pH_2O is enhanced oxidation and at higher pH_2O evaporation rate. The partial pressure of O_2 in the gas is essential because depending on the pO_2 in the gas the addition of H_2O affects differently the oxidation behaviour. It was shown in section 7.1 that increasing the pO_2 in the Ar-O_2 gases the oxidation rate increased. Therefore the addition of H_2O to the Ar-O_2 gas where the pO_2 is low, i.e. Ar-0.1%O_2 must have a much stronger effect on the oxidation rate than to the gases at higher pO_2, i.e. Ar-1%O_2. This is schematically illustrated in Fig. 68.

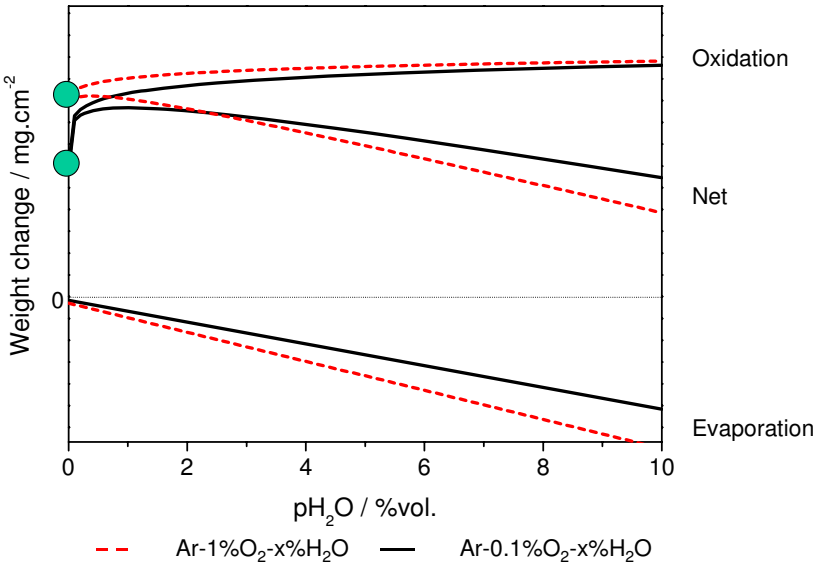

Fig. 68. *Schematic illustration of the effect of water vapour on the oxidation and evaporation rate at low and high pO_2 in Ar-O_2-H_2O gas mixtures*

7.7 Oxidation behaviour of chromium in Ar-H_2-H_2O gas mixtures

Oxidation tests were carried out at 1000°C in various low pO_2 environments generated by mixing H_2 and H_2O at different ratios. For the studies the pH_2O was kept constant and the pH_2 was changed. Additionally two atmospheres with low and high water vapour pressure were chosen and samples were tested for different times up to 312h.

7.7.1 Oxidation in Ar-x%H_2-7%H_2O gas mixtures

Fig. 69 shows weight changes recorded during isothermal oxidation of chromium in different Ar-H_2-H_2O gases at 1000°C. There was always the same amount of H_2O present in the gas, i.e. 7%vol, therefore changes in oxidation behaviour reflected effect of oxygen or/and hydrogen partial pressures.

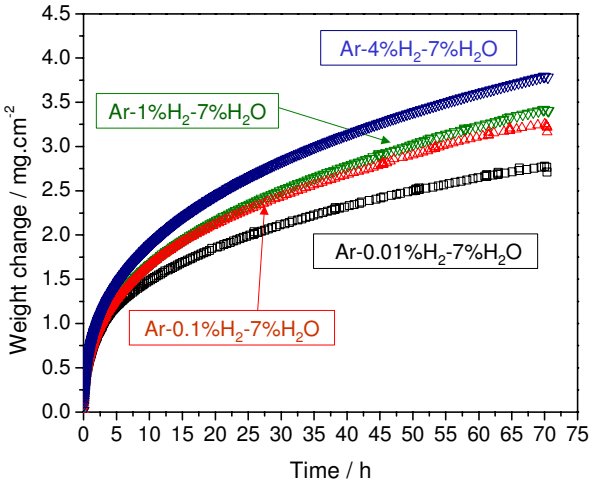

Fig. 69. *Isothermal oxidation of chromium, batch JUG in various, Ar-H_2-H_2O atmospheres at 1000°C*

It was found that the oxidation rate increased when more hydrogen was present in the gas and overall mass gain was generally higher than in dry Ar-O_2 atmospheres. Oxide adherence was relatively good in all cases but some evidence of spallation after cooling to room temperature was found. The extent however, was far less than in dry Ar-O_2 gases. Interesting is the tendency for

oxide spallation being reduced when the pH_2 was increased. Morphologies of the scale formed in the test gases are shown in Fig. 70.

The photographs illustrate the most representative view of morphologies formed but it must be noted that in all tested gases large pores were formed locally near the metal/oxide interface Fig. 71. It was found that the concentration of such pore formation gradually decreased when more hydrogen was present in the gas. Overall the porosity of the oxide scale was affected the most. It was observed that increasing the pH_2 in the gas led to the pores size being reduced. In the Ar-0.01%H_2-7%H_2O a number of relatively large, (around 1μm) pore were formed in the scale and the overall morphology was similar to those formed in only water vapour, Fig. 37. In Ar-4%H_2-7%H_2O scales were free of such large pores.

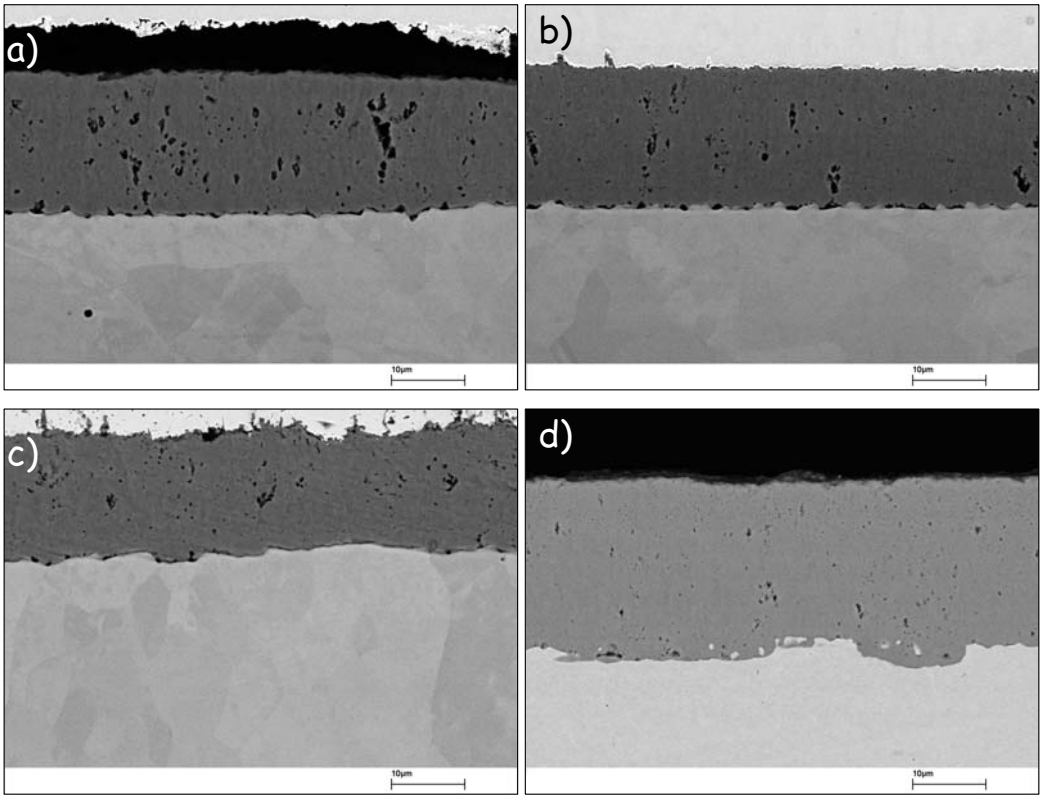

Fig. 70. *SEM image of polished cross-sections of oxide scales formed on chromium, batch JUG after 72h oxidation at 1000°C in a) Ar-0.01%H_2-7%H_2O, b) Ar-0.1%H_2-7%H_2O, c) Ar-1%H_2-7%H_2O and d) Ar-4%H_2-7%H_2O*

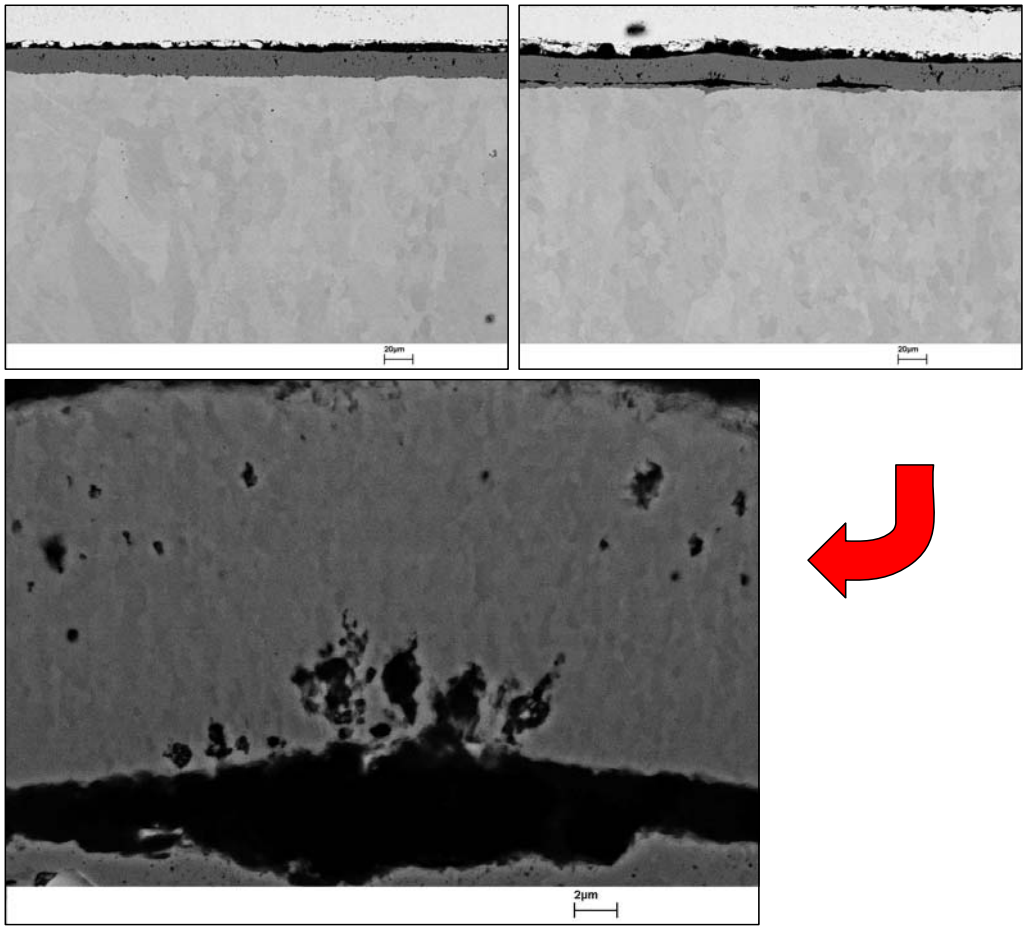

Fig. 71. *SEM images of polished cross-sections of oxide scales formed on chromium, batch JUG after 72h oxidation at 1000°C in Ar-0.01%H_2-7%H_2O, scale morphology was photographed in different regions*

7.7.2 Time dependence of oxidation behaviour of chromium in Ar-H_2-H_2O

Chromium, batch JUG was exposed to Ar-4%H_2-7%H_2O and Ar-3%H_2-30%H_2O at 1000°C for different time up to 312h. For technical reasons a horizontal furnace was used instead of the thermogravimetric setup. Each sample was oxidized separately. This enabled analyses all of scale morphologies formed and at the same time intermediate cooling was avoided. Fig. 72 shows the thickness of the oxide scales measured after the corresponding time exposures.

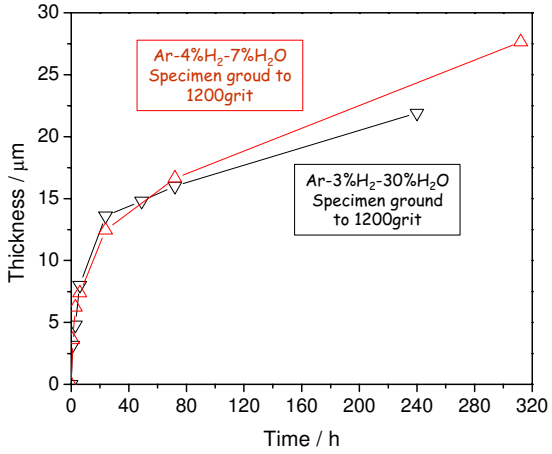

Fig. 72. *Isothermal oxidation of chromium, batch JUG in various, Ar-H_2-H_2O atmospheres at 1000°C, (each experiment was carried out separately in horizontal furnace)*

No significant differences in oxide thickening between samples exposed to Ar-3%H_2-30%H_2O and Ar-4%H_2-7%H_2O were found and in both gases the scale adherences were excellent, Fig. 73 and Fig. 74. After longer oxidation time characteristic type of porosity, was developed inside the scales and well-defined layers were formed. It was particularly pronounced in Ar-3%H_2-30%H_2O, Fig. 73.

Fig. 73. *Metallographic cross-sections of oxide scales formed in Ar-3%H_2-30%H_2O at 1000°C on chromium, batch JUG ground to 1200grit, after oxidation of a) 24h, b) 49h, c) 240h*

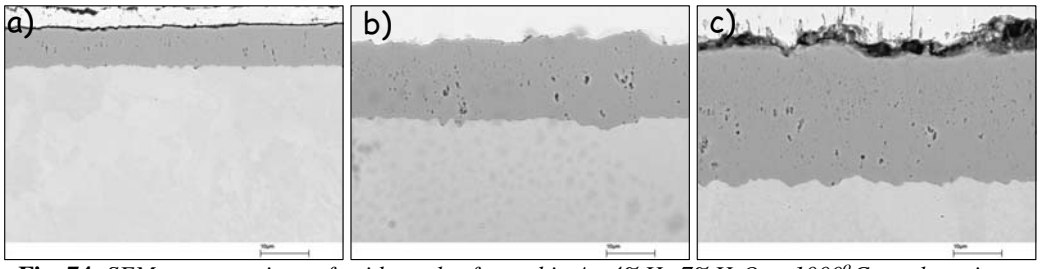

Fig. 74. *SEM cross-sections of oxide scales formed in Ar-4%H_2-7%H_2O at 1000°C on chromium, batch JUG ground to 1200grit, after oxidation of a) 24h, b) 72h, c) 312h*

To confirm such behaviour additional experiments were carried out in Ar-3%H_2-30%H_2O however this time specimens were polished to 1μm prior to oxidation instead of grounding to 1200 grit, Fig. 75. The oxide scale was again composed of two layers, the outer compact and the inner very porous.

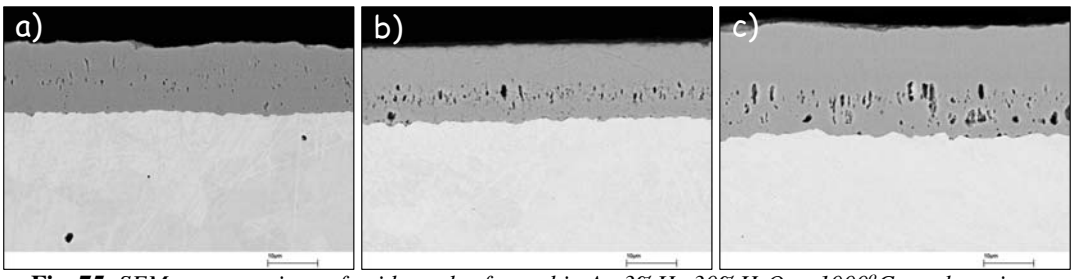

Fig. 75. *SEM cross-sections of oxide scales formed in Ar-3%H_2-30%H_2O at 1000°C on chromium, batch JUG polished to 1μm, after oxidation of a) 24h, b) 49h, c) 240h*

Formation of such duplex structure has been reported for many systems and is usually related to oxidation of alloys or metals of low purity [3,87-89]. In the case of films grown on alloys the two layers usually have different chemical composition and in case of pure metals these layers differ in their microstructure. Studies on different oxides using the sequential $^{16}O/^{18}O$ oxidation techniques showed that final distribution of ^{18}O is consistent with the outer layer of the scale growing by the outward diffusion of cations while the inner layer grows by the inward short circuit transport of oxygen, [90-94].

Atkinson based on the tracer measurements excluded oxygen grain boundary diffusion and suggested penetration of the oxide by gas molecules, [87]. It seems to be in agreement with study of Pritchard who found ^{14}C in the inner layer of duplex films when a second oxidation stage was carried out in $^{14}CO_2$ [95]. This could indicate that formation of the inner porous layer is connected with inner transport of gaseous molecules. It should be noted that this process seems to be time dependent. Atkinson in his other work pointed out that in the early stages of oxidation the inner transport is restricted and depends on the system it started to proceeds at some thickness of the scale, [89]. This suggestion is very reasonable because the porosity usually increases in the scale with the time and therefore the fast diffusion paths in the scale are created. Clear indications of time dependence of pores growth are showed in Fig. 74.

Mrowec et al studied formation of duplex structure during the sulfidation of Fe, [96,97]. The authors proposed that formation of such structure is related with interfacial voids developing at the

metal/oxide interface. In that sense the oxide above the detached area still has a gradient of chemical potential across it and metal ions will continue to migrate outwards. As consequence the metal chemical potential falls and the pO_2 rises. Thus the oxide dissociates sending metals ions outwards through the film and oxygen as gas into the void space, and the oxygen is available for further oxidation of the metal substrate. This process, however seems to be very much dependent on the particular system and composition of external gas.

For instance in the present studies formation of duplex layer structure was very pronounced in Ar-3%H_2-30%H_2O and only to small extent in Ar-4%H_2-7%H_2O, Fig. 73 and Fig. 74. The question arises which factor was the key: water vapour, oxygen or hydrogen partial pressure. Oxygen partial pressure equalled approximately $9x10^{-15}$ and $3x10^{-13}$ atm for Ar-4%H_2-7%H_2O and Ar-3%H_2-30%H_2O respectively. Therefore if the pO_2 were the reason, a similar morphology would be formed in Ar-1%H_2-7%H_2O, Fig. 70c because the oxygen partial pressure was nearly the same as in Ar-3%H_2-30%H_2O, i.e. $1.3x10^{-13}$atm but this was not the case. One could account for action of hydrogen on slowing down pore growth as shown in Fig. 70, however between the Ar-4%H_2-7%H_2O and Ar-3%H_2-30%H_2O gases there was no significant difference in hydrogen content. Therefore the water vapour partial pressure must have been the prime reason of extensive void formation inside the scale. Also studies carried out in Ar-O_2-H_2O atmospheres, section 7.6, indicated that H_2O enhances pore formation, namely larger pores were formed in scales grown in the high water vapour containing atmospheres. The most pronounced scale separation for the outer nonporous and inner porous layer occurred when chromium was oxidized in Ar-1%O_2-10%H_2O, Fig. 62c and this also indicates that the pressure of water vapour must have had a strong influence on pore formation. The exact action of water vapour on the pores development is not completely clear but it is believed that fast adsorption and modification of oxide grains structures seem to be the main factors affected. These aspects were considered in detailed in section 7.3.

Another phenomenon often observed during exposure of chromium to the low pO_2 gases was local formation of very large void near metal/oxide interface, Fig. 76. Two important features are essential to note. First is that although such pronounced separation occurred metal surface was still covered by a layer of oxide which suggests that inward growth still proceeded. And second that the small pores, resulting from dissociation of oxide at the oxide/pore interface are present in the inner oxide scale separated from the substrate. It could be speculate that in the early stages of oxidation, reaction rate was very fast and due to high growth stresses the scale could be detached along pores formed near

the metal/oxide interface. The photographs showed very convincingly that great numbers of whiskers were formed on the surface. This could explain high oxidation rates in the early stages.

It is also important to note that oxide grain formed in low pO_2 gases such as Ar-4%H_2-7%H_2O were extremely fine, Fig. 76. Similar microstructure was found after early stages of oxidation in the Ar-7%H_2O, Fig. 42 and it was proposed that such an oxide morphology development was related to the faster adsorption and dissociation of H_2O at the outer surface than O_2. This aspect was discussed in detailed in section 7.3 and 7.4.

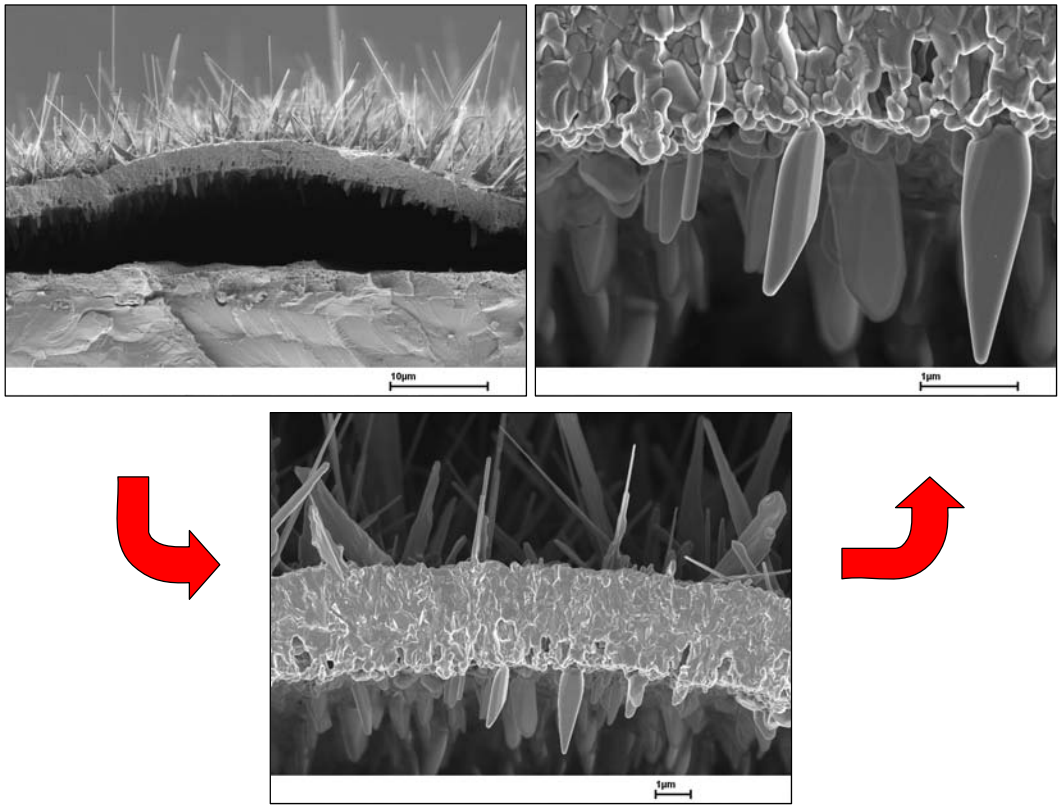

Fig. 76. *SEM fracture sections of oxide scales formed on chromium, batch JUG after 5h oxidation in Ar-4%H_2-7%H_2O at 1000^oC*

Since inward transport of oxygen bearing species seems to be the important factor in understanding oxidation behaviour in low pO_2 gases, especially in term of duplex layer formation, the tracer studies were carried out and are discussed in next section.

7.7.3 Two-stage oxidation in Ar-4%H_2-2%$H_2{}^{16}O$/Ar-4%H_2-2%$H_2{}^{18}O$

To get more information about the way of scale growth process in the Ar-H_2-H_2O atmospheres, the chromium sample was exposed at 1000°C to Ar-4%H_2-2%$H_2{}^{16}O$ for 3 hours and then the atmosphere was changed in-situ to Ar-4%H_2-2%$H_2{}^{18}O$ for another 3h. After that the specimen was analysed by Sputtered Neutrals Mass Spectroscopy to determine the trace distribution in the scale, Fig. 77. The procedure was described in section 6.4.

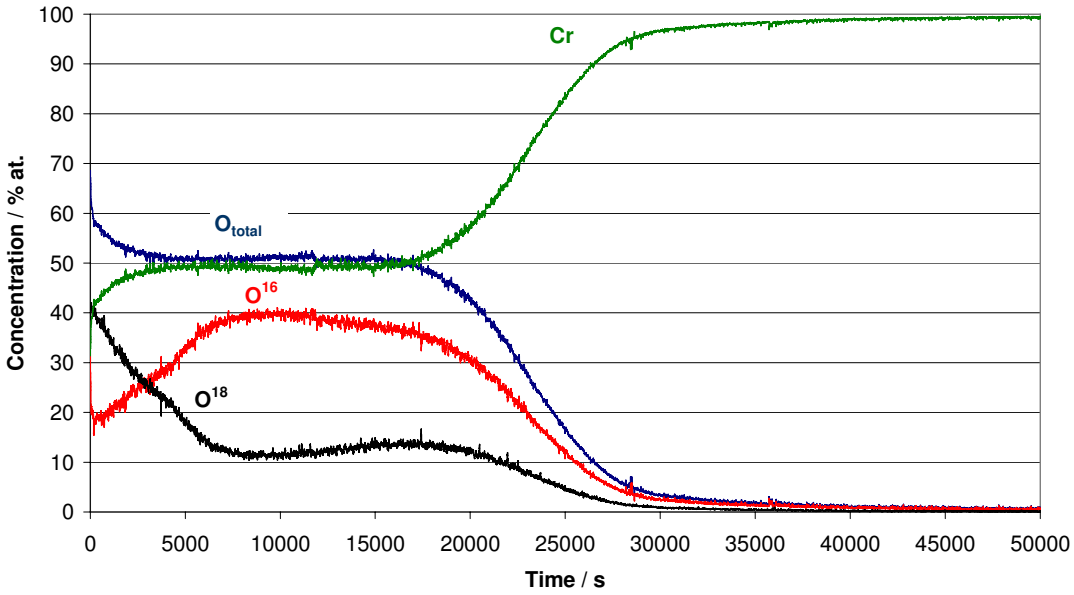

Fig. 77. *Two-stage oxidation of chromium, batch JUG for 3h in Ar-4%H_2-2%$H_2{}^{16}O$ / 3h in Ar-4%H_2-2%$H_2{}^{18}O$ at 1000°C*

It was found that concentration of ^{18}O isotope was high in the outer part of the scale. However, significant enrichment was also seen at the metal/oxide interface. A very similar behaviour was found in case of two-stage oxidation in Ar-2%$H_2{}^{16}O$/Ar-2%$H_2{}^{18}O$, Fig. 38, only the inner enrichment in ^{18}O was less pronounced compared to the Ar-4%H_2-2%$H_2{}^{16}O$ / Ar-4%H_2-2%$H_2{}^{18}O$. It was proposed that it could be an indication that the oxide growth occurred not only at the gas/oxide interface but to some extent also at the metal/oxide interface. Therefore it is believed that oxidation mechanism in Ar-H_2-H_2O must be similar to those in the Ar-H_2O and can be described as in section 7.4.

It was found that exposures of chromium to the Ar-H_2-H_2O generally showed higher oxidation rates and better scale adherence than those formed in the dry Ar-O_2. It was found that the oxide grains formed in Ar-H_2-H_2O were significantly smaller than in the Ar-O_2 and it is believed that such an oxide morphology development was related to the faster adsorption and dissociation of H_2O at the outer surface than O_2. Clear evidence of inward scale growth during oxidation in the Ar-H_2-H_2O was found and it is believed to be a consequence of the smaller oxide grain microstructure. It is suggested that inward oxygen grain boundary diffusion was the most enhanced by the development of the fine-grained microstructure. However, molecular transport of H_2O and H_2 through the scale could also operate and contribute to the inner scale growth due to formation of H_2O/H_2 bridges in scale voids.

7.8 Oxidation behaviour of chromium in multicomponent gas mixtures

7.8.1 General remarks

Reactions of chromium and chromia forming alloys with mixed gases were used to identify conditions under which chromia scales were permeable to carbon and nitrogen. As discussed in previous sections, different oxide scale morphologies and oxidation kinetics were observed, depending on partial pressure of oxygen and water vapour. Introducing N_2 or CO-CO_2 into the reactive gas caused further complication in the oxidation mechanism and has not been well understood so far. However, reactions of chromium with multicomponent gas mixtures are of particular importance in understanding transport mechanisms through chromia scales, because it is commonly considered that the carbides and nitrides can only be formed in the substrate alloy if the growing oxide is permeable to nitrogen or carbon [29-31].

In following studies oxidation tests were carried out in various N_2- or CO-containing atmospheres including low and high pO_2 gases with and without water vapour. Two temperatures were used, 950^{o}C and 1000^{o}C. Specimens were exposed to test atmospheres for various times. As standard exposure time of 72h was chosen to enable comparison of the results with previously studied atmospheres, but also the early stages of oxidation were investigated, 24h.

7.8.2 Oxidation behaviour at 1000°C

Fig. 78 shows the oxidation behaviour of chromium, batch JUG in N_2-1%O_2 and N_2-1%O_2-7%H_2O at 1000°C. In the early stages of oxidation, the weight changes of specimens were similar. However, after approximately 35h a significant increase in the oxidation rate was observed in the N_2-1%O_2-7%H_2O and total weight change recorded after 72h in that atmosphere was higher than in the N_2-1%O_2. Scale adherence in N_2-1%O_2-7%H_2O gas was good and only minor spallation was seen. In contrast, in dry N_2-1%O_2 gas, no speeding up of the oxidation rate was observed during isothermal oxidation and the scale spalled off completely after cooling to room temperature.

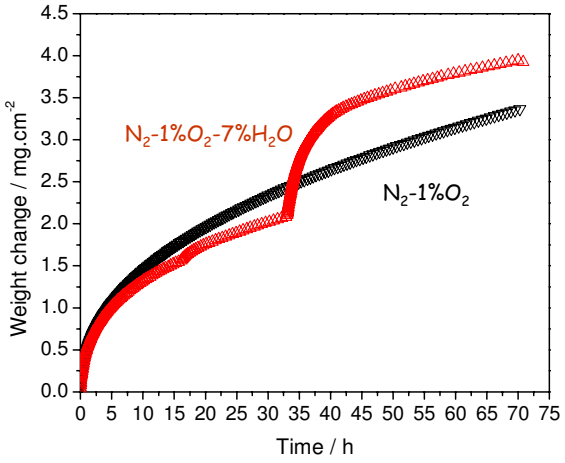

Fig. 78. *Isothermal oxidation of chromium, batch JUG at 1000°C in N_2-1%O_2 and N_2-1%O_2-7%H_2O gases. Scale formed in the N_2-1%O_2 spalled off after cooling to room temperature*

Morphologies of the scale formed in the gases are shown in Fig. 79 and Fig. 80. Care should be taken in evaluating the scale thickness as the presented photomicrographs were taken using fracture sections of the samples. In the N_2-1%O_2-7%H_2O beneath the chromium oxide, a thick layer of nitride was formed. A number of pores were observed in the oxide and especially at the nitride/oxide interface. The nitride layer seemed to be pore-free. During oxide growth the scale heavily buckled and surface cracks were formed along the convoluted area, Fig. 79. In the N_2-1%O_2 the spalled-off scale did not show evidence of nitridation in the outer and inner parts, Fig. 80. The remaining specimen surface was analysed using XRD, Fig. 81 and additionally metallographic cross-section of the sample was performed and examined using SEM coupled with EDX, Fig. 82. CrN and Cr_2N were detected but it must be noted that the nitride layer was significantly thinner than after exposure in the N_2-1%O_2-7%H_2O and it was formed only locally. This suggested that penetration of nitrogen

through oxide scale grown in the N_2-1%O_2 was pretty much restricted compared to the N_2-1%O_2-7%H_2O.

A comparison of the oxidation behaviour of chromium in N_2-1%O_2 and Ar-1%O_2 gases at 1000°C, Fig. 83a, shows that the weight changes in both gases were nearly the same, whereas a similar comparison for N_2-1%O_2-7%H_2O and Ar-1%O_2-7%H_2O revealed a significant increase in oxidation rate in the N_2-containing gas in which thick nitride layer was formed, Fig. 83b. This could also indicate that nitrogen ingress was much lower in N_2-1%O_2 than in N_2-1%O_2-7%H_2O.

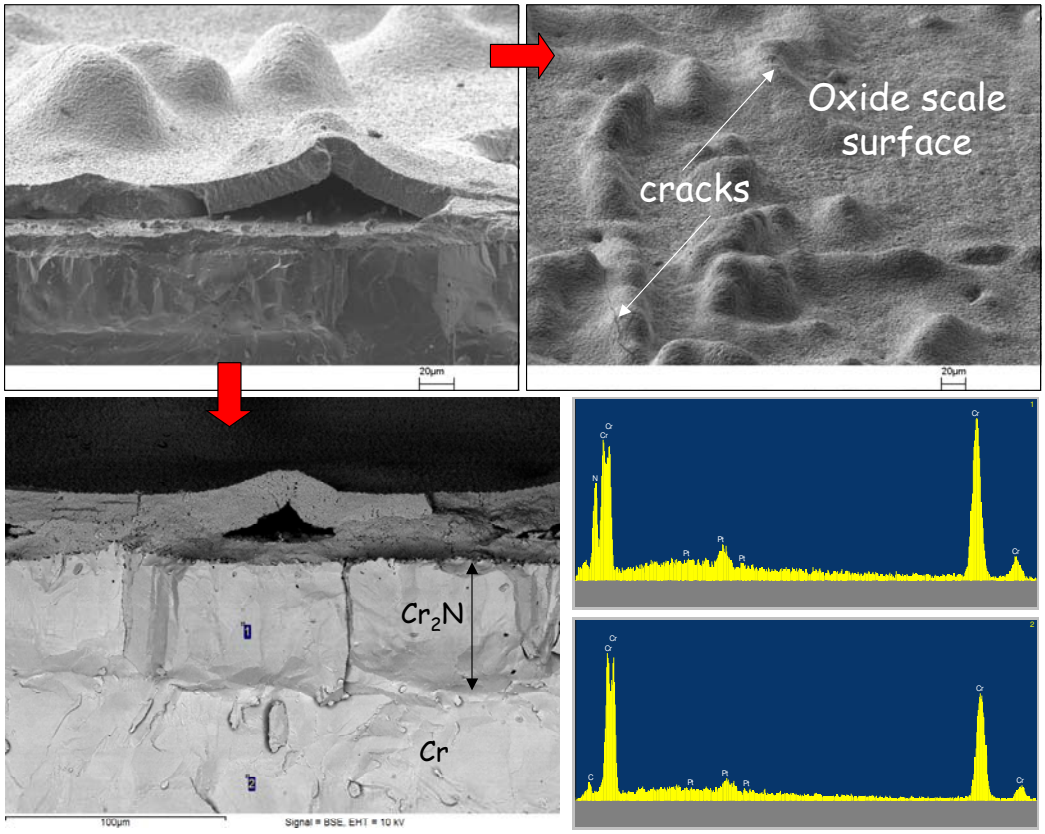

Fig. 79. *SEM cross-sections of scale formed on chromium, batch JUG after 72h isothermal oxidation in the N_2-1%O_2-7%H_2O at 1000°C and EDX spectra taken from points 1 and 2*

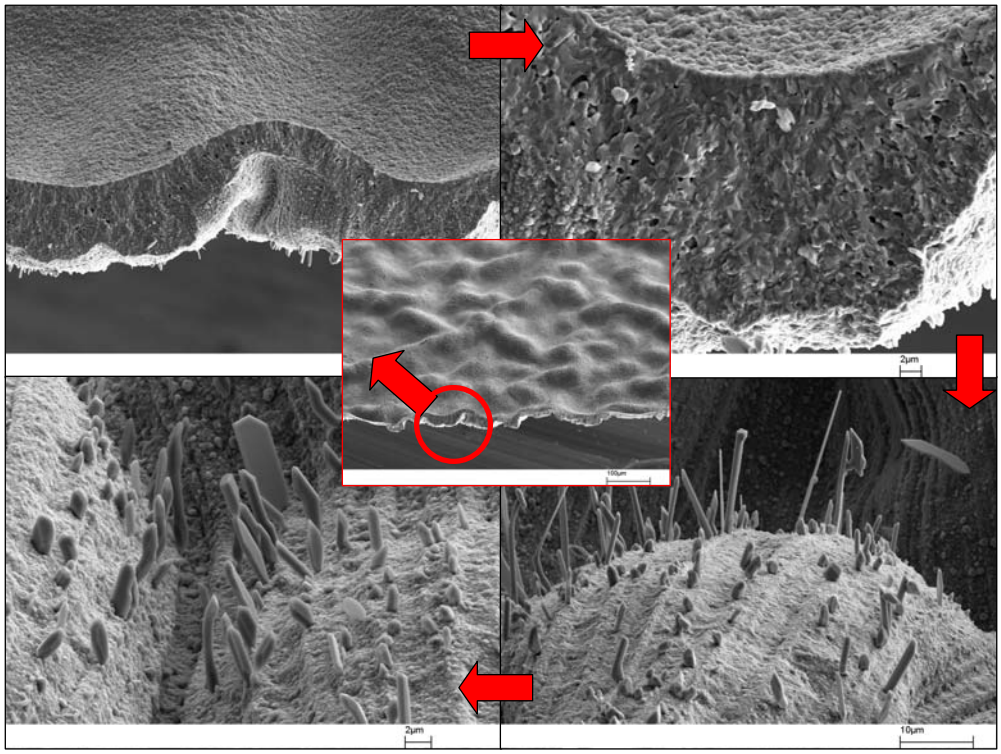

Fig. 80. *SEM sections of scale formed on chromium, batch JUG after 72h isothermal oxidation in the N_2-1%O_2 at 1000^{o}C*

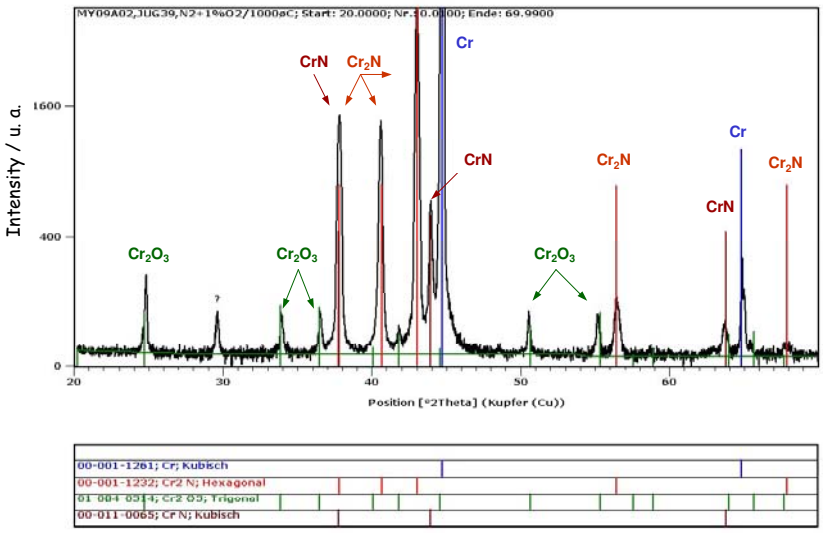

Fig. 81. *XRD patterns recorded on specimen surface, chromium batch JUG oxidized in the N_2-1%O_2 for 72h at 1000^{o}C. The oxide layer spalled off during cooling to room temperature and only metal surface was analysed*

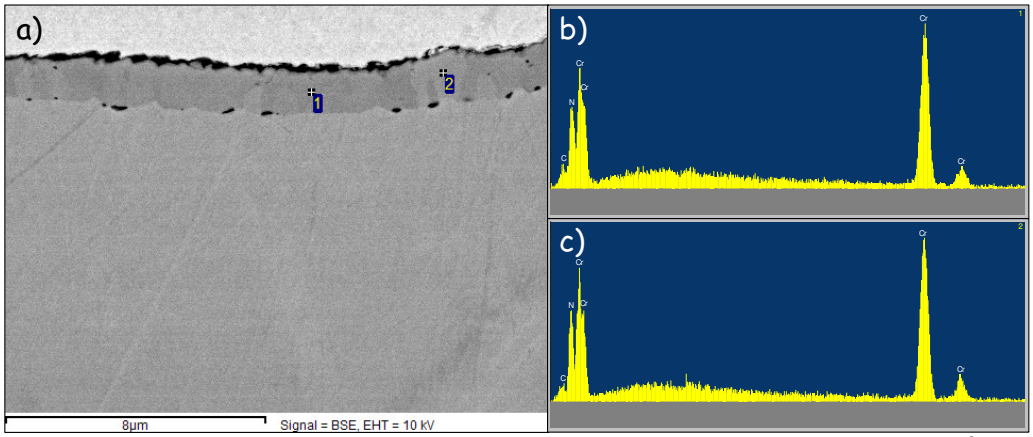

Fig. 82. *a) SEM cross-section of chromium batch JUG exposed to the N_2-1%O_2 for 72h at 1000°C. Scale spalled off during cooling revealing remaining nitrides, b) and c) EDX measured spectra in point 1 and 2*

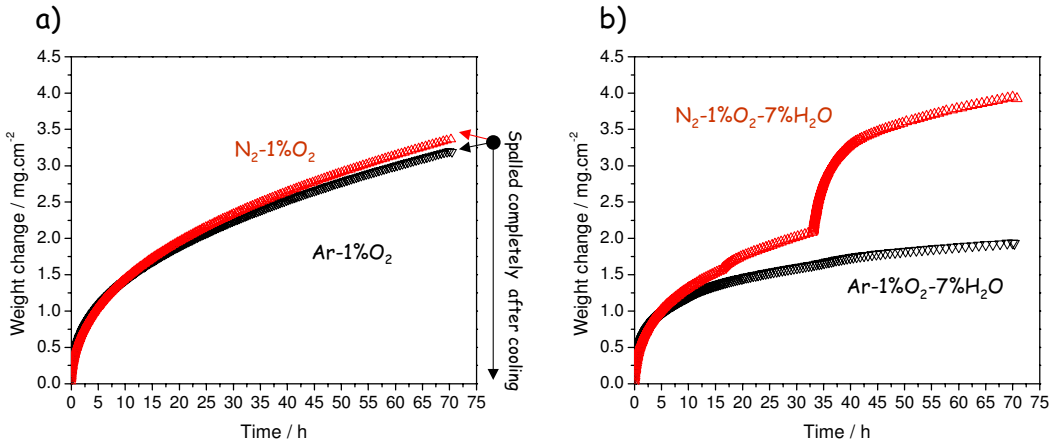

Fig. 83. *Isothermal oxidation of chromium, batch JUG in a) N_2-(Ar-)1%O_2 and b) N_2-(Ar-)1%O_2-7%H_2O gases at 1000°C*

The above study clearly suggested that water vapour played an important role in the transport process of nitrogen through the oxide scale. It was seen that in N_2-1%O_2 gases the scale penetration by nitrogen was significantly reduced compared with the N_2-1%O_2-7%H_2O. It has been reported that nitridation often occurs in chromium when exposed to high pO_2 gases [57-62]. However most of the studies were carried out in laboratory air and the effect of atmospheric conditions such as temperature and humidity was not always considered. Simple calculation shows that air may well contain more than 2 vol. -% of water vapour when humidity and temperature are high and this factor

could be very important in the overall behaviour. Indications that a low concentration of water vapour promotes the formation of nitrides beneath the oxide scale could be found in work of Jacob et al. [68]. These authors performed one- and two-stage oxidations at 800°C in N_2-O_2 and N_2-O_2-H_2O atmospheres using labelled oxygen and nitrogen isotopes, Fig. 84. It both cases evidences of nitrogen in the scale were found. However, only in the N_2-O_2-H_2O gas was significant enrichment observed near the metal/oxide interface.

Another interesting aspect of this study was the periodical weight increase recorded during isothermal exposure in the N_2-1%O_2-7%H_2O gas. This could be related to nitride formation beneath the oxide scale. It is known that the hardness of chromium nitride is considerably higher than that of chromium metal and thus the ability to plastically deform should be lower, when nitrides formed beneath the oxide [68-70]. Buscail et al measured hardness of the chromium nitrides formed beneath oxide scale in synthetic humidified air at different temperatures as a function of depth, Fig. 85, [69]. The authors suggested that the higher hardness of nitrides could hinder plastic deformation of the substrate and thus prevent relaxation of growth stresses. This in turn could promote scale cracking giving periodical access of oxygen to new metallic surface.

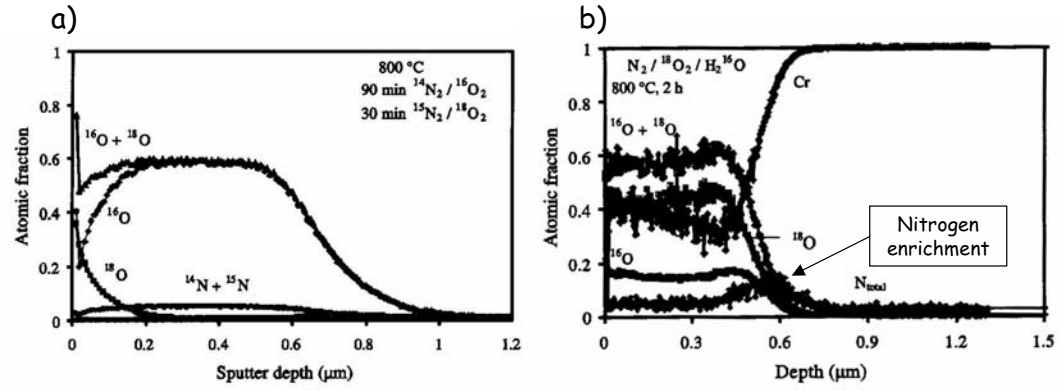

Fig. 84. *Oxygen and nitrogen isotope distribution profiles for chromium after oxidation at 800°C a) two stage oxidation, 90 min in $^{14}N_2$-20%$^{16}O_2$ and 30 min in $^{15}N_2$-20%$^{18}O_2$ and b) one stage oxidation, 120 min in $^{15}N_2$-20%$^{18}O_2$-1%$H_2{}^{16}O$, [68]*

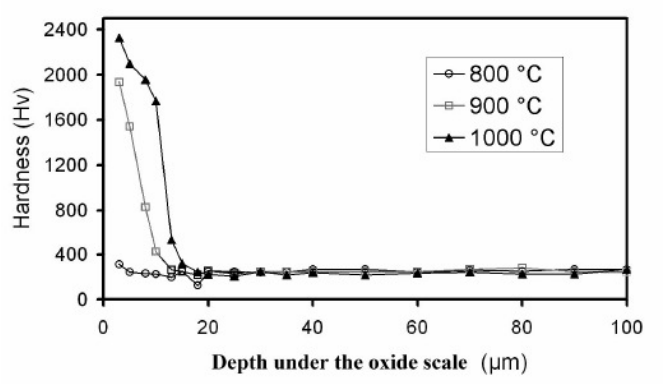

Fig. 85. *Average hardness vs. depth in the metallic substrate below the oxide scale for specimen oxidised in synthetic humidified air at 800, 900 and 1000 °C, during 150 h., [69]*

7.8.3 Oxidation behaviour at 950°C

Sets of experiments were carried out in N_2-containing gases at various oxygen partial pressures. The test temperature was lowered to 950°C to improve oxide scale adherence.

Fig. 86 shows the isothermal oxidation of chromium in various gases containing, 2%vol water vapour. It could be seen that in high pO_2 gases, i.e. N_2-1%O_2-2%H_2O and N_2-20%O_2-2%H_2O, the oxidation rate increased with increasing oxygen partial pressure in the gas but in the low pO_2 gas, N_2-10%H_2-2%H_2O, where molecular oxygen was absent, the oxidation rate was the highest. The morphologies of the oxide scale are shown in Fig. 87. In both high pO_2 gases, the nitride layer was formed beneath oxide scale whereas only chromia was present after exposure to the low pO_2 gas. Additionally it was found that absolute oxygen partial pressure had an influence on oxide cracking during the process. It was found that oxidation rate periodically increased in the N_2-20%O_2-2%H_2O atmosphere. This, however, had hardly any effect on the scale adherence which was good in both gases.

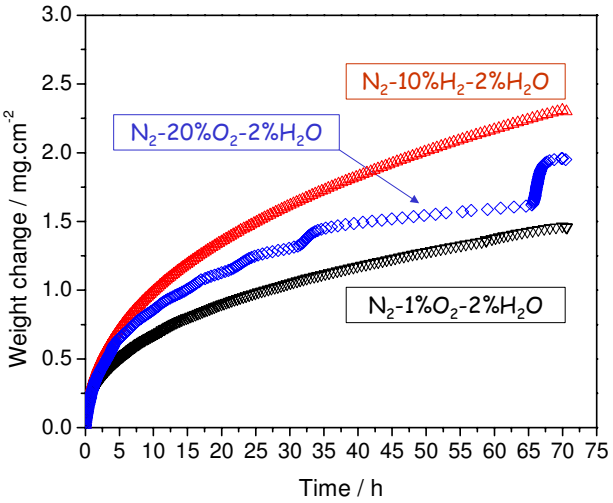

Fig. 86. *Isothermal oxidation of chromium, batch JUG at 950°C in the N_2-1%O_2-2%H_2O, N_2-20%O_2-2%H_2O and N_2-10%H_2-2%H_2O gases*

The important question arises why the nitridation was restrained in N_2-10%H_2-2%H_2O gas and not in N_2-1%O_2-2%H_2O and N_2-20%O_2-2%H_2O gases. This can be related with several factors but fast adsorption of water vapour on the surface seemed to play the major role. It has been established that dissociation and adsorption of H_2O on chromium is very fast compared to O_2 or N_2, [67,68]. Therefore it is expected that increasing the ratio of H_2O to N_2 should result in blocking the access of nitrogen to the surface and hampering nitridation. It is believed that the absolute value of oxygen partial pressure in the gas is also important for the adsorption and dissociation of H_2O and although no data are available for chromia it is very reasonable to assume inverse proportionality, i.e. the lower the pO_2 in the gas the faster the dissociation of water. In that sense in N_2-O_2-H_2O gas more water vapour is required to block nitrogen ingress in comparison to the N_2-H_2-H_2O.

It should be also noted that H_2O could significantly affect the development of chromia scale morphology. It was shown that chromium exposed to Ar-7%H_2O at 1000°C, Fig. 42 formed significantly smaller oxide grains than in Ar-20%O_2, Fig. 41. A similar effect of water vapour may be expected in relevant atmospheres composed of N_2 instead of Ar. If this were the case, the addition of a small amount of water vapour to N_2-O_2 gas could promote nitridation as the inward transport is enhanced and addition of higher concentration of H_2O to N_2-O_2 gas could hamper nitridation because of preferential adsorption of water vapour on the scale surface blocking nitrogen access to

the scale. In chapter 7.8.4 it will be shown that indeed high concentration of water vapour (10%vol.) added to N_2-1%O_2 gas at 950°C completely blocked nitrogen ingress to the scale.

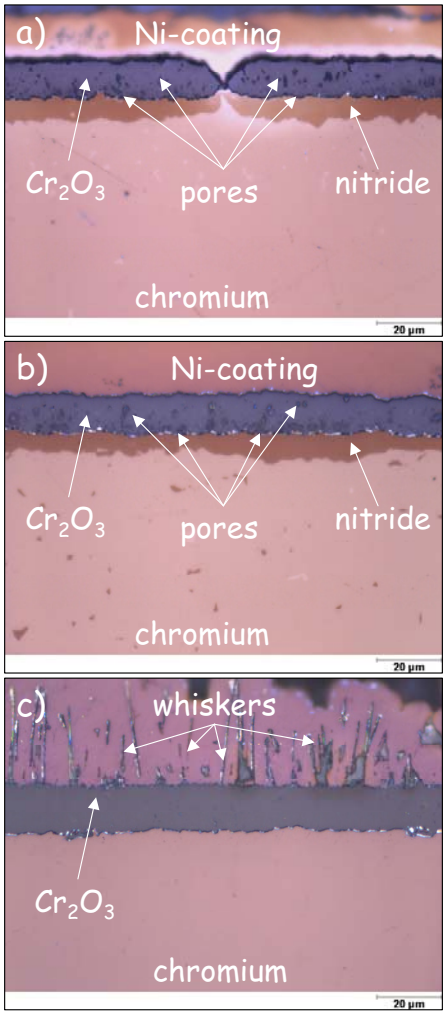

Fig. 87. *Metallographic cross-sections of oxide scale formed on pure chromium after 24h isothermal oxidation of chromium at 950°C in a) N_2-1%O_2-2%H_2O, b) N_2-20%O_2-2%H_2O and c) N_2-10%H_2-2%H_2O, surface was contrasted by sputtering iron oxide on it*

7.8.4 Early stages of oxidation at 950°C

Fig. 88 shows the weight change recorded after 24h exposures of chromium to various N_2-O_2-H_2O gases and Fig. 89 shows an example of the differences in oxidation behaviour. It was found that in N_2-O_2-H_2O or N_2-H_2O atmospheres containing a high concentration of water the weight changes were significantly lower than in gases containing low concentrations of water vapour. This was especially pronounced in all gases containing 10%vol. H_2O, i.e. N_2-1%O_2-10%H_2O, N_2-20%O_2-10%H_2O and N_2-40%O_2-10%H_2O. In the N_2-1%O_2, N_2-1%O_2-0.05%H_2O as well as N_2-1%H_2O the weight changes were substantially higher, even up to three times in comparison to high water vapour content gases. It was observed that the addition of water vapour affected scale adherence and formation of nitride beneath the oxide scale.

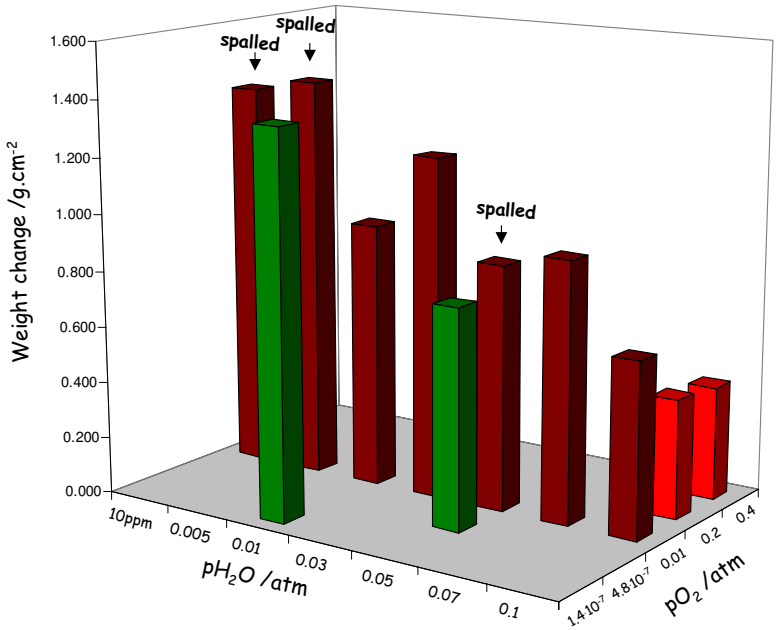

Fig. 88. *Weight change after 24h isothermal oxidation of chromium, batch JUG at 950°C in atmospheres containing various amount of H_2O*

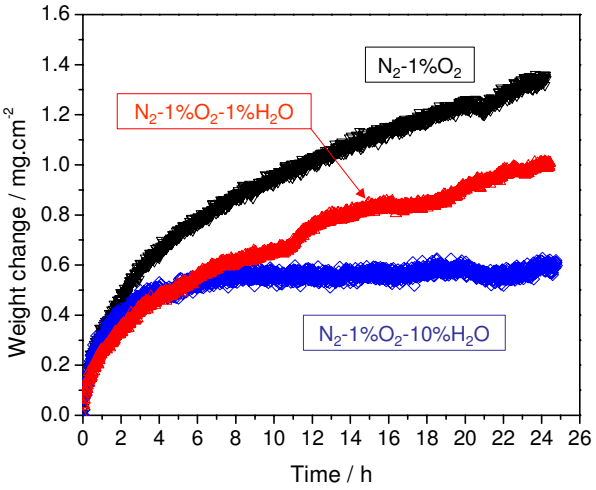

Fig. 89. *Isothermal oxidation of chromium, batch JUG at 950°C in gases containing various amount of H_2O. Scale formed in the N_2-1%O_2 spalled off during cooling to room temperature*

Scale morphologies formed in N_2-1%O_2 containing different amount of water vapour are shown in Fig. 90. The compositions of the scales formed in the test gases are shown in Table 15. The uptake of nitrogen and oxygen was calculated based on the measurement of the scale thickness and weight change recorded by TGA. For calculation it was assumed that only Cr_2O_3 and Cr_2N were formed. A thick sublayer of nitride beneath the oxide was observed in N_2-1%O_2-1%H_2O gas, Fig. 90a. The nitride thickness differed substantially along the sample length and was in the range of 2-6µm. At the oxide/nitride interface, a large number of pores were formed and the oxide scale was often detached from the alloy. The outer part of the scale was considerably more dense. In the N_2-1%O_2-3%H_2O a much thinner layer of nitride was found and often the nitride layer was plucked out during metallography preparation, Fig. 90b. Similar was the case in the N_2-1%O_2-7%H_2O, only the nitride layer was thinner and less porosity was present at the substrate/oxide interface, Fig. 90c. In N_2-1%O_2-10%H_2O the formation of nitride was completely blocked and only minor porosity formed at the metal/oxide interface, Fig. 90d. The oxide scale spalled in few places but in general the alloy/oxide interface was very intact and the oxide adhered much better to the metal than in other gases. In some gases, i.e. N_2-1%O_2, N_2-1%O_2-0.5%H_2O and N_2-1%O_2-5%H_2O the scale spalled off after cooling to room temperature. Most likely that such behaviour is related to the porosity formed at the nitride/oxide interface. In that case the remaining nitride layer should be present on the metal surface. To check this, specimen surfaces (without spalled scale) were analysed using XRD technique, Fig. 91.

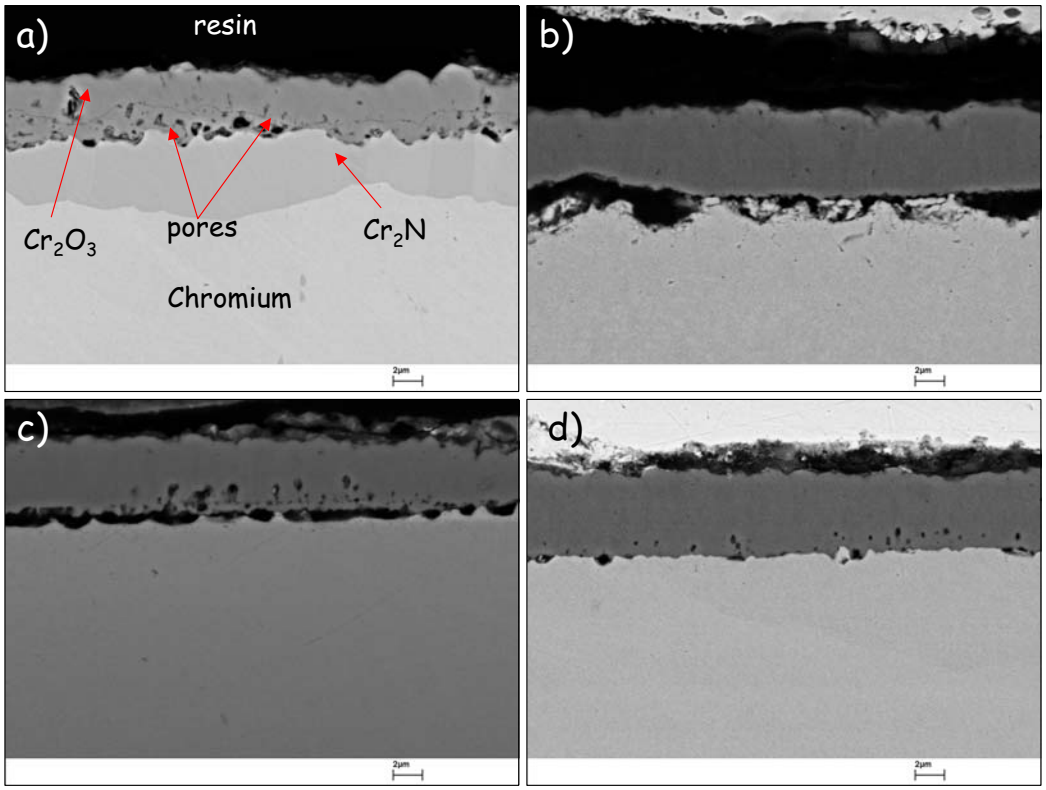

Fig. 90. *SEM cross sections of chromium, batch JUG after isothermal oxidation at 950°C in a) N_2-1%O_2-1%H_2O b) N_2-1%O_2-3%H_2O, c) N_2-1%O_2-7%H_2O and d) N_2-1%O_2-10%H_2O. Scales formed in N_2-1%O_2, N_2-1%O_2-0.5%H_2O and N_2-1%O_2-3%H_2O spalled off during cooling to room temperature*

Table 15. *Weight changes and estimated compositions of the scales formed on chromium after 24 h isothermal oxidation in various gases at 950°C*

Atmosphere	TGA W/A, mg.cm^{-2}	Thickness of Cr_2O_3 layer, µm	Thickness of Cr_2N layer, µm	O_2 uptake mg.cm^{-2}	N_2 uptake mg.cm^{-2}
N_2-1%O_2	1.38	Spalled			
N_2-1%O_2-0.5%H_2O	1.42	Spalled			
N_2-1%O_2-1%H_2O	0.94	3.4	3.4	0.64	0.30
N_2-1%O_2-3%H_2O	1.21	5.4	2	1.03	0.18
N_2-1%O_2-5%H_2O	0.87	Spalled			
N_2-1%O_2-7%H_2O	0.92	5.4	0.9	0.85	0.07
N_2-1%O_2-10%H_2O	0.62	5.4	0.0	0.62	0.00
N_2-20%O_2-10%H_2O	0.42	4.0	0.0	0.42	0.00
N_2-40%O_2-10%H_2O	0.40	4	0.0	0.40	0.00
N_2-1%H_2O	1.37	7.6	5.7	1.01	0.36
N_2-5%H_2O	0.78	5.7	0.5	0.75	0.03
N_2-4%H_2-4%H_2O	1.49	12	0.0	1.49	0.00

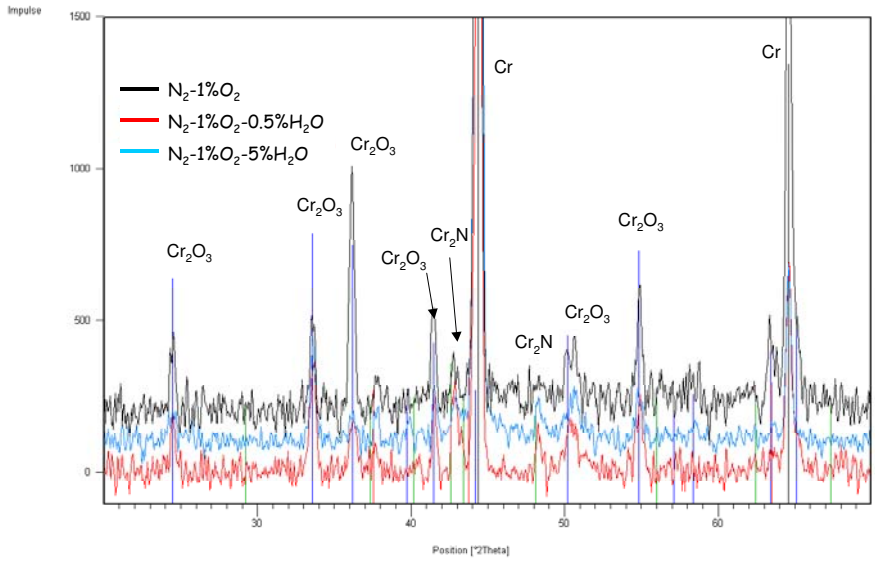

Fig. 91. *XRD – patterns taken from surfaces of chromium, batch JUG after 24h isothermal oxidation at 950°C in various N_2-O_2-H_2O gases*

In all analysed samples evidence of a nitride layer was found. It is interesting, however, to note that the intensity peaks originating from Cr_2N in N_2-1%O_2, N_2-1%O_2-0.5%H_2O and N_2-1%O_2-5%H_2O were in the ration of 3:8:3. If the intensity signal were considered to be dependent on the nitride layer thickness, then the presented results could also suggest that the addition of small concentration of water vapour to the dry N_2-O_2 gas promotes nitrogen penetration through the scale, but higher concentrations block nitrogen ingress. The indications that water vapour when present in high concentrations hampers nitridation were clearly seen in this work, Fig. 90d. The blocking effect of water vapour on the nitrogen uptake was also found in N_2-H_2O gases. In N_2-1%H_2O a thick layer of nitride was formed locally along the metal length, Fig. 92a. In N_2-5%H_2O the nitride layer was much thinner and only in the specimen corner became thicker, Fig. 92b.

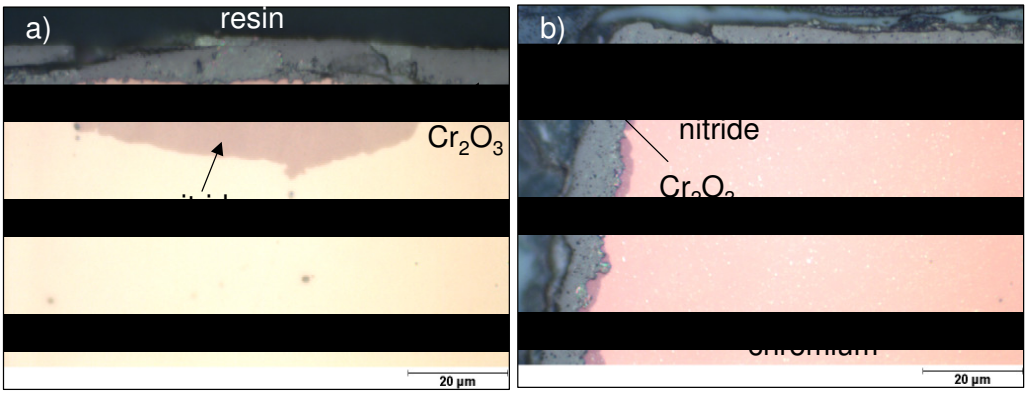

Fig. 92. *Metallographic cross sections after 24h isothermal oxidation of chromium, batch JUG at 950°C in a) N_2-1%H_2O and b) N_2-5%H_2O, surface was contrasted by sputtering iron oxide on it*

To explain the blocking effect of water vapour in N_2-O_2-H_2O gases containing a high concentration of H_2O, competitive adsorption at the outer oxide surface is suggested. The H_2O molecules are considered to be adsorbed preferentially onto the surface and when present in sufficient amount act as a barrier for N_2 adsorption. Ehlers et al proposed a similar interpretation to explain the enhanced oxidation of the 9%Cr steel in water vapour containing gases, [98]. Considering the entry of the molecular species into the scale proceed according to the surface adsorption equilibria

$$H_2O(g) + S = [H_2O/S] \tag{43}$$

$$N_2(g) + S = [N_2/S] \tag{44}$$

where S represents a vacant surface site, and H_2O/S, N_2/S represent adsorbed species. Assuming that at any instant during scale development, surface sites are conserved, then

$$M = [S] + [N_2/S] + [H_2O/S] \tag{45}$$

where, M is a constant and square brackets denote area concentrations. Eliminating [S] between Eqns. (43), (44) and (45), one finds

$$[H_2O/S] = \frac{M \cdot K_1 \cdot p_{H_2O}}{1 + K_1 \cdot p_{H_2O} + K_2 \cdot p_{N_2}} \tag{46}$$

$$[N_2/S] = \frac{M \cdot K_1 \cdot p_{N_2}}{1 + K_1 \cdot p_{H_2O} + K_2 \cdot p_{N_2}} \tag{47}$$

And its follows immediately that

$$\left[\frac{H_2O/S}{N_2/S}\right] = \frac{K_1 \cdot p_{H_2O}}{K_2 \cdot p_{N_2}} \tag{48}$$

This competitive adsorption process could indicate that, if water vapour is present in the atmosphere containing N_2 at certain condition, the H_2O can preferentially be adsorbed at the gas/oxide surface. Anghel et al investigated adsorption of different molecules onto zirconia and chromia. Based on the results the authors proposed the tendency of adsorption in the following order: $N_2<H_2<CO<H_2O$, [67]. Jocob et al. using SIMS measurements found that on chromium oxidized at 800^{o}C in N_2-20%O_2-1%H_2O, the oxide scale contained oxygen arising from the water vapour to an extent of about one-third of the total amount of oxygen, [68]. A similar behaviour but in Ar-O_2-H_2O atmosphere was also found in this work. In Ar-1%O_2-2%H_2O the extent of oxide arising from water vapour was approximately 5 times higher than oxide arising from O_2. Such behaviour also indicates that adsorption of H_2O is much more effective than monomolecular O_2. The presented examples support the view of different tendencies for molecular adsorption of H_2O and N_2 molecules on surfaces at high temperatures and as such could support the proposed blocking effect of water vapour when present in high amount compared to N_2.

It has been already noted that different adsorption onto the outer surface could affect the scale morphology, i.e. grain growth or porosity distribution and this effect could also play an important role. This aspect was considered in detailed in section 7.3. The following experiments were designed to provide better understanding of this phenomenon. Chromium was exposed to N_2-4%H_2-4%H_2O for 24h at 950^{o}C and no evidence of nitridation was found beneath the scale. In a second experiment, however, chromium was oxidized in the same atmosphere for 24h, but after that time the reaction gas was in-situ changed for next 24h to N_2. The scale was thicker but again no evidence of nitridation was to be found. The differences in oxide thickness resulted from further oxidation of chromium in N_2. The N_2 gas contained approximately 10ppm of oxygen and considering the gas flow conditions this amount was sufficiently high to supply oxygen for the scale growth.

The lack of nitrides beneath the oxide scale after exposure to N_2-4%H_2-4%H_2O gas could be explained again by fast adsorption of water vapour molecules onto the surface, very likely additionally enhanced because of the low oxygen partial pressure in the gas. Two-stage exposure to N_2-4%H_2-4%H_2O / N_2 suggested that the absence of Cr_2N beneath the scale was associated with the modification of scale morphology, because neglecting contaminations there was only N_2 in the gas. For example during exposure to N_2, the oxide grains grew (because there was no more water vapour to inhibit the process), the grain boundaries concentration reduced and in turn inward scale transport was hampered thus preventing nitrogen ingress.

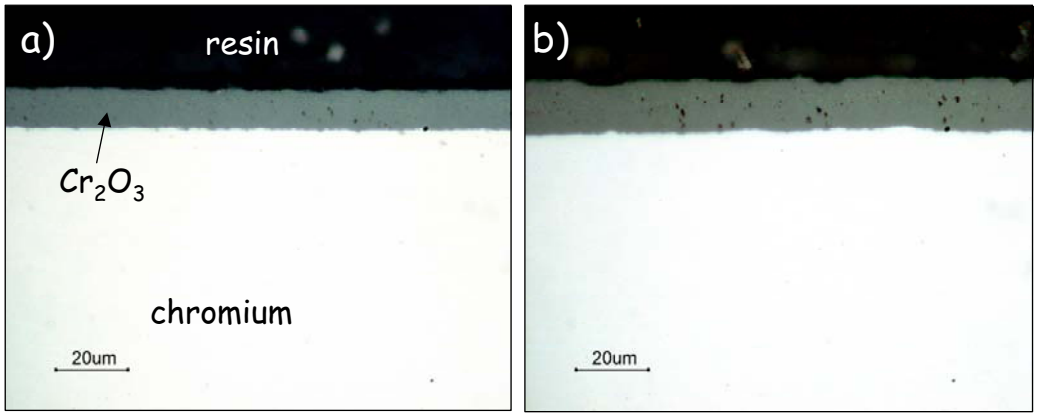

Fig. 93. *Cross sections after isothermal oxidation of chromium, batch JUG at 950°C in a) 24h in N_2-4%H_2-4%H_2O, b) 24h in N_2-4%H_2-4%H_2O / 24h in N_2*

Another aspect of oxidation of chromium in N_2-O_2-H_2O which seems to be important is the evaporation of Cr-bearing species due to formation of volatile hydroxide. This problem was particularly pronounced in gases where the partial pressures of H_2O and O_2 were high, Table 10. Similarly, as described in section 7.6.3, the chromium flux was estimated for the test gases, Table 11.

Table 5. *Partial pressure of $CrO_2(OH)_2$ and estimated flux of chromium, T=950°C*

Atmosphere	$p_{CrO_2(OH)_2(g)}$ *atm*	J_{Cr} $g \cdot cm^{-2} \cdot s^{-1}$	*Chromium mass loss after 24h oxidation* $mg \cdot cm^{-2}$
N_2-1%O_2-0.5%H_2O	$3.5x10^{-9}$	$4.1x10^{-13}$	$3.5x10^{-5}$
N_2-1%O_2-1%H_2O	$6.9x10^{-9}$	$8.1x10^{-13}$	$7.0x10^{-5}$
N_2-1%O_2-3%H_2O	$2.1x10^{-8}$	$2.4x10^{-12}$	$2.1x10^{-4}$
N_2-1%O_2-5%H_2O	$3.4x10^{-8}$	$4.1x10^{-12}$	$3.5x10^{-4}$
N_2-1%O_2-7%H_2O	$4.8x10^{-8}$	$5.7x10^{-12}$	$4.9x10^{-4}$
N_2-1%O_2-10%H_2O	$6.9x10^{-8}$	$8.1x10^{-12}$	$7.0x10^{-4}$
N_2-20%O_2-10%H_2O	$6.5x10^{-7}$	$7.7x10^{-11}$	$6.6x10^{-3}$
N_2-40%O_2-10%H_2O	$1.1x10^{-6}$	$1.3x10^{-10}$	$1.1x10^{-2}$

The calculated values of the chromium loss due to evaporation are too low to explain the weight changes observed in N_2-O_2-H_2O gases containing high concentrations of water vapour, Fig. 88. Therefore as suggested in section 7.6.3 there is probably another parameter which the presented model did not take into account. For example, the model described above assumed that the evaporation surface was flat and this was not a real case because the scale roughness increases that surface area. Besides if some of the pores developed in the scale were open, the evaporation surface could highly increase. This is schematically shown in Fig. 63.

7.8.5 Oxidation in CO-CO_2-H_2O gas mixtures

The main purpose of this study was to establish whether H_2O could block carburization of chromium or not. Specimens were exposed for 24 h to three different CO-containing gases, i.e. pure CO, CO-2%CO_2 and CO-2%CO_2-1%H_2O at 950°C, Fig. 94. The highest oxidation rate was observed in the atmosphere containing water vapour. In all cases the scale was attached very well to the metal surface, but substantial differences in morphology were observed. Beneath the oxide scale in pure CO and in CO-2%CO_2, precipitation of carbide beneath oxide scale was observed, Fig. 95a and b. In CO gas pores were found located mainly at the oxide/carbide interface. The scale formed in CO-2%CO_2 gas mixture was much denser and carbide precipitations were formed locally. When 1%vol of H_2O was added to CO-2%CO_2, hardly any carbides were found and at the same time only minor pores were seen, Fig. 95c. Although no carbide was formed in CO-2%CO_2-1%H_2O the oxidation rate was the fastest. It suggests that presence of water vapour species enhanced the oxide scale growth for chromium oxidized in CO-CO_2 gas mixtures.

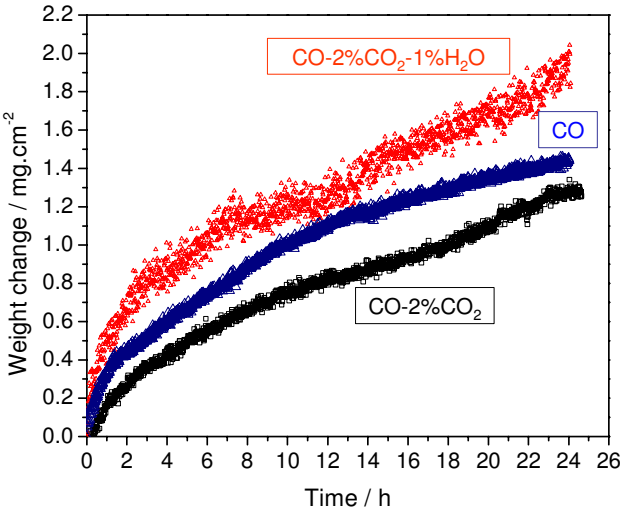

Fig. 94. *Isothermal oxidation of chromium, batch JUG at 950°C in CO - containing atmospheres*

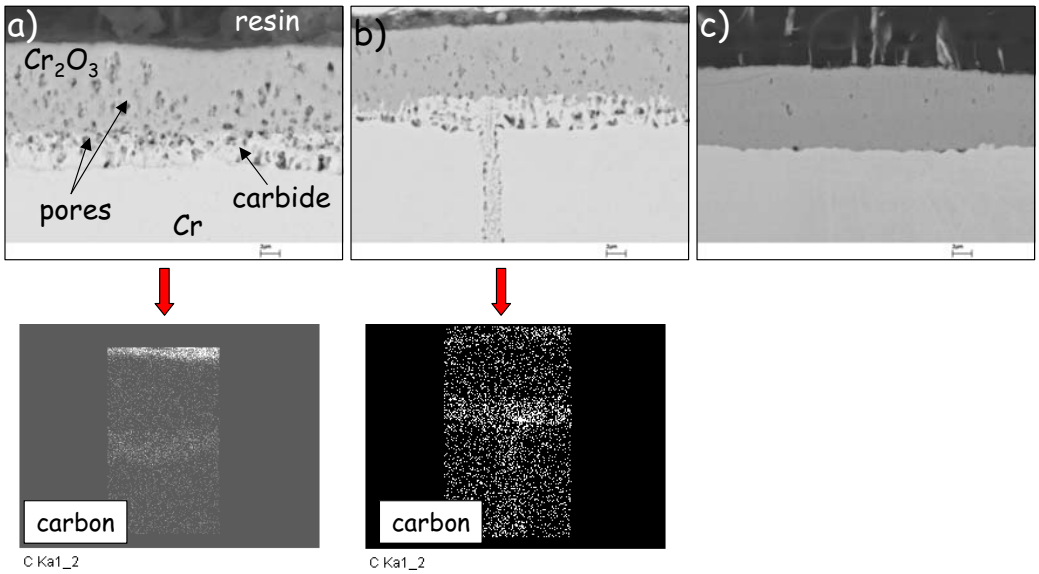

Fig. 95. *SEM cross sections of chromium, batch JUG after isothermal oxidation at 950°C in a) CO, b) CO-2%CO_2, c) CO-2%CO_2-1%H_2O and EDX carbon mapping of formed scale*

The presented results clearly show that even small additions of water vapour to the CO-2%CO_2 gas markedly affect both oxidation rate and scale morphology. The penetration of carbon was hampered and as consequence no carbide were formed on the metal. It is important to note that at the same time the oxidation rate increased and was higher even in the pure CO gas where the thick carbide layer was formed. This indicates that adsorption of water vapour was favourable and thus the contribution of CO for the oxide growth was lower. Such observations are in good agreement with literature findings, [67-71]. Anghel et al found that upon addition water vapour to the CO gas at 600°C, the dissociation rate of CO on Cr decreased which was interpreted as a blocking effect of water. Subsequent removal of water from the gas again increased dissociation of CO, [67]. Turkdogan et al investigated the early stages of oxidation of iron to wüstite, [71]. They found that the activation energy at 850-1150°C in H_2/H_2O was much lower than in case for oxidation in CO-CO_2 mixtures. Therefore it is believed that blocking effect of water vapour can be interpreted as a competitive adsorption between CO and H_2O molecules at the outer surface of the scale and similar dependency could be derived as in equations (44-48).

The lack of carbides in the CO-2%CO_2-1%H_2O gas may result from lower activity of carbon in the gas. Assuming that the reacting gas was well equilibrated, the activity of carbon would not change

much by introducing 1%vol. H_2O, Table 5. But if one takes into account that water vapour was preferentially adsorbed at the surface, the decrease in carbon activity at the scale surface could be significantly reduced and in turn it could be a reason for decarburization. Therefore it is believed that fast adsorption and dissociation of water vapour at the outer surface of the scale was the main reason of observed decarburization.

- Oxidation behaviour of chromium in multicomponent gas mixtures, Summary -

Studies of the oxidation behaviour of chromium, batch JUG in multicomponent gas mixtures revealed that scale growth was affected by water vapour and oxygen partial pressure.

The early stages of oxidation at 950^{o}C showed that the addition of H_2O to an N_2-1%O_2 gas improves scale adherence and modified oxide susceptibility to nitrogen penetration. When water vapour is added to the gas in small amounts, (N_2-1%O_2-1%H_2O) it promotes nitrogen ingress in the scale, however when more H_2O is present in the gas (N_2-1%O_2-10%H_2O) the nitridation is hampered. Such behaviour is suggested to be a consequence of enhanced surface reaction by water vapour and competitive adsorption between H_2O and N_2. It is proposed that H_2O inhibited grain growth and in turn promoted inward transport through the scale. Therefore, if small amounts of H_2O are present in the N_2-O_2-H_2O gas, the nitridation could be enhanced. However, if more H_2O is added, although fast diffusion paths for nitrogen ingress still existed, the nitridation is hampered because water vapour is blocking nitrogen adsorption at the outer surface of the scale.

The blocking effect of water vapour at the oxide surface was especially pronounced in low pO_2 gases such as N_2-4%H_2-4%H_2O. Indications were found that in such atmospheres adsorption and dissociation of H_2O is even faster than in N_2-O_2-H_2O gases and thus lower concentrations of water vapour are needed in the gas to block adsorption and inward transport of nitrogen.

The blocking effect of water vapour at the oxide surface was also found in CO-2%CO_2-1%H_2O gas. It appeared that 1%vol. of H_2O was sufficient to block carbon ingress and hamper carburization.

8. Studies of oxidation behaviour of high purity chromium, batch DUR

In this study chromium batch DUR of higher purity than batch JUG was chosen. Comparing contamination level, Table 3, it is seen that carbon level was lowered from 70 to less than 10ppm. The investigations were designed in the way to give an overall picture of behaviour of this chromium batch in different oxygen partial pressure with and without water vapour.

8.1 Oxidation behaviour at 1000°C

Mass gain after 72 h isothermal exposure in all tested atmospheres is shown in Fig. 96 and relative amount of oxide which was spalled after cooling to room temperature in Fig. 97. For presenting the effect of oxygen and water vapour partial pressures both parameters are shown on the diagram. For dry gas Ar-20%O_2 and Ar-1%O_2 10 ppm of water vapour was assumed. Comparisons showed that chromium specimens oxidized faster and adhered better to the metal in low pO_2 atmosphere containing water vapour than in dry, high pO_2 gases.

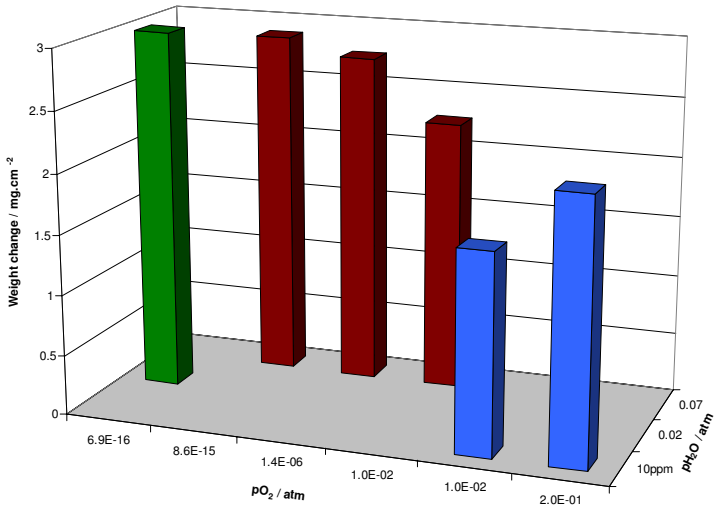

Fig. 96. *Weight change after 72h isothermal oxidation of chromium, batch DUR at 1000°C in tested atmospheres*

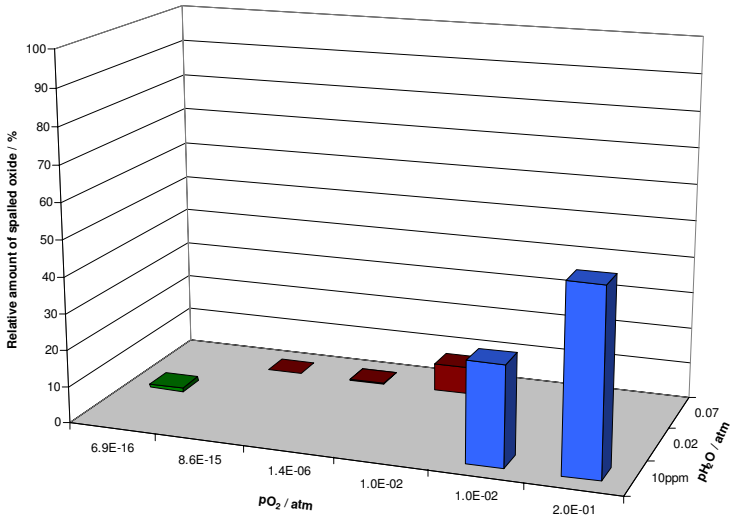

Fig. 97. *Relative amount of spalled oxide after cooling to room temperature chromium specimens, batch DUR which were exposed for 72h to tested atmospheres at 1000°C*

In case of dry Ar-O_2 gases it was found that oxidation rate increases at higher oxygen pressures, Fig. 98a. During exposures to Ar-20%O_2 speeding up in oxidation rate was observed figure, Fig. 98b. Few authors has already been reported such behaviour [1,12-16]. It is believed that growth stresses building up in the scale led to buckling and cracking during the oxidation process what in turn resulted in periodical increase in scaling rate.

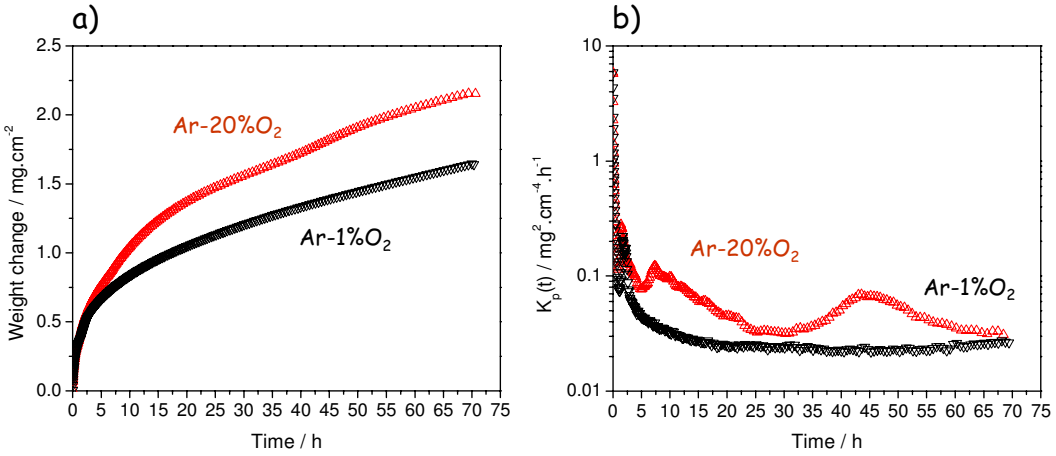

Fig. 98. *Isothermal oxidation of chromium, batch DUR in Ar-1%O_2 and Ar-20%O_2 at 1000°C, a) weight change and b) K_p as a function of time*

This seems to be confirmed by the scale morphologies. In Ar-20%O_2 the oxide developed two layers scale with clear evidences of buckling Fig. 99a. The outer was thin and compact with grain size in the range of few hundreds nanometres whereas the inner was porous and grain size were even few micrometres large. These two layers were locally detached and in the places where the contact was lost outer layer was bulged. Cracks were seen on the oxide surface. These were probably formed during cooling to the room temperature but similar cracks could be imagined to occur during the scale growth. Development of such oxide type is schematically illustrated in Fig. 100. Different morphology was formed when chromium was oxidized in Ar-1%O_2. The scale was compact and no evidences of buckling and double layer formation were found, Fig. 99b. The scale developed characteristic voidage at the metal/oxide interface and locally was completely separated from the metal, the reason for poor oxide adhering. The grains sizes were large and in the range of few micrometres.

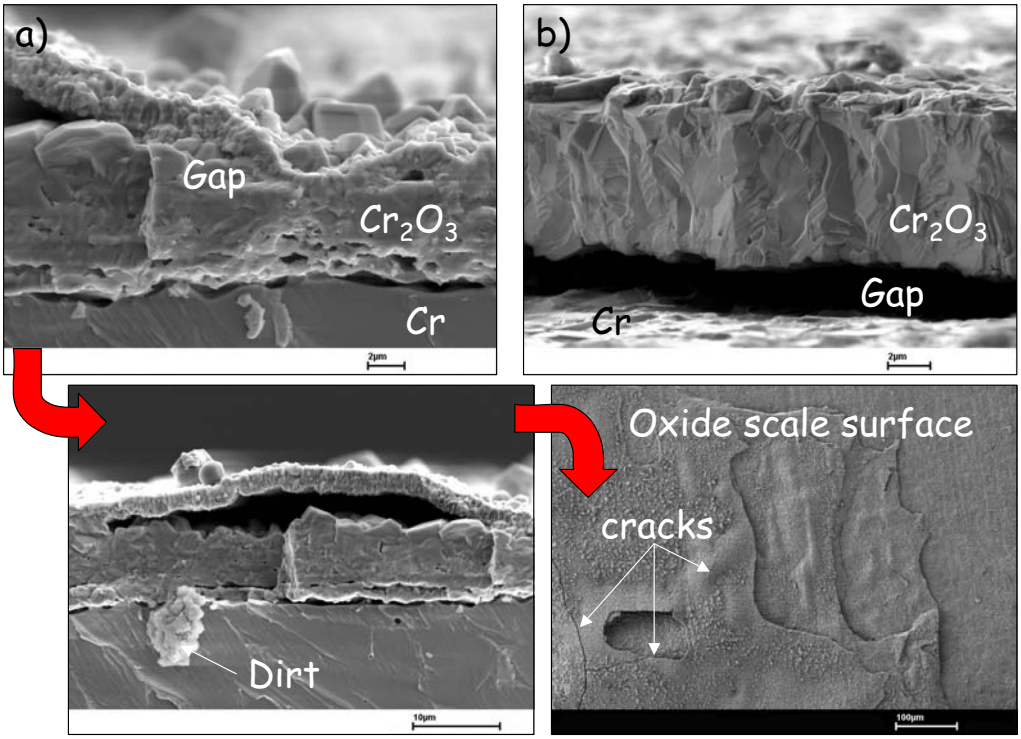

Fig. 99. *SEM fractured-sections of oxide scales formed on chromium, batch DUR, after 72h oxidation at 1000°C in a) Ar-20%O_2, b) Ar-1%O_2,*

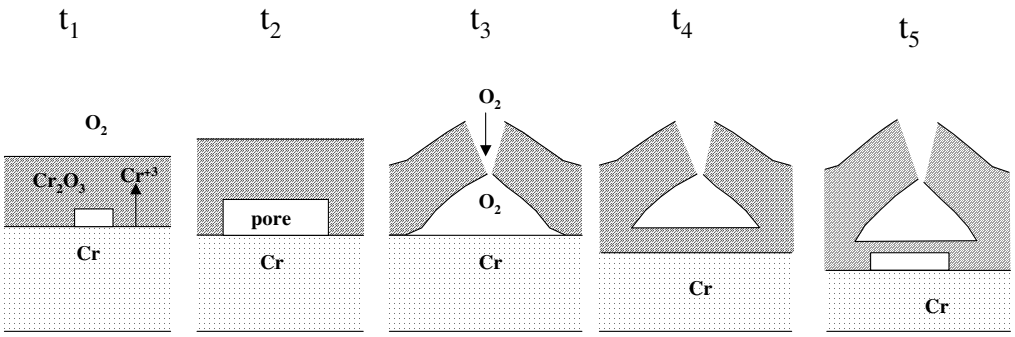

Fig. 100. *Schematic development of oxide formation on chromium in dry Ar-O_2 gases at pO_2 sufficiently high to exceed ability of scale to deform plastically, [40]*

In Ar-H_2-H_2O specimens oxidized much faster than in Ar-O_2 atmospheres. Similar rate was recorded in both tested gases, Fig. 101a. The metal/oxide interface was free of voids and oxide adherence was excellent in all tested gases Fig. 101. In both Ar-4%H_2-2%H_2O and Ar-4%H_2-7%H_2O the scale was compact and only small pores around few hundreds nanometres in diameter could be seen. It should be noted that contrary to batch JUG, Fig. 76, no evidences of inner buckling were found. It appears that contamination could be one of the factors, which affect inner buckling at low pO_2 gases.

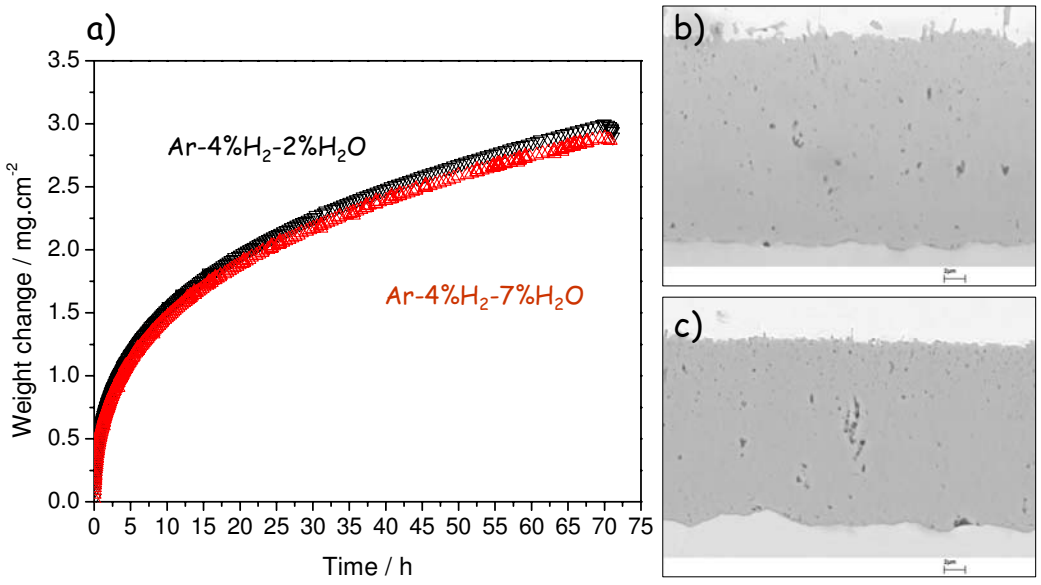

Fig. 101. *Isothermal oxidation of chromium, batch DUR in Ar-H_2-H_2O gases at 1000°C, a) weight change, b) morphology of scale formed in Ar-4%H_2-2%H_2O and c) Ar-4%H_2-7%H_2O at 1000°C*

Comparing oxidation behaviour in Ar-O_2-H_2O and Ar-H_2O gases one finds higher weight change in Ar-7%H_2O than in Ar-1%O_2-7%H_2O, Fig. 102a. Similar type of scale morphologies formed in both gases and large pores developed within the scale, however the extent was higher in Ar-7%H_2O than in Ar-1%O_2-7%H_2O, Fig. 102b and c. Good oxide adhering was maintained after cooling to room temperatures in both gases.

It is suggested that because of H_2O and O_2 presence in Ar-1%O_2-7%H_2O gas the evaporation was enhanced due to formation of volatile $CrO_2(OH)_2$ and in turn the weight change recorded in that gas was lower than in Ar-7%H_2O. The effect of gas composition in Ar-O_2-H_2O atmospheres was discussed in detail in section 7.6.

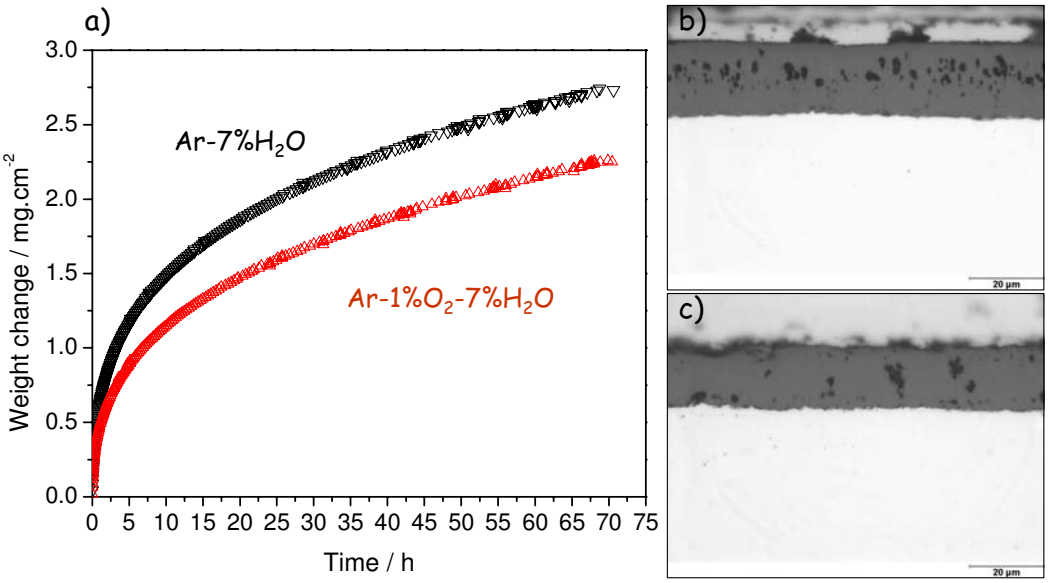

Fig. 102. *Isothermal oxidation of chromium, batch DUR in Ar-O_2-H_2O gases at 1000°C, a) weight change vs. time, b) morphology of scale formed in Ar-7%H_2O and c) Ar-1%O_2-7%H_2O at 1000°C*

It must be noted that important difference in oxidation behaviour in Ar-O_2-H_2O gases between batch JUG and DUR was observed. Studies on both batches showed that weight change decreased when 1%vol of O_2 was added to the Ar-7%H_2O gas, however on batch DUR the weigh change in such mixture, i.e. Ar-1%O_2-7%H_2O, was higher compared to Ar-1%O_2 whereas on batch JUG it was lower, Fig. 103. Since the purity of batches was different it is believed that the effect of water vapour could be shifted depending on the chromium used. Important to note that purity level seems to have

a particular impact on the oxidation behaviour of chromium in dry Ar-O_2 gases. This aspect will be further discus in chapter 10.

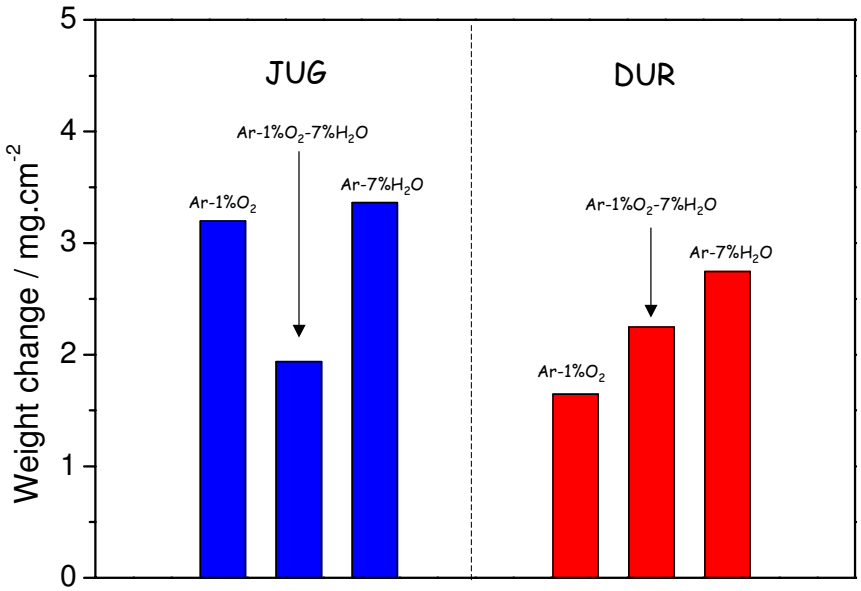

Fig. 103. *Comparison of weight changes after isothermal oxidation of chromium batches JUG and DUR at 1000°C in Ar-1%O_2, Ar-1%O_2-7%H_2O and Ar-7%H_2O atmospheres*

8.2 Oxidation behaviour at 1050°C

The same set of experiments as in Fig. 96 was carried out in 1050°C, Fig. 104. The data show similar trend as observed at 1000°C, i.e. weight change was higher in Ar-H_2-H_2O gases than in Ar-O_2. Similar also was the effect of atmosphere on the oxide scale adherence, Fig. 105.

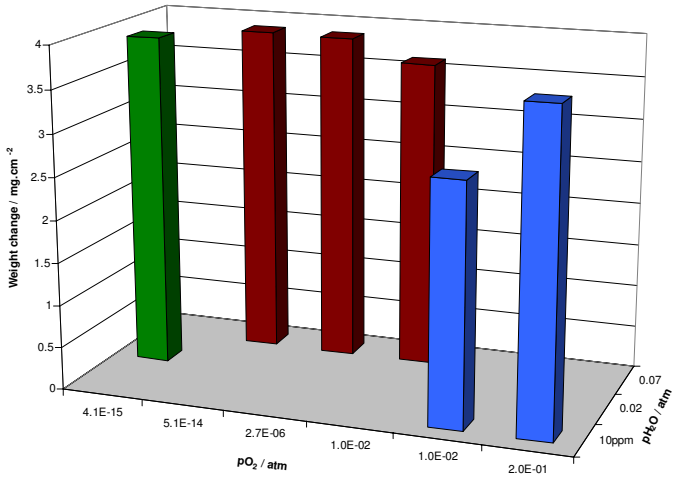

Fig. 104. *Weight change after 72h isothermal oxidation of chromium, batch DUR at 1050°C in tested atmospheres*

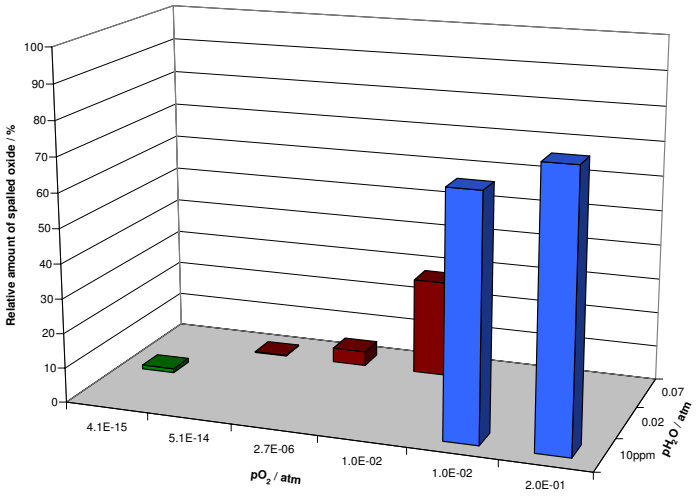

Fig. 105. *Relative amount of spalled oxide after cooling to room temperature chromium specimens, batch DUR which were exposed for 72h to tested atmospheres at 1050°C*

In dry Ar-O_2 gases similar to 1000°C it was found that weight change increased at higher oxygen pressures, Fig. 106a. Also during exposures to Ar-20%O_2 increasing oxidation rate was observed, Fig. 106b. This effect however was more significant in this temperature than at 1000°C. Scale morphologies confirmed such behaviour. In Ar-20%O_2 the entire oxide was damaged with pores and buckles all over the scale whereas in Ar-1%O_2 the scale was compact and no evidences of buckling were found, Fig. 107a and b. Both scales developed characteristic voidage at the metal/oxide interface.

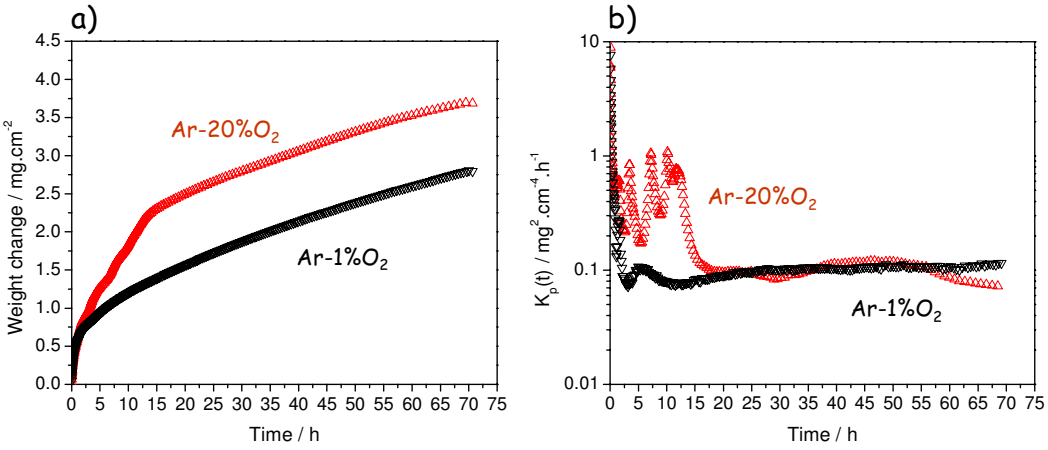

Fig. 106. *Isothermal oxidation of chromium, batch DUR in Ar-1%O_2 and Ar-20%O_2 at 1050°C, a) weight change and b) K_p as a function of time*

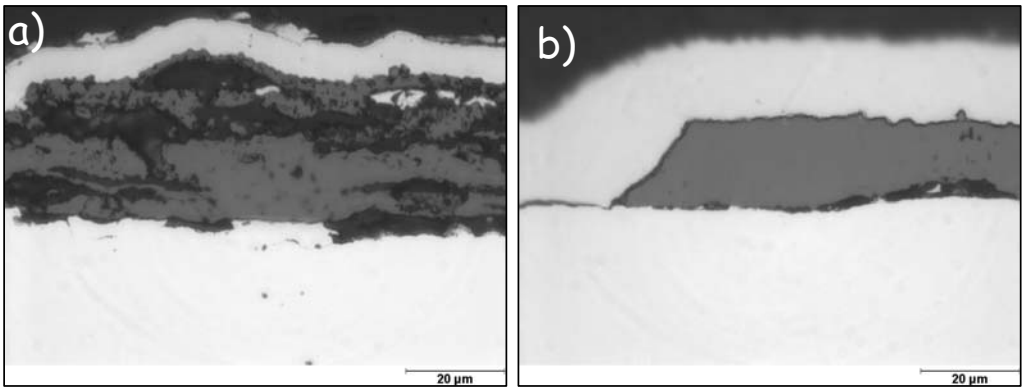

Fig. 107. *Metallographic cross-sections of oxide scales formed on chromium, batch DUR after 72h oxidation at 1050°C in a) Ar-20%O_2, b) Ar-1%O_2*

In the Ar-H_2-H_2O specimens oxidized much faster than in dry Ar-O_2 atmospheres. Similar rate was recorded in both tested gases and excellent scale adhering was observed, Fig. 108a-c. Oxides were

compact but in Ar-4%H_2-7%H_2O larger pores appeared in the scale whereas in 4%H_2-2%H_2O the pores were smaller and seemed to be in less number. No evidences of inner buckling were found.

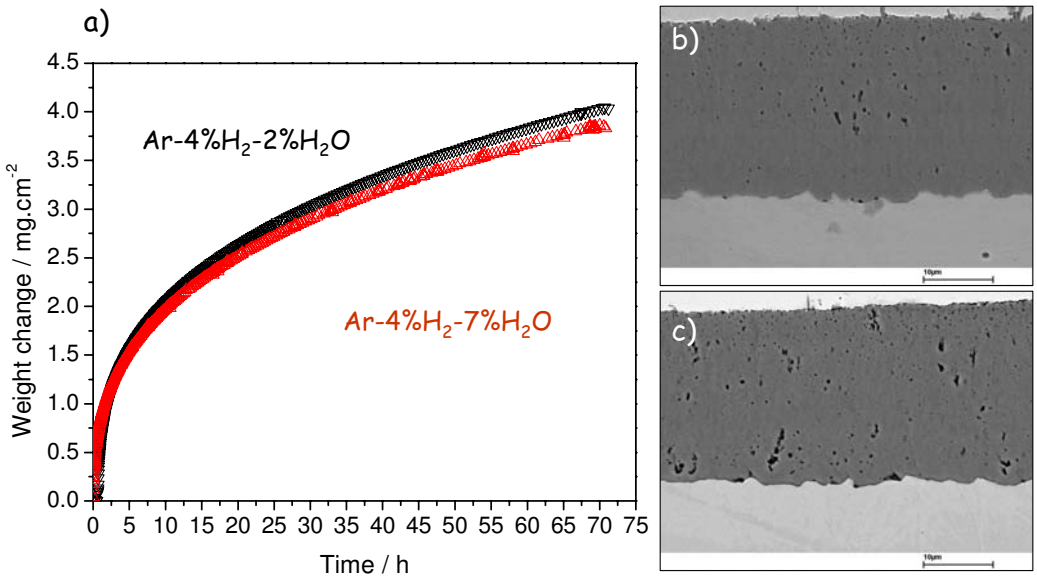

Fig. 108. *Isothermal oxidation of chromium, batch DUR in Ar-H_2-H_2O gases at 1050°C, a) weight change vs. time, b) morphology of scale formed in Ar-4%H_2-2%H_2O and c) Ar-4%H_2-7%H_2O*

Similar tendency in oxidation behaviour was also found between Ar-O_2-H_2O and Ar-H_2O gases as was found at 1000°C. The weight change was higher in Ar-7%H_2O than in Ar-1%O_2-7%H_2O, Fig. 109a. Oxide scales formed in both gases showed similar morphologies and very good adherence was maintained after cooling to room temperature, Fig. 109b, and c. Large pores were found in both oxide scales, however the extent seemed to be higher in Ar-H_2O than in mixed gas.

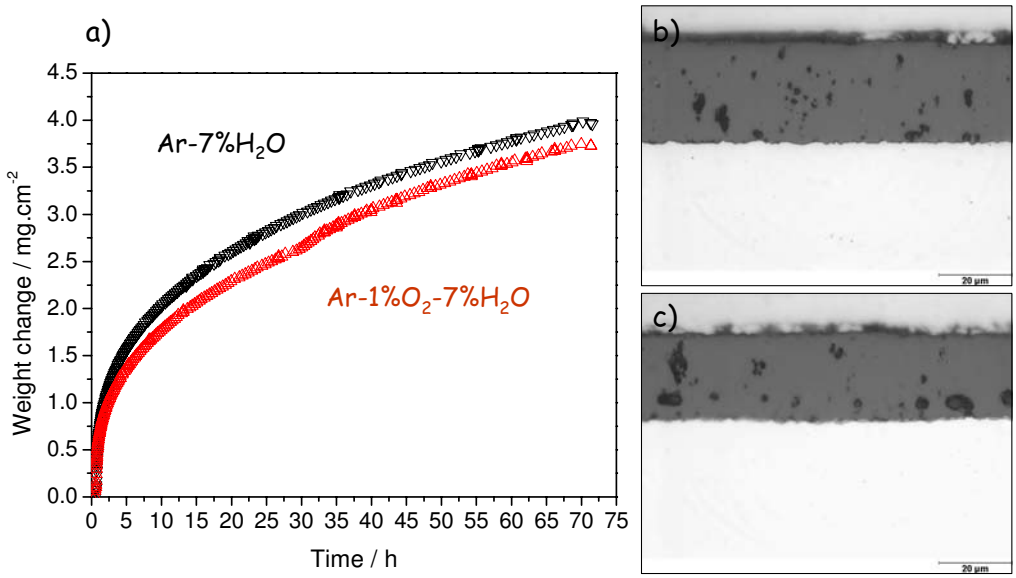

Fig. 109. *Isothermal oxidation of chromium, batch DUR in Ar-O_2-H_2O gases at 1050°C, a) weight change, b) morphology of scale formed in Ar-7%H_2O and c) Ar-1%O_2-7%H_2O*

8.3. Time dependence on oxide adherence

In fracture mechanical concepts, the oxide scale adherence is described to depend on the oxide scale thickness and the tendency to scale spalling is expected therefore to vary with exposure time, [100]. To check whether this was also the case for specimens oxidized in the present test gases, additional experiments with varying exposure times in dry Ar-20%O_2, Fig. 110a and wet Ar-7%H_2O, Fig. 110b were carried out. For that set of experiments higher temperature, i.e. 1050°C was chosen to enable adherence differences be more pronounced. The relative amount of spalled oxide after cooling was plotted in another diagram, Fig. 111. It appears that spallation increased with increasing exposure time in case of exposures to Ar-20%O_2. A different behaviour with time was seen in Ar-7%H_2O gas, in that case the extent of spalling was far less substantial than after exposure to high-pO_2 gas and did not appear to be time dependent. Selected scale morphologies are shown in Fig. 112. In Ar-20%O_2 after short 5h oxidation time oxide scale appeared to be dense but indications of scale cracking have already been present. Longer exposure, i.e. 20h showed the scale already damaged with many pores in the bulk and it is believed to be the consequence of periodical speeding up in oxidation rate due to

stresses development as illustrated in Fig. 100. In Ar-7%H_2O the scale remains well adherent to the metal after longer times and only pores increased their size.

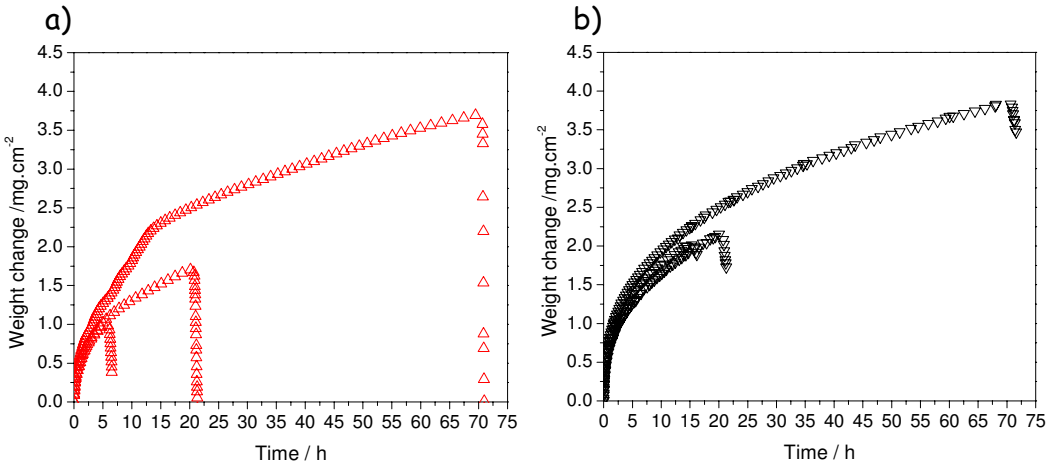

Fig. 110. *Weight change during isothermal oxidation of chromium, batch DUR at 1050°C and after cooling to room temperature a) Ar-20%O_2 b) Ar-7%H_2O. The cooling process started at that point of time in which the weight change became negative and this indicated oxide spallation*

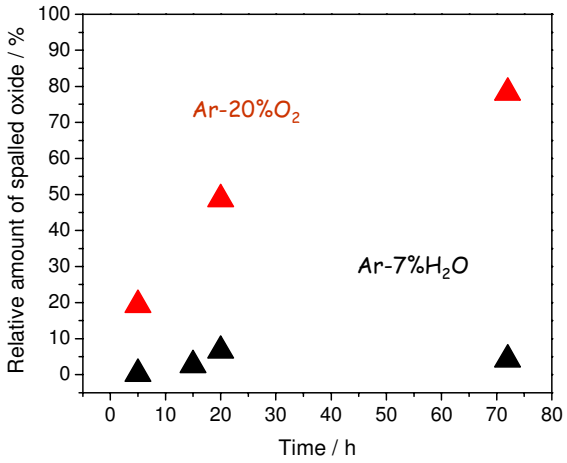

Fig. 111. *Relative amount of spalled oxide after cooling to room temperature. Oxide was formed on chromium, batch DUR exposure to Ar-20%O_2 and Ar-7%H_2O for various time at 1050°C and cooled to room temperature after the process*

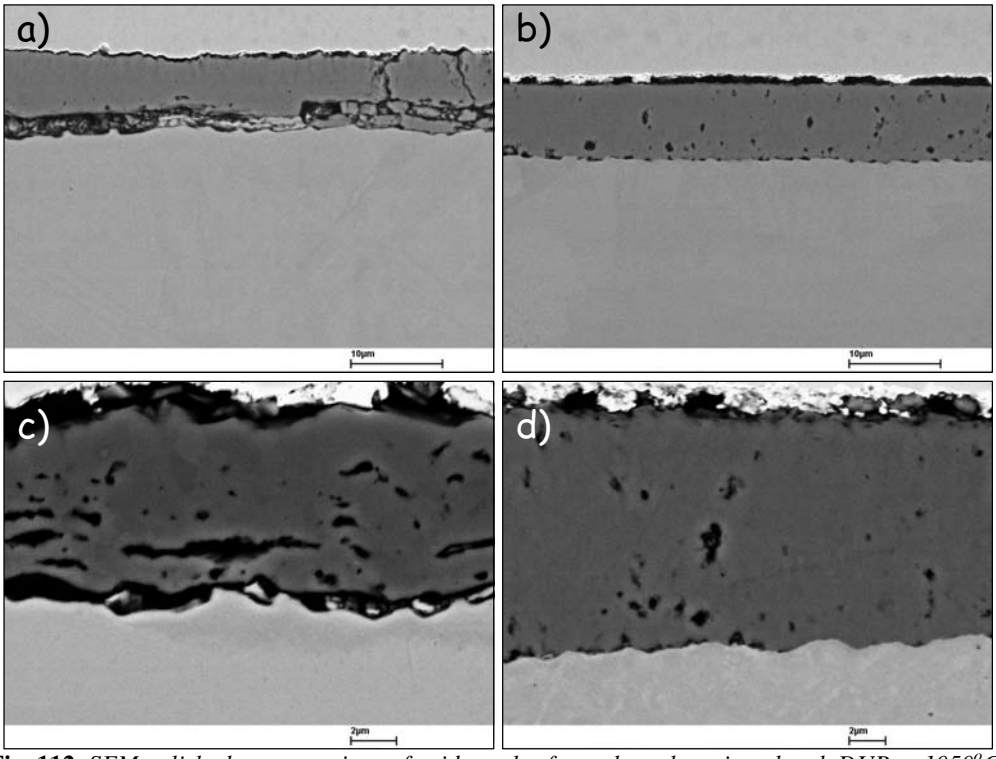

Fig. 112. *SEM polished cross-sections of oxide scales formed on chromium, batch DUR at 1050°C after oxidation in Ar-20%O_2 for a) 5h, c) 20h and in Ar-7%H_2O for b) 5h and d) 20h*

9. Studies of oxidation behaviour of low purity chromium, batch KER

Commercial chromium batch KER, Table 3 was studied. It can be seen that this batch was contaminated in carbon and sulphur the most compare to other chromium batches. The presence of these elements in metal or alloy is widely considered to have a negative effect on the oxidation behaviour and on scale adherence in particular, [1-3,38,44]. However it must be noted that not only the influence of carbon and sulphur was essential because number of elements played a different roles on the material behaviour during the high temperature exposures and depending on the valance and element's stability a different action could be expected. All these factors would be difficult to take into considerations and therefore the purpose of this study was to show how different could be the oxidation behaviour of chromium depending on purity rather than speculating on the possible effect of each element separately. Still remarks are made in relation to carbon and sulphur impurities because it is believe that these elements could have a particular effect on the oxide scale adherence. Fig. 113 shows oxidation kinetics, Fig. 114 relative amounts of spalled off oxide and Fig. 115 oxide scale morphologies formed on the chromium, batch KER after exposure to tested gas at 1000°C.

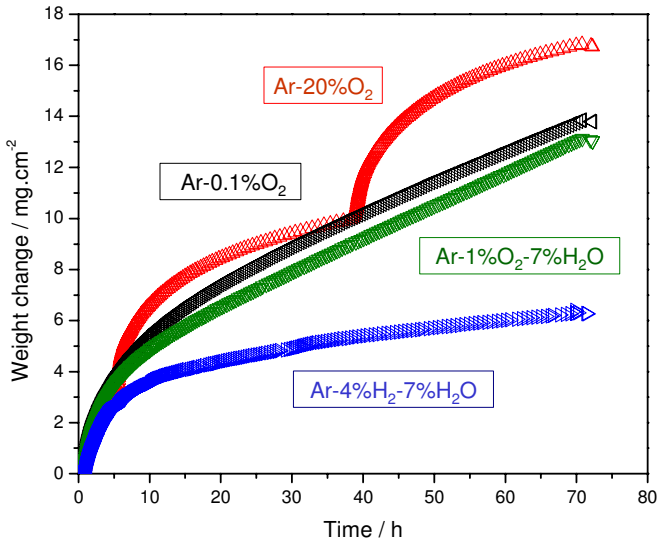

Fig. 113. *Isothermal oxidation of chromium, batch KER in various gases at 1000°C*

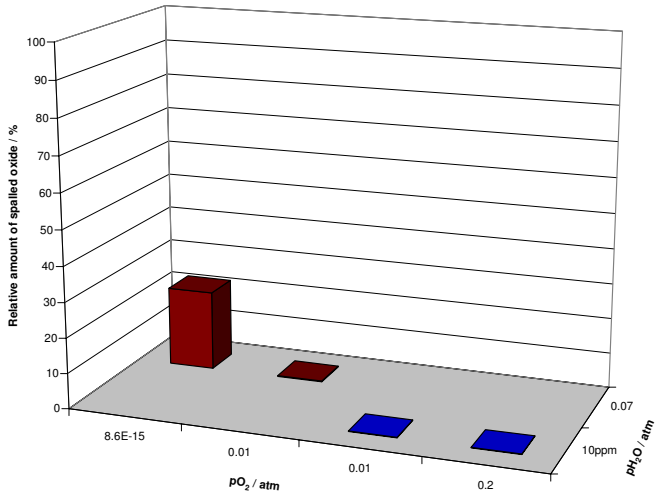

Fig. 114. *Relative amount of spalled oxide after cooling to room temperature chromium specimens, batch KER which were exposed for 72h to tested atmospheres at 1000°C*

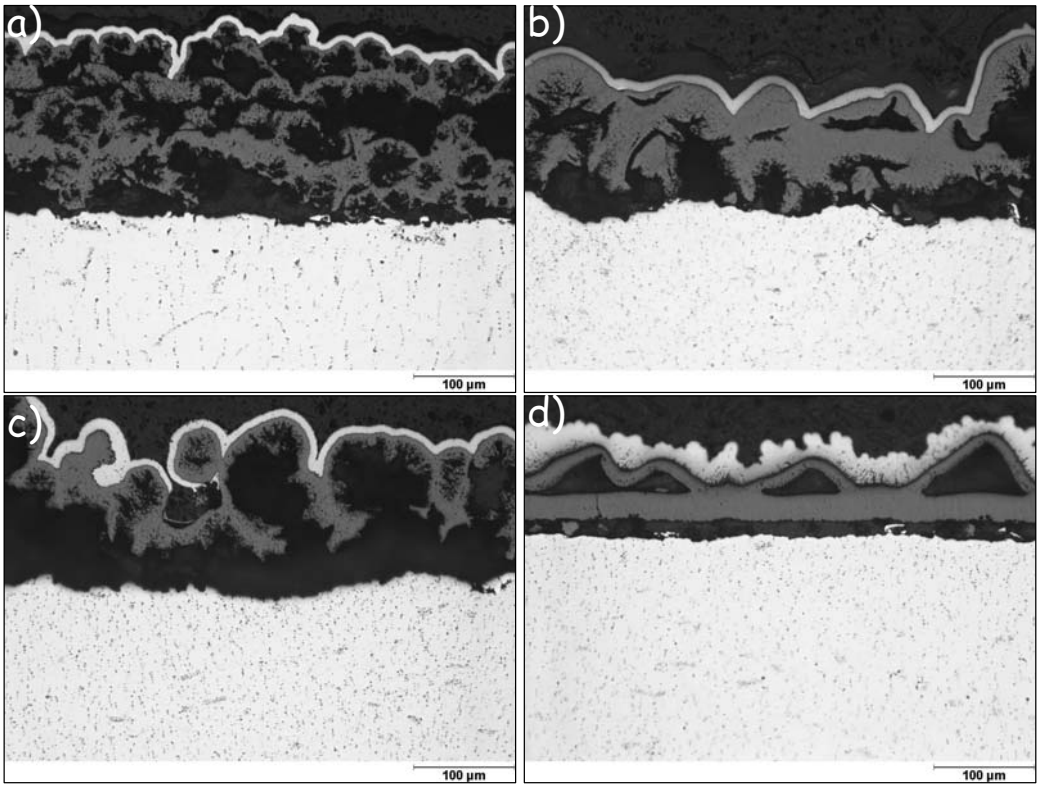

Fig. 115. *Metallographic cross-sections of oxide scales formed on chromium, batch KER after 72h oxidation at 1000°C in a) Ar-20%O_2, b) Ar-1%O_2, c) Ar-1%O_2-7%H_2O, d) Ar-4%H_2-7%H_2O*

It can be seen that weight change was remarkably higher in all tested gases in comparison to previously tested batch JUG and DUR. In Ar-O_2 gases similar dependency on the pO_2 was observed as in batches JUG and DUR, i.e. highest weigh change at higher oxygen partial pressure. Similarly to batch DUR but more pronounced during the exposure to Ar-20%O_2 periodically increases in oxidation rate was observed, Fig. 98 and Fig. 113. Morphology of such scale showed significant damage of the scale and pores and gaps all over the oxide. The scale formed in Ar-1%O_2 seemed to be denser but also in that case numbers of large pores were formed.

Addition of water vapour to the Ar-1%O_2 did not change significantly oxidation rate and scale adherence. In both gases the scale was porous and strongly buckled. The slightly lower weight change in the Ar-1%O_2-7%H_2O compare to the Ar-1%O_2 could be related with enhanced evaporation due to formation of $CrO_2(OH)_2$. This aspect was discussed in chapter 7.6.

Oxidation in low pO_2 atmosphere, here the Ar-4%H_2-7%H_2O showed the lowest weight change among all tested gases and the most compact scale formed. Still a number of pores/buckles were present in the scale and the metal/oxide interface was also porous. The extent of porous was however much lower than in the case of O_2 containing gases.

The presented results suggest that pores formation was particularly severe in Ar-O_2 gases. It could be explained by extensive formation of CO at the metal/oxide interface. The studies of many authors showed that carbon present in the metal can diffuse to the interface and form CO_2 and CO, which subsequently are being removed outwards through the cavities and pores, [1-3,99]. Such process is schematically illustrated for the oxidation of steel, Fig. 116, [2]. Also the findings of that work indicated the diffusion of carbon from the metal to the metal/oxide interface, Fig. 39 and Fig. 67. Particularly interesting from the point of present work, was the study of Graham and Caplan, who carried out oxidation on pure Ni with different carbon content, [99]. The authors exposed pure Ni of different purity in carbon i.e.100, 9 and 2 ppm atomic at 1270^oC for 20h. To analyse gases, the oxidized sheets were placed on the flanged in a metal, ultrahigh vacuum apparatus below chisel which could be raised magnetically and drop onto the specimen to break into the oxide. By breaking the oxide the pulse of CO_2 released was recorded by mass spectrometer. It was found that average CO_2 peak heights for the three grades of oxidized Ni were in the ratio 100:8:0. Further analysis by spark-source mass spectroscopy showed that oxidation reduced the carbon levels from 100:9:2 to 17:2:2 ppm atomic carbon indicating that during oxidation maximum possible CO_2 production

would be in 83:7:0, which was in agreement with observed CO_2 peak heights. At the same time observation of scale morphologies shown that many voids formed throughout the oxide on the Ni with 100 ppm atomic carbon and few on the low-carbon Ni except near the oxide metal interface. This experiments demonstrated that cavities in the NiO scale contained CO_2 at appreciable pressures and that amount of cavity is related to the carbon content of the nickel. As the conclusion authors suggested that impurities apparently could have significant effect on the formation of cavities in oxide layer.

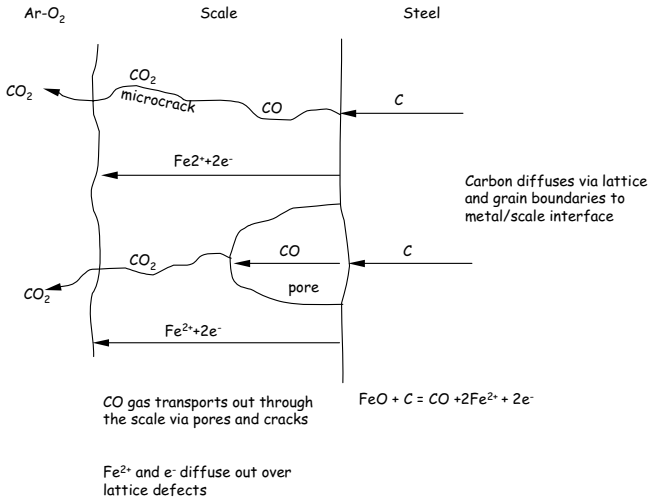

Fig. 116. *Schematic illustration of chromium transport in Ar-O_2 gases in cases of voidage formation at the metal/oxide interface, [2]*

It could be speculated that formation of heavily porous scale on the chromium batch KER in Ar-1%O_2 and Ar-20%O_2 gases resulted from carbon removal during the process shown in Fig. 116. To verifying whether it was the case or not the contamination of carbon in chromium batch KER was analysed before and after exposure to Ar-1%O_2 gas. To do so the oxide scale was removed from the metal surface after oxidation, ground to 1200 grit and then analysed. It was found the carbon content was substantially reduced approximately from the 120ppm (before exposure) to 1ppm (after exposure). This could be evidenced that formation of voids in the bulk scale formed on chromium in dry Ar-O_2 gases is related with presence of carbon, Fig. 115b.

Fig. 117 shows the partial pressure of the gaseous CO(g), CO_2(g) and Cr(g) in equilibrium with solid Cr(s), Cr_2O_3 and $Cr_{23}C_6$(s) vs. temperature. It can be seen, that the CO partial pressure is quite high,

i.e. $p_{CO} \approx 4 \cdot 10^{-5} atm$. Therefore one could expect that increasing carbon content in the metal promotes pore growth and this indeed was observed experimentally in this work, Fig. 99b and Fig. 115a. Additionally, if the pO_2 in the external gas increased, more voids could be generated at the metal/oxide interface due to vacancies condensations, equation (24) and Fig. 31 and by this larger extent of free-metal surface could be revealed at that interface. Grabke and co-workers [101] suggested that trace elements such as carbon could segregate at the metal/oxide interface contributing to pore growth by formation of CO gas when free metal surface are revealed. Fig. 115 clearly shows that oxide scales formed in Ar-20%O_2 were much more porous than in Ar-1%O_2 and it might be the consequences of larger free-metal surface present at the metal/oxide interface.

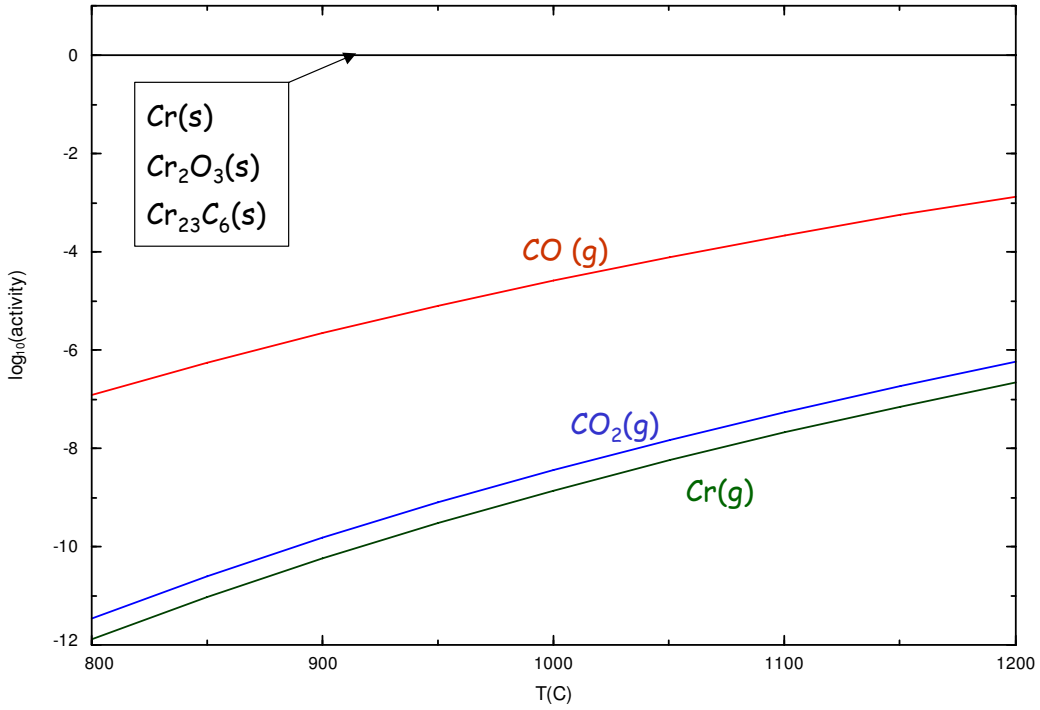

Fig. 117. *Temperature dependence of gaseous CO, CO_2 and Cr in equilibrium with solid Cr, Cr_2O_3 and $Cr_{23}C_6$, [63]*

10. Effect of impurities on the oxidation behaviour of chromium

Findings of this work presented in previous sections clearly indicate that purity of the chromium was an important factor in overall oxidation behaviour. The apparent differences were especially pronounced in exposures to high pO_2 gases. The weight changes recorded during exposure of three chromium batches, JUG, DUR and KER, Table 3, to the Ar-1%O_2 at 1000°C are shown in Fig. 118a. Similar comparison but in the Ar-4%H_2-7%H_2O is presented in Fig. 118b. The same tendency, i.e. the purest the chromium specimen the slower oxidation rate was found, however the extent of changes were much less apparent in Ar-4%H_2-7%H_2O than in Ar-1%O_2 gas.

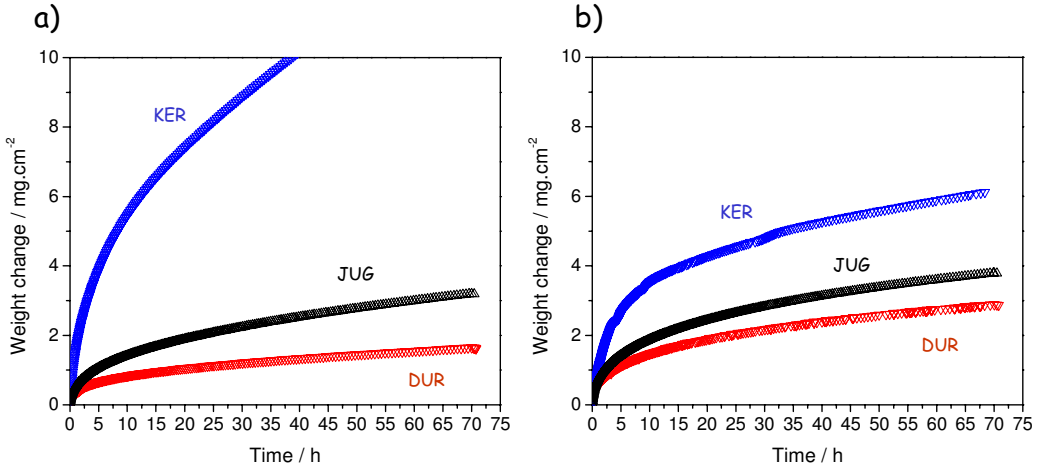

Fig. 118. *Isothermal oxidation of chromium batches JUG, DUR and KER of various purity, Table 3 at 1000°C in a) Ar-1%O_2, b) Ar-4%H_2-7%H_2O gas mixtures*

The oxidation of purest chromium batch DUR in Ar-1%O_2 did not show any porosity in the bulk scale possibly thanks to very low carbon concentration, Fig. 99b. The voids were only concentrated at the metal/oxide interface. The oxidation of commercial chromium batch KER showed a number of pores all over the scale and poor adherence to the metal. The oxide scale formed on batch JUG in Ar-1%O_2 spalled off during cooling to room temperature. The contamination in carbon in this batch was higher than in batch DUR but substantially lower than in batch KER. It was thought that if carbon was a factor contributing to formation of poor adhering scale, reducing it level in that batch could improve scale adherence. This was done by oxidation the specimen previously exposed to Ar-

1%O_2 for second time. Before testing the specimen surface was ground to 1200grit to remove carbon which could be concentrated near metal surface. Oxidation behaviour is shown in Fig. 119a and the morphology of "reoxidized" specimen in Fig. 119b.

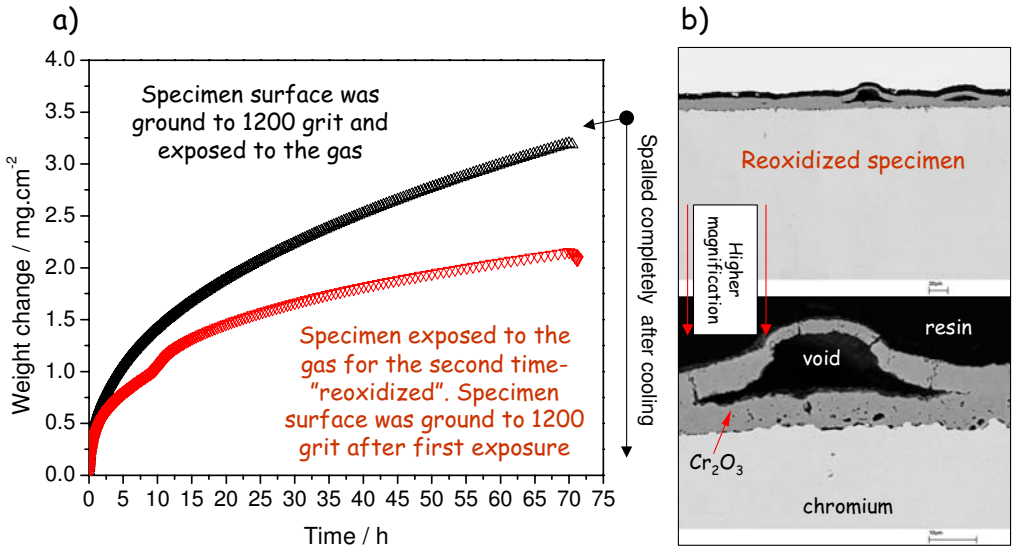

Fig. 119. *a) Isothermal oxidation of chromium, batch JUG prepared in various ways in dry Ar-1%O_2 atmospheres at 1000°C, b) SEM cross section of the reoxidized specimen*

It was seen that such procedure improved oxide adherence and scale did not spalled off after cooling to room temperature. Still some voids were present in the bulk scale and at the metal/oxide interface. Interesting to notice that oxidation rate was reduced for the "reoxidized" specimen. This could be the effect of "purification" process. During first exposure various elements could diffuse to the metal/oxide interface concentrated near the metal surface and after grounding the specimen surface the impurities level could reduce. Depending on the valance of these elements the defect structure of the oxide could be affected and therefore reducing its concentration in the chromium the oxidation rate could be lower, [1].

Another approach was taken for further evidences confirming that contamination could strongly affect oxidation behaviour of chromium. The chromium batch JUG was prepared according to the usual procedure i.e. ground to 1200 grit however the thickness of the specimen was reduced to 0.2 mm, (standard thickness was 2mm). It was believed that reducing specimen thickness the carbon reservoir was also reduced and "purification" in the sample during high temperature exposure could

be more effective. Two different atmospheres, Ar-1%O_2 and Ar-4%H_2-7%H_2O were examined. Oxidation behaviours of specimens with reduced thickness were compared to specimens with standard thickness and shown in Fig. 120. Scale morphologies are shown in Fig. 121. For illustration purposes the approximated thickness of scale formed on the standard thickness specimen in Ar-1%O_2 was drawn.

Apparent decrease in oxidation rate was observed in both tested atmospheres for specimen with reduced thickness. Different chromium purity seemed to have much stronger effect in Ar-O_2 gas. In that gas the scale formed on specimen with reduction thickness was quite compact, only in the inner part of the scale pores were present. In case of Ar-H_2-H_2O atmosphere overall porosity was lower in modified sample and oxide scale adherence was excellent in both specimens.

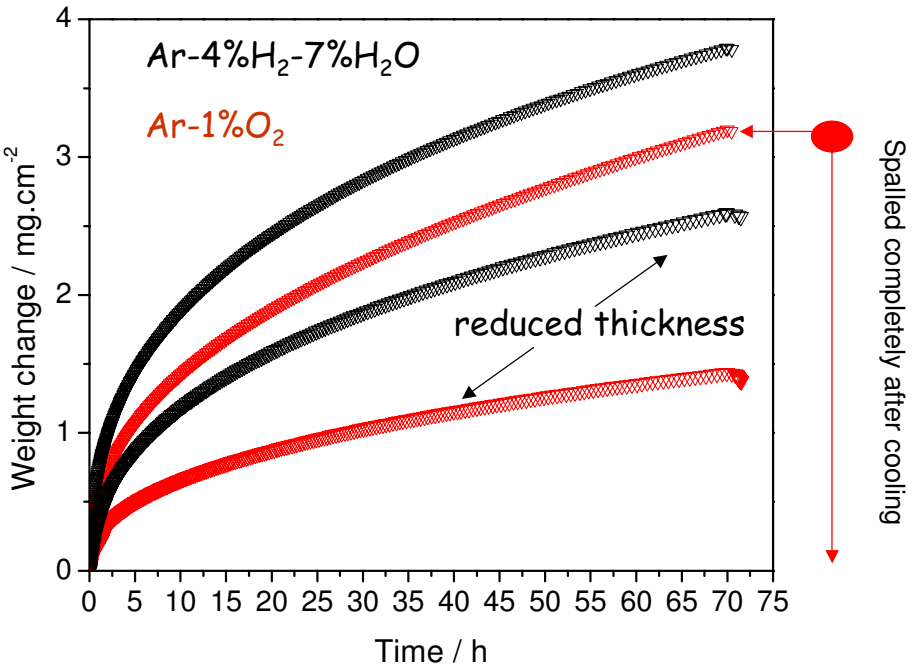

Fig. 120. *Isothermal oxidation of chromium, batch JUG of standard 2mm thickness and reduced to 0.2 mm in Ar-1%O_2 and Ar-4%H_2-7%H_2O at 1000^{o}C*

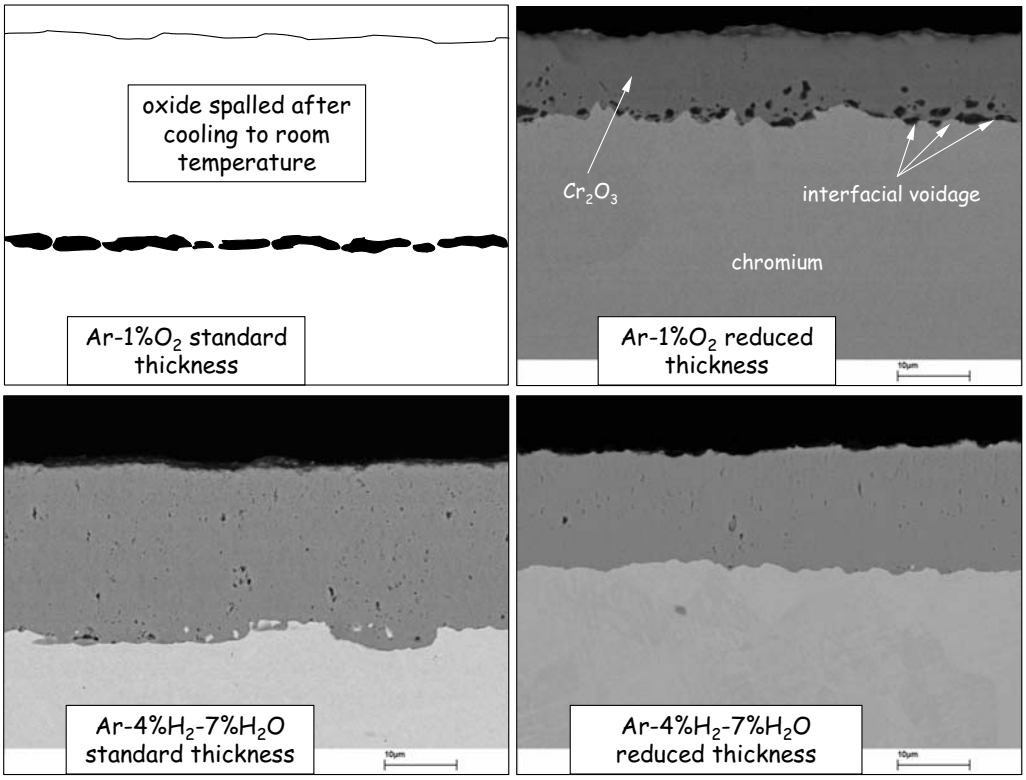

Fig. 121. *SEM cross-sections of oxide scales formed on chromium, batch JUG, after 72h oxidation at 1000^{o}C, standard and reduced thickness of the specimen*

11 Conclusions

Several methods were applied to investigate the oxidation behaviour of chromium in high and low pO_2 gases. Thermogravimetric measurements of weight change during exposure of chromium to different gases enabled the oxidation kinetics to be determined. Metallographic and SEM examinations were applied to characterize the scale morphology in terms of pore development and scale adherence. More detailed information of the scale microstructure such as oxide grain size was obtained using TEM combined with FIB techniques. By using tracer studies and SNMS measurements, it was possible to determine the transport processes in the growing oxide scale. XRD studies of the oxidized samples allowed different phases to be characterized. This was particularly useful for the scales formed in multicomponent gas mixtures such as N_2-O_2-H_2O.

The results of this work clearly indicate that the oxidation behaviour of chromium depends on many factors; not only should the experimental atmosphere be taken into account, but also the purity of the specimen and its geometry. The factors which were found to play a major role in the oxidation of chromium are shown schematically in Fig. 122.

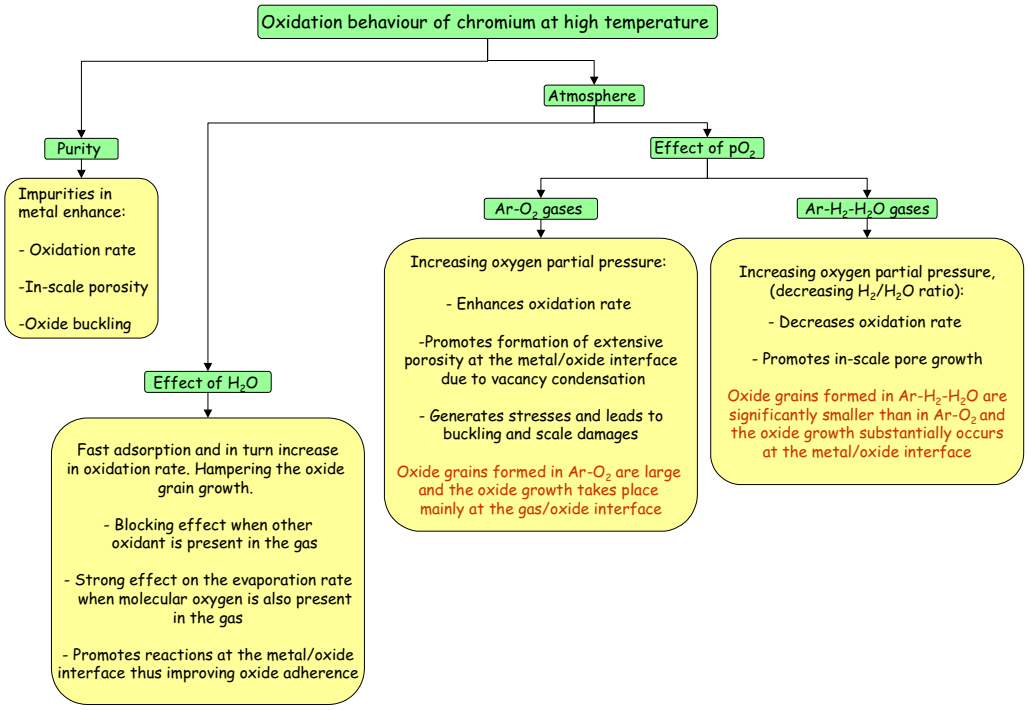

Fig. 122. *Schematic illustration of factors which play a major role during oxidation of chromium*

- Purity of chromium and specimen geometry -

The purity of chromium was shown to affect substantially both oxidation rate and oxide scale adherence. This finding is a key factor in the interpretation of the scatter observed in the literature on oxidation kinetics of pure chromium. Chromium specimens of different purity were investigated and it was observed that purer chromium had a lower oxidation rate and produced a less porous oxide scale. This behaviour was particularly pronounced in Ar-O_2 gases. The presence of trace elements could account for the enhanced oxidation rate due to modifications in defect concentrations in the oxide, and poor scale adherence was probably affected by carbon, which forms the volatile oxide CO at the chromium/chromia interface at pressure of $4x10^{-5}$atm.

- Atmosphere -

To make the effect of atmosphere easier to understand, a few categories of commonly used gases are considered.

Ar-O_2 gases

Clear indications of oxygen partial pressure effects on oxidation rate and adherence were found in Ar-O_2 gases. Increasing the pO_2 in such gas mixtures enhanced the oxidation rate and promoted pore formation at the metal/oxide interface which in turn led to extensive oxide spallation during cooling to room temperature. At the same time growth stresses became higher and the oxide tended to form buckle-type morphologies. Periodical increases in oxidation rate occurred at higher oxygen pressures and as a consequence the scale morphology differed substantially, depending on the pO_2. At reduced oxygen pressures, a very dense scale was formed with no evidence of buckling whereas at higher oxygen pressures a more porous scale was observed. This is schematically illustrated in Fig. 123. Oxide grains were relatively large and if the scale did not crack during exposure, the bulk scale was nearly pore-free in Ar-O_2 mixtures with low O_2 concentration. Therefore it is believed that in Ar-O_2 gases, scale compactness and adherence are affected mainly by the oxygen partial pressure.

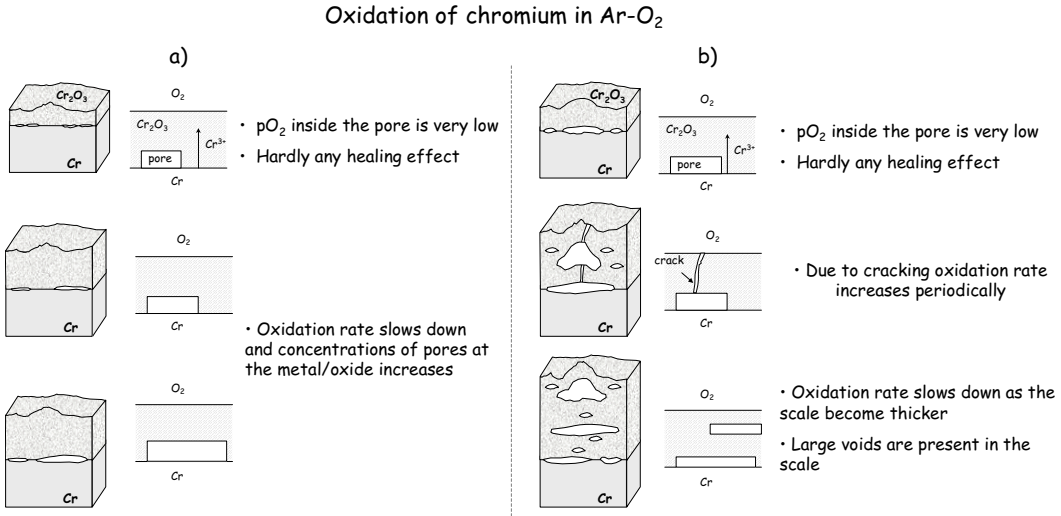

Fig. 123. *Schematic development of oxide formation on pure chromium in dry Ar-O_2 gases, a) low O_2 concentration b) high O_2 concentration*

Ar-H_2-H_2O gases

Exposures to the Ar-H_2-H_2O generally showed higher oxidation rates and better scale adherence than those formed in the dry Ar-O_2. It was found that the oxide grains formed in the Ar-H_2-H_2O were significantly smaller than in the Ar-O_2 and it is believed that such an oxide morphology development was related to the faster adsorption and dissociation of H_2O at the outer surface compared with O_2. Clear evidence of inward scale growth during oxidation in the Ar-H_2O and Ar-H_2-H_2O was found and it is believed to be a consequence of the smaller oxide grain size. It is suggested that inward oxygen grain boundary diffusion was most enhanced by the development of the fine-grained microstructure. However, molecular transport of H_2O and H_2 through the scale could also operate and contribute to the inner scale growth due to formation of H_2O/H_2 bridges in scale voids. This is illustrated schematically in Fig. 124.

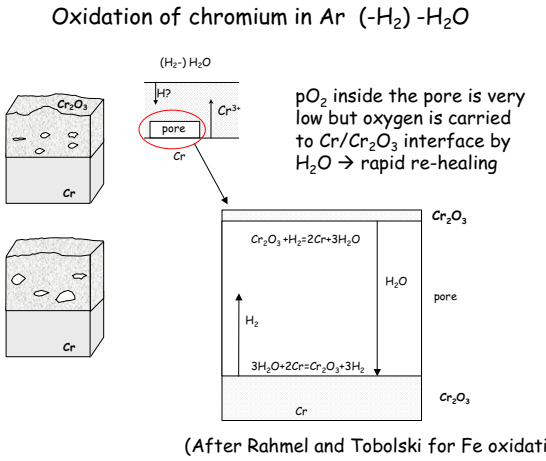

Fig. 124. *Schematic development of oxide formation on pure chromium in H_2-H_2O gases*

- Ar-O_2-H_2O -

The oxidation behaviour of chromium in such gas systems seems to be complex because of several processes operate at the same time. First of all oxygen and water vapour partial pressures are important here. This is because the addition of water vapour could have a weaker or stronger effect depending on the pO_2 in the gas. Small additions of H_2O to the Ar-O_2 gas in which the pO_2 is low would result in enhanced oxygen uptake due to faster adsorption of water vapour at the surface. Larger additions of water vapour to Ar-O_2 where the pO_2 is higher would promote the formation of $CrO_2(OH)_2$ and in turn enhance the evaporation rate.

Multicomponent gas mixtures

Studies on the oxidation behaviour of chromium in multicomponent gas mixtures revealed that scale growth was affected by water vapour and oxygen partial pressure. It was also found that the formation of nitrides and carbides beneath the oxide scale could be affected by water vapour present in the atmosphere.

It was shown that water vapour added to N_2-O_2 gases at 950°C in small amounts, e.g. N_2-1%O_2-1%H_2O, enhanced nitrogen ingress to the metal/scale interface and when added in sufficiently high amounts, i.e. N_2-1%O_2-10%H_2O, completely hindered nitridation. Such behaviour may be a

consequence of enhanced water vapour surface reaction and competitive adsorption between H_2O and N_2. It is believed that H_2O inhibited grain growth which in turned promoted inward transport through the scale. Therefore, if small amounts of H_2O are present in the N_2-O_2-H_2O gas nitridation is enhanced. However, if more H_2O is added, despite fast diffusion paths for nitrogen ingress still existing, nitridation ia hampered because water vapour is blocking nitrogen adsorption at the outer surface of the scale. The blocking effect of water vapour at the surface was especially pronounced in low pO_2 gases such as N_2-4%H_2-4%H_2O and CO-2%CO_2. It is believed that in such atmospheres adsorption and dissociation of H_2O is enhanced by the low oxygen partial pressure and therefore dissociation of water vapour is even faster than in the N_2-O_2-H_2O.

12 References

1. P. Kofstad, *High Temperature Corrosion, Elsevier Applied Science Publisher Ltd 1998, 132*
2. N. Birks, G.H. Meier, *Introduction to High Temperature Oxidation of Metals 1982, 74*
3. S. Mrowec and T. Weber, *Gas Corrosion of Metals, National Bureau of Standards, Washington, DC, 1978*
4. H. Hindam, and D.P. Whittle; *Oxid. Met. 18 (1982) 245*
5. W.C. Hagel; *Trans. Am. Soc. Met., 56 (1963) 538*
6. C.A. Phalnikar, *E.B. Evans and W.M. Baldwin, Jr.; J. Electrochem. Soc., 103 (1956) 429*
7. L. Cadiou and J. Paidassi ; *Mem. Sci. Rev.Metall, 66 (1969) 217*
8. D. Caplan and M. Cohen; *J. Electrochem. Soc. 112 (1964)5*
9. D. Caplan and M. Cohen; *J. Electrochem. Soc. 108 (1961) 438*
10. D. Caplan and G.J. Sproule; *Oxid. Met., 9 (1975) 459*
11. D.J. Young and M. Cohen; *J. Electrochem. Soc., 124 (1977) 775*
12. P. Kofstad and K.P. Lillerud; *J. Electrochem. Soc., 127 (1980) 2410*
13. P. Kofstad and K.P. Lillerud; *J. Electrochem. Soc., 127 (1980) 2397*
14. P. Kofstad, K.P. Lillerud; *Oxid. Met., 17 (1982) 177*
15. K.P. Lillerud and P. Kofstad, *Oxid. of Met., vol. 17, (1982), p. 195*
16. K.P. Lillerud and P. Kofstad, *Oxid. of Met., vol. 17, (1982), p. 127*
17. B. Tveten, G. Hultquist, and T. Norby, *Oxid. Met., 1999 51 (3/4) 221*
18. B. Tveten, G. Hultquist, and D. Wallinder, Oxid. Met., 2001. 55 (3/4) 279
19. G. Hultquist, B. Tveten, and E. Hoerlund, *Oxid. Met., 2000 54 (1/2) 1*
20. D.L. Douglass, P. Kofstad, A. Rahmel and G.C. Wood, *Oxid. Met., 45 5/6 (1996) 529*
21. M. Hänsel, W.J. Quadakkers and D.J. Young; *Oxid. Met., 59 3/4 (2003) 285*
22. W.J. Quadakkers, J.F. Norton, H.J. Penkalla, U. Breuer, A. Gil, T. Rieck and M. Hänsel, *3rd Conference on 'Microscopy of Oxidation', The Institute of Metals, [Edts. S.B. Newcomb, J.A. Little], (1996) 221*
23. W.J. Quadakkers, J.F. Norton, S. Canetoli, K. Schuster and A. Gil, *3rd Conference on 'Microscopy of Oxidation', The Institute of Metals, [Edts. S.B. Newcomb, J.A. Little], (1996) 609*
24. W.J. Quadakkers, J. Piron-Abellan, V. Shemet and L. Singheiser, *Mat. at High Temp., 20 (2003) 115*

25. W.J. Quadakkers, P.J. Ennis, J. Zurek and M. Michalik, *Workshop on Scale Growth and Exfoliation in Steam Plant, NPL, Teddington, U.K., 3-5 September 2003 Proceeding to be published in Mat's. at High Temp., in Press*
26. P.J. Ennis, M. Michalik, W.J. Quadakkers and J. Zurek, *International Journal of Pressure Vessels and Piping, In Press*
27. W.J. Quadakkers, H. Greiner and W. Köck, *Proc. First European Solid Oxide Fuel Cell Forum, 3-7 October 1994, Lucerne, Schwitzerland, p. 525*
28. P. Martinz and W. Köck, *Industrie, 46, (1993) p. 26*
29. X.G. Zheng and D.J. Young, *Oxid. Met., 42, 3/4 (1994) p.163*
30. X.G. Zheng, *Diss. UNSW Sydney, 1993*
31. D. J Young, *Simultaneous oxidation and carburisation of chromia forming alloys*, In Press
32. A.U. Saybolt and D.H. Haman, *Trans. Met. Soc. AIME 230, (1964) 1294*
33. W. J. Quadakkers, *Lecture of High Temperature Corrosion, Forschungszentrum Jülich, 2002*
34. N. Pilling and R. Bedworth, *J. Inst. Metals 29, (1923) 529*
35. G. Tammann, *Z. Anorg. Allg. Chem. 111, (1920) 78*
36. E.W.A. Young, P.C. M. Stiphout and J.H.W. de Wit, *J. Electrochem. Soc., 132 (1985) 884*
37. T. Matsui and K. Naito J. Nucl. *Mater., 120 (1984) 115*
38. P.Y. Hou, *Oxid. Met., 52 (1999) 337*
39. E.A. Gulbransen and K.F. Andrew, *J. Electrochem. Soc., 104 (1957) 334*
40. M. Michalik, M. Hänsel, J. Zurek, L. Singheiser and W.J. Quadakkers, *Mat. at High Temp., Proceedings of the Sixth International Conference on the Microscopy of Oxidation, University of Birmingham, England (2005) 39*
41. E.A. Polman, T. Fransen and P.J. Gellings, *Oxid. Met. 32 (1989) 433*
42. G.M. Raynaud and R.A. Rapp, *Mictrostruct. Sci. 12 (1985) 197*
43. A. Yamauchi, K. Kurokawa and H. Takahashi, *Oxid. Met., 59 (2003) 517*
44. H. C. Graham and H. H. Davis, *J. American Society 54, (1971), p.89*
45. G.C. Fryburg, F.J. Kohl and C.A. Stearns, *J. Electrochem. Soc., 121 (1974) 953*
46. R.T. Grimley, R.P. *Burns and M.G. Inghram, J. Chem. Phys., 34 (1961) 664*
47. M. Farber and R.D. Srivastava, *Combust. Flame, 20 (1973) 43*
48. B.B. Ebbinghaus, *Combust. Flame, 93 (1993) 119*
49. B.B. Ebbinghaus, *Report of the Lawrence Livermore National Laboratory, UCRL-JC-115742 (1993)*
50. M. Hänsel, *Diss. RWTH Aachen, Jül-3583, September 1998, ISSN0944-2952*

51. H. Asteman, J. -E. Swensson, L. -G. Johansson, *Corrosion Science 4 (2002) 2635*
52. H. Asteman, J. -E. Swensson, M. Norell and L. –G. Johansson, *Oxid. Met., 54 (2000) 11*
53. H. Asteman, J. -E. Swensson, L. –G. Johansson and M. Norell, *Oxid. Met., 52 (1999) 95*
54. H. Asteman, J. -E. Swensson, L. -G. Johansson, *Oxid. Met., 57 (2002) 193*
55. K. Hilpert, D. Das. M. Miller, D.H. Peck, R. Weiss, *J. Electrochem. Soc 143 (1996) 3642*
56. E.J. Opila, *NASA Glenn Research Centre, Cleveland, OH (2005), unpublished research*
57. T. Mills, *J.Less common Metals, 26 (1972) 223*
58. W. Hagel, *Trans. ASM, 56(1963) 583*
59. G.R. Wilms and T.W. Rea*, J. Less-Common Met. 1, 152 (1959)*
60. G.R. Wilms and T.W. Rea, *J. Less-Common Met. 3, 234 (1961)*
61. C.A. Snavely and C.L Faust, *J. Electrochem. Soc. 97, 99 (1950)*
62. V.I. Arkharov, V.N. Konev and I.S. Trakhtenberg, *Phys. Met. Metall. 5, 164 (1957)*
63. C. Balle, A.D. Pelton, W.J. Thompson, G. Eriksson, K. Hack, P. Chartrand, S. Degterov, J. Melancon, S. Petersen, *FactSage 5.1, Copyright Thermfact 1976*
64. W.J. Quadakkers, A. Elschner, H. Holzbrecher, K. Schmidt, W. Speier and H. Nickel, *Mikrochim. Acta 102 (1992) 197*
65. W.J. Quadakkers, A. Elschner, W. Speier and H. Nickel, *Appl. Surf. Sci. 52 (1991) 271*
66. W.J. Quadakkers, H. Holzbrecher, K.G. Briefs and H. Beske, *Oxid. Met., 32 (1989) 67*
67. C.Anghel, E. Hörnuld, G. Hultquist, M. Limbäck, *Appl. Surf. Sci. 233 (2004) 392*
68. Y.P. Jacob, V.A.C. Haanappel, M.F. Stroosnijder, H. Buscail, P. Fielitz, G. Borchardt, *Corros. Sci. 44 (2002) 2027*
69. H. Buscail, Y.P. Jacob. M.F. Stroosnijder, E. Caudron, R. Cueff, F.Rabaste and S. Perrier, *Materials Science Forum 461 (2004) 93*
70. I. Murris, Y.P. Jacob, V.A.C. Haanappel, M.F. Stroosnijder, *Oxid. Met., in press*
71. E.T. Turkdogan, W.M. McKewan and L. Zwell, *J. Phys. Chem. 69 (1965) 327*
72. G. Hultquist and P. Szakálos, *J. Atm. Chem. in press*
73. T.Akermark, *Oxid. Met., 50 (1998) 167*
74. K. Larsson, H. Björkman and K. Hjort, *J. Appl. Phys. 90 (2001) 1026*
75. J. Zurek, D.J. Young, E. Essumann, M.Hänsel, H.J. Penkalla. L.Niewolak, W.J. Quadakkers, *submitted to publication*
76. W.D. Kingery, H.K. Bowen and D.R. Uhlmann, *Introduction to Ceramics, New York (1976)*
77. K.W. Lay, *Material Science Research, Proceedings of the Third International Conference on Sintering and Related Phenomena, University of Notre Dame, (1972) 65*

78. J. Lis and R. Pampuch, Spiekanie, AGH, Kraków (2000)
79. A.Rahmel and J.Tobolski, *Corro. Sc., 5 (1965) 333*
80. C. T. Fuji and R.A. Meussner, *J. Electrochem. Soc., 111 (1964) 1215*
81. A. Yamauchi, Y. Yamauchi, Y. Hirohate, T. Hino and K. Kurokawa, *Materials Science Forum 522 (2006) 163*
82. W.M. Kays and M.E. Crawford, *Convective Heat and Mass Transfer, McGraw-Hill, New York, (1980)*
83. T.K. Scherwood, R.L. Pigford and C.R. Wilke, *Mass Transfer, McGraw-Hill, New York, (1975)*
84. D.R. Poirier, G.H. Geiger, *Transport Phenomena in Materials Processing, Pennsylvania (1994)*
85. D.R. Gaskell, *An Introduction to Transport Phenomena in Materials Engineering, Macmillan, New York (1992)*
86. D.J. Young and B.A. Pint, *Oxid. Met., in press*
87. A. Atkinson*, Rev. Mod. Phys. 57 (1985) 437*
88. A. Atkinson and R.I. Taylor, *Philo. Mag. A 39 (1979) 581*
89. A. Atkinson and R.I. Taylor, *Philo. Mag. A 43 (1982) 979*
90. A. Atkinson, R.I. Taylor and P.D. Goode, *Oxid. Met. 13 (1979) 519*
91. M.R. Taylor, J.M. Calvert, D.G. Less and D.B. Meadowcroft, *Oxid. Met. 14 (1980) 499*
92. J.S. Sheasby and J.D. Brown, *Oxid. Met., 5 (1978) 405*
93. C. Gleave, J.M. Calvert, D.G. Lees and P.C. Rowlands, *Proc. R. Soc. London Ser. A 379 (1982) 409*
94. A.M. Pritchard, J.E. Antill, K.R. Cottell, K.A. Peakall, and A.E. Truswell, *Oxid. Met. 9 (1975) 181*
95. A.M. Pritchard, N.E.W. Hartley, J.F. Singleton and A.E. Truswell, *Corros. Sci. 20 (1980) 1*
96. S. Mrowec, *Corros. Sci. 7 (1967) 563*
97. S. Mrowec and K. Przybylski, *Oxid. Met. 11 (1977) 365*
98. J. Ehlers, D.J. Young, E.J. Smaardijk, A.K. Tyagi, H.J. Penkalla, L. Singheiser and W.J Quadakkers, *Corro. Sci., 48(2006) 3428*
99. M.J. Graham and D. Caplan, *J. Electrochem. Soc., 201 (1973) 769*
100. M. Schütze, *Protective Oxide Scales and Their Breakdown,London (1997)*
101. H.J. Grabke, M.Steinhorst, H. Brumm and D. Wiemer, *Oxid. Met. 35 (1991) 199*

Acknowledgements

The authors would like to thank the German Research Foundation for the financial support and all the people which have contributed to this work, especially;

the Central Department of Technology (ZAT), Research Centre Jülich;

the Central Division of Analytical Chemistry (ZCH), Research Centre Jülich;

the High Temperature Corrosion group and the Electron Microscope unit at the University of New South Wales, Sydney, Australia;

and especially our colleagues at the Institute of Energy Research, (IEF-2), Research Centre Jülich in which this work was carried out.

Schriften des Forschungszentrums Jülich
Reihe Energietechnik / Energy Technology

1. **Fusion Theory**
   Proceedings of the Seventh European Fusion Theory Conference
   edited by A. Rogister (1998); X, 306 pages
   ISBN: 978-3-89336-219-6

2. **Radioactive Waste Products 1997**
   Proceedings of the 3rd International Seminar on Radioactive Waste Products held in Würzburg (Germany) from 23 to 26 June 1997
   edited by R. Odoj, J. Baier, P. Brennecke et al. (1998), XXIV, 506 pages
   ISBN: 978-3-89336-225-7

3. **Energieforschung 1998**
   Vorlesungsmanuskripte des 4. Ferienkurs „Energieforschung“
   vom 20. bis 26. September 1998 im Congrescentrum Rolduc und
   im Forschungszentrum Jülich
   herausgegeben von J.-Fr. Hake, W. Kuckshinrichs, K. Kugeler u. a. (1998),
   500 Seiten
   ISBN: 978-3-89336-226-4

4. **Materials for Advances Power Engineering 1998**
   Abstracts of the 6th Liège Conference
   edited by J. Lecomte-Beckers, F. Schubert, P. J. Ennis (1998), 184 pages
   ISBN: 978-3-89336-227-1

5. **Materials for Advances Power Engineering 1998**
   Proceedings of the 6th Liège Conference
   edited by J. Lecomte-Beckers, F. Schubert, P. J. Ennis (1998),
   Part I XXIV, 646, X pages; Part II XXIV, 567, X pages; Part III XXIV, 623, X pages
   ISBN: 978-3-89336-228-8

6. **Schule und Energie**
   1. Seminar Energiesparen, Solarenergie, Windenergie. Jülich, 03. und 04.06.1998
   herausgegeben von P. Mann, W. Welz, D. Brandt, B. Holz (1998), 112 Seiten
   ISBN: 978-3-89336-231-8

7. **Energieforschung**
   Vorlesungsmanuskripte des 3. Ferienkurses „Energieforschung“
   vom 22. bis 30. September 1997 im Forschungszentrum Jülich
   herausgegeben von J.-Fr. Hake, W. Kuckshinrichs, K. Kugeler u. a. (1997),
   505 Seiten
   ISBN: 978-3-89336-211-0

8. **Liberalisierung des Energiemarktes**
   Vortragsmanuskripte des 5. Ferienkurs „Energieforschung“
   vom 27. September bis 1. Oktober 1999 im Congrescentrum Rolduc und
   im Forschungszentrum Jülich
   herausgegeben von J.-Fr. Hake, A. Kraft, K. Kugeler u. a. (1999), 350 Seiten
   ISBN: 978-3-89336-248-6

9. **Models and Criteria for Prediction of Deflagration-to-Detonation Transition (DDT) in Hydrogen-Air-Steam-Systems under Severe Accident Conditions**
   edited by R. Klein, W. Rehm (2000), 178 pages
   ISBN: 978-3-89336-258-5

10. **High Temperature Materials Chemistry**
    Abstracts of the 10th International IUPAC Conference, April 10 - 14 2000, Jülich
    edited by K. Hilpert, F. W. Froben, L. Singheiser (2000), 292 pages
    ISBN: 978-3-89336-259-2

11. **Investigation of the Effectiveness of Innovative Passive Safety Systems for Boiling Water Reactors**
    edited by E. F. Hicken, K. Verfondern (2000), X, 287 pages
    ISBN: 978-3-89336-263-9

12. **Zukunft unserer Energieversorgung**
    Vortragsmanuskripte des 6. Ferienkurs „Energieforschung“
    vom 18. September bis 22. September 2000 im Congrescentrum Rolduc und
    im Forschungszentrum Jülich
    herausgegeben von J.-Fr. Hake, S. Vögele, K. Kugeler u. a. (2000),
    IV, 298 Seiten
    ISBN: 978-3-89336-268-4

13. **Implementing Agreement 026**
    For a Programme of Research, Development and Demonstration on Advanced Fuel Cells: Fuel Cell Systems for Transportation. Annex X. Final Report 1997 - 1999
    edited by B. Höhlein; compiled by P. Biedermann (2000), 206 pages
    ISBN: 978-3-89336-275-2

14. **Vorgespannte Guß-Druckbehälter (VGD) als berstsichere Druckbehälter für innovative Anwendungen in der Kerntechnik**
    Prestressed Cast Iron Pressure Vessels as Burst-Proof Pressure Vessels for Innovative Nuclear Applications
    von W. Fröhling, D. Bounin, W. Steinwarz u. a. (2000) XIII, 223 Seiten
    ISBN: 978-3-89336-276-9

15. **High Temperature Materials Chemistry**
Proceedings of the 10th International IUPAC Conference
held from 10 to 14 April 2000 at the Forschungszentrum Jülich, Germany
Part I and II
edited by K. Hilpert, F. W. Froben, L. Singheiser (2000), xvi, 778, VII pages
ISBN: 978-3-89336-259-2

16. **Technische Auslegungskriterien und Kostendeterminanten von SOFC- und PEMFC-Systemen in ausgewählten Wohn- und Hotelobjekten**
von S. König (2001), XII, 194 Seiten
ISBN: 978-3-89336-284-4

17. **Systemvergleich: Einsatz von Brennstoffzellen in Straßenfahrzeugen**
von P. Biedermann, K. U. Birnbaum, Th. Grube u. a. (2001), 185 Seiten
ISBN: 978-3-89336-285-1

18. **Energie und Mobilität**
Vorlesungsmanuskripte des 7. Ferienkurs „Energieforschung“
vom 24. September bis 28. September 2001 im Congrescentrum Rolduc und im Forschungszentrum Jülich
herausgegeben von J.-Fr. Hake, J. Linßen, W. Pfaffenberger u. a. (2001), 205 Seiten
ISBN: 978-3-89336-291-2

19. **Brennstoffzellensysteme für mobile Anwendungen**
von P. Biedermann, K. U. Birnbaum, Th. Grube u. a. (2002)
PDF-Datei auf CD
ISBN: 978-3-89336-310-0

20. **Materials for Advances Power Engineering 2002**
Abstracts of the 7th Liège Conference
edited by J. Lecomte-Beckers, M. Carton, F. Schubert, P. J. Ennis (2002), c. 200 pages
ISBN: 978-3-89336-311-7

21. **Materials for Advanced Power Engineering 2002**
Proceedings of the 7th Liège Conference
Part I, II and III
edited by J. Lecomte-Beckers, M. Carton, F. Schubert, P. J. Ennis (2002), XXIV, 1814, XII pages
ISBN: 978-3-89336-312-4

22. **Erneuerbare Energien: Ein Weg zu einer Nachhaltigen Entwicklung?**
Vorlesungsmanuskripte des 8. Ferienkurs „Energieforschung“
vom 23. bis 27. September 2002 in der Jakob-Kaiser-Stiftung, Königswinter
herausgegeben von J.-Fr. Hake, R. Eich, W. Pfaffenberger u. a. (2002), IV, 230 Seiten
ISBN: 978-3-89336-313-1

23. **Einsparpotenziale bei der Energieversorgung von Wohngebäuden durch Informationstechnologien**
von A. Kraft (2002), XII, 213 Seiten
ISBN: 978-3-89336-315-5

24. **Energieforschung in Deutschland**
Aktueller Entwicklungsstand und Potentiale ausgewählter nichtnuklearer Energietechniken
herausgegeben von M. Sachse, S. Semke u. a. (2002), II, 158 Seiten, zahlreiche farb. Abb.
ISBN: 978-3-89336-317-9

25. **Lebensdaueranalysen von Kraftwerken der deutschen Elektrizitätswirtschaft**
von A. Nollen (2003), ca. 190 Seiten
ISBN: 978-3-89336-322-3

26. **Technical Session: Fuel Cell Systems of the World Renewable Energy Congress VII**
Proceedings
edited by D. Stolten and B. Emonts (2003), VI, 248 pages
ISBN: 978-3-89336-332-2

27. **Radioactive Waste Products 2002 (RADWAP 2002)**
Proceedings
edited by R. Odoj, J. Baier, P. Brennecke and K. Kühn (2003), VI, 420 pages
ISBN: 978-3-89336-335-3

28. **Methanol als Energieträger**
von B. Höhlein, T. Grube, P. Biedermann u. a. (2003), XI, 109 Seiten
ISBN: 978-3-89336-338-4

29. **Hochselektive Extraktionssysteme auf Basis der Dithiophosphinsäuren: Experimentelle und theoretische Untersuchungen zur Actinoiden(III)-Abtrennung**
von S. A. H. Nabet (2004), VI, 198 Seiten
ISBN: 978-3-89336-351-3

30. **Benchmarking-Methodik für Komponenten in Polymerelektrolyt-Brennstoffzellen**
von Matthias Gebert (2004), 194 Seiten
ISBN: 978-3-89336-355-1

31. **Katalytische und elektrochemische Eigenschaften von eisen- und kobalthaltigen Perowskiten als Kathoden für die oxidkeramische Brennstoffzelle (SOFC)**
von Andreas Mai (2004), 100 Seiten
ISBN: 978-3-89336-356-8

32. **Energy Systems Analysis for Political Decision-Making**
edited by J.-Fr. Hake, W. Kuckshinrichs, R. Eich (2004), 180 pages
ISBN: 978-3-89336-365-0

33. **Entwicklung neuer oxidischer Wärmedämmschichten für Anwendungen in stationären und Flug-Gasturbinen**
von R. Vaßen (2004), 141 Seiten
ISBN: 978-3-89336-367-4

34. **Neue Verfahren zur Analyse des Verformungs- und Schädigungsverhaltens von MCrAlY-Schichten im Wärmedämmschichtsystem**
von P. Majerus (2004), 157 Seiten
ISBN: 978-3-89336-372-8

35. **Einfluss der Oberflächenstrukturierung auf die optischen Eigenschaften der Dünnschichtsolarzellen auf der Basis von a-Si:H und µc-Si:H**
von N. Senoussaoui (2004), 120 Seiten
ISBN: 978-3-89336-378-0

36. **Entwicklung und Untersuchung von Katalysatorelementen für innovative Wasserstoff-Rekombinatoren**
von I.M. Tragsdorf (2005), 119 Seiten
ISBN: 978-3-89336-384-1

37. **Bruchmechanische Untersuchungen an Werkstoffen für Dampfkraftwerke mit Frischdampftemperaturen von 500 bis 650°C**
von L. Mikulová (2005), 149 Seiten
ISBN: 978-3-89336-391-9

38. **Untersuchungen der Strukturstabilität von Ni-(Fe)-Basislegierungen für Rotorwellen in Dampfturbinen mit Arbeitstemperaturen über 700 °C**
von T. Seliga (2005), 106 Seiten
ISBN: 978-3-89336-392-6

39. **IWV-3 Report 2005. Zukunft als Herausforderung**
(2005), 115 Seiten
ISBN: 978-3-89336-393-3

40. **Integrierter Photodetektor zur Längenmessung**
von E. Bunte (2005), XI, 110 Seiten
ISBN: 978-3-89336-397-1

41. **Microcrystalline Silicon Films and Solar Cells Investigated by Photoluminescence Spectroscopy**
by T. Merdzhanova (2005), X, 137 pages
ISBN: 978-3-89336-401-5

42. **IWV-3 Report 2005. Future as a challenge**
(2005), 115 pages
ISBN: 978-3-89336-405-3

43. **Electron Spin Resonance and Transient Photocurrent Measurements on Microcrystalline Silicon**
by T. Dylla (2005), X, 138 pages
ISBN: 978-3-89336-410-7

44. **Simulation und Analyse des dynamischen Verhaltens von Kraftwerken mit oxidkeramischer Brennstoffzelle (SOFC)**
von M. Finkenrath (2005), IV, 155 Seiten
ISBN: 978-3-89336-414-5

45. **The structure of magnetic field in the TEXTOR-DED**
by K.H. Finken, S.S. Abdullaev, M. Jakubowski, M. Lehnen, A. Nicolai, K.H. Spatschek (2005), 113 pages
ISBN: 978-3-89336-418-3

46. **Entwicklung und Modellierung eines Polymerelektrolyt-Brennstoffzellenstapels der 5 kW Klasse**
von T. Wüster (2005), 211 Seiten
ISBN: 978-3-89336-422-0

47. **Die Normal-Wasserstoffelektrode als Bezugselektrode in der Direkt-Methanol-Brennstoffzelle**
von M. Stähler (2006), VI, 96 Seiten
ISBN: 978-3-89336-428-2

48. **Stabilitäts- und Strukturmodifikationen in Katalysatordispersionen der Direktmethanolbrennstoffzelle**
von C. Schlumbohm (2006), II, 211 Seiten
ISBN: 978-3-89336-429-9

49. **Eduktvorbereitung und Gemischbildung in Reaktionsapparaten zur autothermen Reformierung von dieselähnlichen Kraftstoffen**
von Z. Porš (2006), XX, 182, XII Seiten
ISBN: 978-3-89336-432-9

50. **Spektroskopische Untersuchung der poloidalen Plasmarotation unter dem Einfluß statischer und dynamischer Ergodisierung am Tokamak TEXTOR**
von C. Busch (2006), IV, 81 Seiten
ISBN: 978-3-89336-433-6

51. **Entwicklung und Optimierung von Direktmethanol-Brennstoffzellstapeln**
von M. J. Müller (2006), 167 Seiten
ISBN: 978-3-89336-434-3

52. **Untersuchung des reaktiven Sputterprozesses zur Herstellung von aluminiumdotierten Zinkoxid-Schichten für Silizium-Dünnschichtsolarzellen**
von J. Hüpkes (2006), XIV, 170 Seiten
ISBN: 978-3-89336-435-0

53. **Materials for Advanced Power Engineering 2006**
Proceedings of the 8th Liège Conference
Part I, II and III
edited by J. Lecomte-Beckers, M. Carton, F. Schubert, P. J. Ennis (2006), Getr. Pag.
ISBN: 978-3-89336-436-7

54. **Verdampfung von Werkstoffen beim Betrieb von Hochtemperaturbrennstoffzellen (SOFC)**
von M. Stanislowski (2006), IV, 154 Seiten
ISBN: 978-3-89336-438-1

55. **Methanol as an Energy Carrier**
edited by P. Biedermann, Th. Grube, B. Höhlein (2006), XVII, 186 pages
ISBN: 978-3-89336-446-6

56. **Kraftstoffe und Antriebe für die Zukunft**
Vorlesungsmanuskripte des 1. Herbstseminars „Kraftstoffe und Antriebe für die Zukunft“ vom 9.-13. Oktober 2006 an der TU Berlin
herausgegeben von V. Schindler, C. Funk, J.-Fr. Hake, J. Linßen (2006), VIII, 221 Seiten
ISBN: 978-3-89336-452-7

57. **Plasma Deposition of Microcrystalline Silicon Solar Cells: Looking Beyond the Glass**
by M. N. van den Donker (2006), VI, 110 pages
ISBN: 978-3-89336-456-5

58. **Nuclear Energy for Hydrogen Production**
by K. Verfondern (2007), 186 pages
ISBN: 978-3-89336-468-8

59. **Kraft-Wärme-Kopplung mit Brennstoffzellen in Wohngebäuden im zukünftigen Energiesystem**
von C. H. Jungbluth (2007), XI, 197 Seiten
ISBN: 978-3-89336-469-5

60. **Finite Element Simulation of Stress Evolution in Thermal Barrier Coating Systems**
by P. Bednarz (2007), XIV, 121 pages
ISBN: 978-3-89336-471-8

61. **Modellierung der Prozesse in katalytischen Rekombinatoren**
von J. Böhm (2007), VI, 116 Seiten
ISBN: 978-3-89336-473-2

62. **Entwicklung einer Heliumstrahldiagnostik zur Messung der Elektronendichte und – temperatur mit hoher räumlicher und zeitlicher Auflösung**
von U. Kruezi (2007), IV, 151 Seiten
ISBN: 978-3-89336-476-3

63. **IEF-3 Report 2007. Von Grundlagen bis zum System**
(2007), 164 Seiten
ISBN: 978-3-89336-479-4

64. **Entwicklung eines Direkt-Methanol-Brennstoffzellensystems der Leistungklasse kleiner 5 kW**
von M. Nölke (2007), 194 Seiten
ISBN: 978-3-89336-481-7

65. **Effect of geometry and composition of Cr steels on oxide scale properties relevant for interconnector applications in Solid Oxide Fuel Cells (SOFCs)**
by P. Huczkowski, W.J. Quadakkers (2007), 159 pages
ISBN: 978-3-89336-484-8

66. **Netzwerke Grundlagenforschung erneuerbare Energien und rationelle Energieanwendung**
Statusseminar 12. + 13. März 2007
(2007), 222 Seiten
ISBN: 978-3-89336-485-5

67. **Effect of water vapour on growth and adherence of chromia scales on pure chromium**
by M. Michalik, M. Hänsel, W. J. Quadakkers (2007), 133 pages
ISBN: 978-3-89336-486-2

This work provides a comprehensive analysis of the oxidation behaviour of chromium with different purity level at high temperature in atmospheres with different oxygen partial pressure. The main aim of the work was to elucidate the effect of water vapour on adherence, volatilization and mass transport through the oxide scale. Another aspect of the study was to determine the effect of material impurities, especially of carbon, on oxidation behaviour in the different test environments.

Author

Marek Michalik studied at the Academy of Mining and Metallurgy in Cracow, Poland and at the University of Ghent, Belgium. Since 2002 he has been working at the Research Centre Juelich, Germany in the Institute of Energy Research. The contents of this book have been submitted to the Technical University of Aachen, (RWTH Aachen) in fulfilment of the requirements for a Doctor of Engineering degree.

Institute of Energy Research
IEF-2 Materials Microstructure and Characterization

The research topics of IEF-2 are focussed on the development and characterization of materials for efficient gas and steam power plants, for high temperature fuel cells and for future fusion reactor components subjected to high thermal loads. The scientific expertises of the institute cover microstructural investigations, surface analysis techniques and the physical, chemical, mechanical and corrosion behaviour of metallic high temperature materials and of ceramic materials used either as structural components or as elements of coating systems.

Forschungszentrum Jülich
in der Helmholtz-Gemeinschaft

Band / Volume 67
ISBN 978-3-89336-486-2

Energietechnik
Energy Technology